

**STRAY GAS MIGRATION: MULTICOMPONENT MASS TRANSFER
EFFECTS ON DISSOLUTION AND PERSISTENCE OF GAS IN THE
SUBSURFACE**

by

Nicholas Alick Ashmore

A thesis submitted to the Department of Civil Engineering

In conformity with the requirements for

the degree of Master of Applied Science

Queen's University

Kingston, Ontario, Canada

(January, 2021)

Copyright ©Nicholas Ashmore, 2021

Abstract

As the development of deep geological gas reserves increases in the coming years, concern has been raised regarding potential environmental impacts including stray gas migration. The goal of this research was to improve investigation techniques at suspected stray gas migration sites by studying multicomponent mass transfer effects on the dissolution and persistence of trapped gas in the subsurface, and potential changes to one of the principal source identification tools, hydrocarbon ratios, over time. This goal was achieved by conducting small-scale (5.3 cm length, 7.2 cm diameter) column experiments, in which single- and multicomponent natural gas mixtures were trapped in sand. Water was pumped through the column, and dissolved gas concentrations were monitored over time. The experiments were simulated using a reactive transport code, MIN3P. Further simulations were conducted to investigate the effects of background dissolved gases on the persistence of gas in the subsurface, and potential changes in hydrocarbon ratios due to multicomponent mass transfer. Additionally, a set of calculations were conducted to determine potential errors for hydrocarbon (and other dissolved gas) ratios due to the misinterpretation of analytical results, and how the use of hydrocarbon ratios may be impacted in practice.

MIN3P was successfully used to simulate the dissolution of both single- and multicomponent source trapped gases in porous media. Laboratory and numerical simulations showed that the aqueous concentrations during gas dissolution are generally insensitive to dissolved background gas concentration, but that gas persistence is highly sensitive to background gases. Multicomponent mass transfer can lead to variation in hydrocarbon ratios over time due to differences in gas partitioning properties, and as such they should be coupled with other identification methods. Furthermore, hydrocarbon ratios should be calculated using an equivalent gas pressure when interpreting dissolved gas concentrations, as other interpretations can lead to significant error (a factor of 1.15 to 2.67 under the conditions considered in this study). The findings of this research demonstrate that it is important to consider multicomponent effects in stray gas migration, as the presence of multiple components in both the source and the background has substantial impact on the dissolution of gas in the subsurface.

Co-Authorship

This thesis has been prepared in manuscript format. Chapter 2, ‘Multicomponent mass transfer effects on the dissolution of stray gas: gas persistence and interpretation of hydrocarbon ratios’ was co-authored by N.A. Ashmore and K.G. Mumford. Scope, methodologies, and the experimental setup were developed by both authors. Numerical modeling, data collection, analysis and interpretation were conducted by N.A. Ashmore with input and guidance from K.G. Mumford. The manuscript was written by N.A. Ashmore and edited by K.G. Mumford.

Chapter 3, ‘Calculation of gas ratios for use in source identification for stray gas migration’ was co-authored by N.A. Ashmore, K.G. Mumford, C.J.C. Van De Ven and L.J. Molofsky. Scope and methodologies were developed by all authors. Calculation approach was developed by N.A. Ashmore with input and guidance C.J.C. Van De Ven and K.G. Mumford. Calculations, analysis and interpretation were conducted by N.A. Ashmore with input and guidance from K.G. Mumford. The manuscript was written by N.A. Ashmore and edited by K.G. Mumford.

Acknowledgements

Thank you to my supervisor, Dr. Kevin Mumford, for his wealth of knowledge and academic curiosity. His dedication and support helped me produce work I can be proud of through particularly challenging times. Thank you to Stan Prunster and Nathan Mullins, whose technical support and help in the lab made this work possible. Thank you to Paula Whitley, Dr. Allison Rutter, Mesha Thompson, Dr. Graham Cairns and Dale Marecak at the Queen's Analytical Services Unit and Michael Nightingale at the University of Calgary for the technical support and knowledge. Thank you to everyone in the groundwater research group for getting me through lots of long days in both the office and the lab, and for always being willing to listen to my ideas and offer advice. Thank you to the administration staff, faculty and students in the Civil Department. Thank you to my friends for making my time at Queen's so special and creating memories that will last a lifetime.

Thank you to Emily, for her love and encouragement, and always putting a smile on my face. Thank you to my family for their love and support through the years. Thank you to my siblings Emma, Ian and Tim for always giving me someone to look up to. Thank you to my mom, for always encouraging me strive to make the world a better place. Thank you to my dad, who is always willing to chat about my research and can always make me laugh. And to both my mom and dad for their love, support, and encouragement.

Table of Contents

Abstract.....	ii
Co-Authorship.....	iii
Acknowledgements.....	iv
List of Figures.....	vii
List of Tables.....	x
List of Abbreviations.....	xi
List of Symbols.....	xii
Chapter 1 Introduction.....	1
1.1 Background.....	1
1.1.1 Well Design and Causes of Gas Migration.....	3
1.1.2 Gas Migration Dynamics.....	5
1.1.3 Leak detection.....	9
1.1.4 Source Identification.....	10
1.1.5 Mass Transfer.....	13
1.2 Research Need.....	17
1.3 Research Objectives.....	17
1.4 Thesis Organization.....	18
1.5 References.....	19
Chapter 2 Multicomponent mass transfer effects on the dissolution of stray gas: gas persistence and interpretation of hydrocarbon ratios.....	26
2.1 Introduction.....	26
2.2 Lab-Scale Experiments.....	34
2.2.1 Experimental Design.....	34
2.2.2 Dissolved Gas Quantification.....	37
2.3 Numerical Modeling.....	38
2.3.1 Model Description.....	38
2.3.2 Model Implementation.....	40
2.4 Results and Discussion.....	43
2.4.1 Single-component (Methane) Dissolution.....	43
2.4.2 Impact of Dissolved Background Gases.....	46
2.4.3 Multicomponent Source Dissolution.....	49
2.5 Summary and Conclusions.....	54

2.6 References.....	56
Chapter 3 Calculation of gas ratios for use in source identification for stray gas migration	61
3.1 Introduction.....	61
3.2 Conceptual Model and Calculation Approach	64
3.2.1 Conceptual Model.....	64
3.2.2 Ratio Definitions.....	66
3.2.3 Ratio Calculations.....	67
3.2.4 Dissolved Gas Sampling Scenarios.....	70
3.3 Results and Discussion	72
3.3.1 Headspace Ratio.....	72
3.3.2 Aqueous Mass and Molar Ratio.....	74
3.3.3 Equivalent Gas Ratio	75
3.3.4 Effects of Dilution.....	75
3.3.5 Addition of non-hydrocarbon gases.....	77
3.4 Summary and Conclusions.....	78
3.5 References.....	79
Chapter 4 Conclusions and Recommendations.....	83
4.1 Summary and Conclusions.....	83
4.2 Recommendations for Future Work.....	86
4.3 Contributions.....	87
4.4 References.....	87
Appendix A Supplemental Figures (Chapter 2).....	88
Appendix B Bromide Tracer Tests (Chapter 2).....	92
Appendix C Sand Characterization (Chapter 2)	94
Appendix D Experimental Apparatus (Chapter 2).....	97
Appendix E Methane Calibration Data (Chapter 2).....	100

List of Figures

- Figure 1.1. Map of North American shale deposits. The largest Canadian deposits are located in Alberta and British Columbia, with smaller deposits in other provinces and territories (US EIA via CCA, 2014). . 2
- Figure 1.2. Conceptual sketch of potential gas sources and failure mechanisms leading to gas migration. Text labeled a) and b) indicate potential gas sources. Stray gas can travel through multiple different pathways (black lines) and be expressed at the well head as surface casing vent flow or near well gas migration, or gas may enter the aquifer leading to far field gas migration. 4
- Figure 1.3. Conceptual sketch of stray gas migration in shallow aquifers. Gas pools under low permeability regions, and flows upwards at the edge of the low permeable region as a point source release. In homogenous regions, continuous gas channels form in a parabolic pattern from the release point. Stray gas is then expressed as either an aqueous expression after dissolution (red), or as a surface expression emitted to the atmosphere (grey arrows)..... 7
- Figure 1.4. Bernard plots with varying levels of complexity (a) Simplified Bernard diagram adapted from Cahill et al. (2018). Multicomponent mass transfer (added in the current study) is shown by the red arrow, and is a proposed mechanism that increases the hydrocarbon ratio due to multicomponent mass transfer. (b) More complex Bernard diagram used in hydrocarbon fingerprinting. Post genetic processes are shown with black arrows, which cause transition between zones. Differences in biogenic (or microbial) and thermogenic delineations between (a) and (b) highlight the empirical nature of gas fingerprinting using hydrocarbon composition and isotopic signature..... 11
- Figure 1.5. O₂ elution curves, with comparison between the experimental data (circles), kinetic theory (thick black line), local equilibrium assumption (thin black line) and a Sherwood correlation (dotted line) for two flow velocities (Geistlinger et al., 2005). 17
- Figure 2.1. Conceptual model for a natural gas leak in the subsurface (a) during active leak when gas pools below low permeability heterogeneities as it travels upwards and becomes trapped in the subsurface, an aqueous phase natural gas plume develops as groundwater dissolves the trapped gaseous phase, and gas is emitted as a surface flux, and (b) post-repair when dissolution continues, but trapped gas becomes disconnected and surface emission stops. Curved arrows indicate partitioning, as background gases partition into the gas phase, and natural gas partitions into the aqueous phase. At the left side of each diagram, the hashed line and grey fill represent a well casing and cement respectively..... 28
- Figure 2.2. Adapted Bernard diagram (Bernard et al., 1976; Cahill et al., 2018; Etiope et al., 2009; McIntosh et al., 2019; Whiticar, 1999). Change due to multicomponent mass transfer is shown by the red

arrow, and is a proposed mechanism of increases in hydrocarbon ratio due to competitive multicomponent mass transfer. Post genetic processes are shown by black arrows, which cause transition between zones. Delineations vary between studies due to the empirical nature of gas fingerprinting. 31

Figure 2.3. Diagram of experimental equipment used to conduct gas emplacement and dissolution experiments. Valves at tubing intersections allowed changes in water flow direction between the gas emplacement and dissolution phases of each experiment. Tubing in grey is 1/8" ID flexible PTFE tubing, and tubing in dashed yellow lines is 1/8" ID copper pipe used for gas transport. Images of lab equipment appear in Appendix D. 35

Figure 2.4. Measured (symbols) and simulated (lines) aqueous effluent concentrations for the (a) single-component (methane) and (b) multicomponent experiments. Experimental data points match the colours of the simulated data. Concentrations that are only simulated (no experimental data) are shown as dotted lines. Simulated average gas saturations throughout the column are shown as a dashed line. Asterix symbol plotted on right axis at 12 pore volumes is the mean experimental final gas saturation. Error bars indicate 95% confidence interval on the mean for both measured concentrations and final gas saturation based on four experiments. Data from individual experiments appears in Appendix A. 43

Figure 2.5. Mole fractions in the gas phase for the (a) single-component (methane) and (b) multicomponent simulations SC-Sim and MC-Sim. Mole fractions are those in the trapped gas adjacent to the column's effluent edge. Simulated average gas saturations throughout the column are shown as a dashed black line. 45

Figure 2.6. Simulated effluent concentrations (a, solid lines) and gas saturations (b, dashed lines) for methane dissolution for a range of background dissolved gas concentration from the SC-Sim simulations. 47

Figure 2.7. Pore volumes until extinction for a highly thermogenic multicomponent source and a source entirely composed of methane (MC-BG and SC-BG). Pore volumes until extinction ($S_g = 0$) is plotted on the y-axis in pore volumes for corresponding relative background gas concentrations (f). 48

Figure 2.8. Hydrocarbon ratio over the duration of the multicomponent experiments (symbols) and MC-Sim simulations (line). Ratios are calculated in terms of partial pressure. The source gas has a hydrocarbon ratio of 5.67. 51

Figure 2.9. Hydrocarbon ratio during natural gas dissolution predicted in the MC-Sources simulations. Each line represents a different initial hydrocarbon ratio ranging from 3 (highly thermogenic - 75% methane) to 1000 (biogenic - 99.9% methane). 53

Figure 3.1. Conceptual model of a gas leak from an energy well that travels up along the outside of the well from either the production formation or an intermediate non-target formation. Source gas is collected from the surface casing and groundwater samples are collected downgradient of the leak. 65

Figure 3.2. Analysis process for a dissolved gas sample beginning with a source gas partitioning to the aqueous phase. The dissolved gas is collected through aqueous sampling, and measured by headspace displacement. After the headspace gas is measured by GC analysis, mass balance calculations are used determine the dissolved gas composition. Through Henry’s Law equilibrium calculations, the initial composition is determined based on the dissolved gas composition. 68

Figure 3.3. Different compositional ratios for an initial source gas with a hydrocarbon ratio of 1000 (highlighted in red). Each line represents a different depth of sample to simulate higher hydrostatic pressure and thus higher gas solubility for a) 500 mL of sample collected, and b) 250 mL of sample collected. 72

Figure 3.4. Calculated compositional ratios for varying dilution factor. The initial source gas has a ratio of 1000, and the sampling collection depth is 30 m. 500 mL of sample is collected, and a minimum of 30 mL of headspace is needed for each sample, with helium added when exsolution alone does not produce enough gas. 76

Figure 3.5. Different compositional ratios from an initially biogenic source gas with atmospheric nitrogen added. 77

Figure 3.6. Different compositional ratios for an initial He/CH₄ ratio of 0.02. 500 mL of sample is collected, and a minimum of 30 mL of headspace is required. No additional helium is added to the system and as such a 0 m depth is neglected. 78

List of Tables

Table 2.1. Summary of column experiments	36
Table 2.2. Simulations	42
Table 2.3. Model Parameters	42
Table 2.4. Physicochemical properties of volatile compounds.....	42
Table 3.1. Scenarios for gas sampling and analysis calculations.....	71
Table 3.2. Henry's Law coefficients for volatile compounds.....	72

List of Abbreviations

AER	Alberta Energy Regulator
AMO	Aqueous molar
AMS	Aqueous mass
ASW	Air-saturated water
BCOGC	British Columbia Oil and Gas Commission
CCA	Council of Canadian Academies
DI	Deionized
EQG	Equivalent gas
FID	Flame-ionization detector
GB	Grey bromobutyl
GC	Gas chromatograph
HS	Headspace
LEA	Local equilibrium assumption
MC	Multicomponent
NAPL	Non-aqueous phase liquid
NEBC	National Energy Board of Canada
PTFE	Polytetrafluoroethylene
SC	Single-component
SCVF	Surface casing vent flow
SER	Saskatchewan Energy Regulation
SG	Source gas
STP	Standard temperature and pressure
US EIA	United States Energy Information Administration
US EPA	United States Environmental Protection Agency
VOA	Volatile Organic Compound

List of Symbols

Symbol	Parameter
α	Longitudinal dispersivity (L)
c	Aqueous phase solute concentration in bulk solution (ML^{-3})
C^g	Gaseous concentration (mol L^{-3})
C^T	Total concentration (mol L^{-3})
C^w	Aqueous concentration (mol L^{-3})
c^w	Aqueous concentration (ML^{-3})
c_s	Aqueous phase concentration of immiscible fluid (ML^{-3})
d	Column diameter (L)
d_{50}	Mean grain size (L)
D'	Depth (L)
D_g	Free diffusion coefficient in gas (L^2T^{-1})
D_w	Free diffusion coefficient in water (L^2T^{-1})
δ	Stagnant film thickness (L)
f	Fraction of total gas pressure (-)
F	Dilution factor (-)
H_i	Henry's constant ($\text{L}^2\text{T}^{-2}\text{mol}^{-1}$)
J	Mass flux ($\text{ML}^{-2}\text{T}^{-1}$)
k_l	Mass transfer coefficient (LT^{-1})
L	Column Length (L)
n^g	Moles in gas (mol)
n^w	Moles in water (mol)
θ	Porosity (-)
ρ	Density of water (ML^{-3})
P	Total gas pressure ($\text{ML}^{-1}\text{T}^{-2}$)
p	Partial pressure ($\text{ML}^{-1}\text{T}^{-2}$)
P_w	Water pressure ($\text{ML}^{-1}\text{T}^{-2}$)
Q	Darcy flux (LT^{-1})
R	Ideal Gas Constant ($\text{ML}^2\text{T}^{-2}\text{K}^{-1}\text{mol}^{-1}$)
S_g	Gas saturation (-)
T	Temperature (K)

v	Pore water velocity (LT^{-1})
V^w	Volume of water (L^3)
y	Mole fraction in gas (-)

Chapter 1

Introduction

1.1 Background

Advances in extraction technology for deep geological gas reserves has led to substantial increases in energy well development in both Canada and the United States (Cahill et al., 2019; CCA, 2014; US EPA, 2016). Natural gas is projected to surpass coal in global energy consumption by 2030 (US EIA, 2019). In the United States, tight shale resources will account for more than 90% of dry natural gas by 2050 (US EIA, 2020), while in Canada they will account for 80% of natural gas production by 2035 (NEBC, 2013). Increased development of the substantial North American shale deposits (Figure 1.1) has been met with public concern regarding environmental impacts including increased greenhouse gas emissions and degradation of surface water and groundwater resources (CCA, 2014; Kang et al., 2014; Rice et al., 2018; Vengosh et al., 2014). Of particular concern is the potential for releases of natural gas into the subsurface known as stray gas migration (Gorody, 2012; Jackson et al., 2013). Estimates of the prevalence of stray gas migration vary greatly, and attribution of methane detected in the subsurface to a source is particularly challenging due to the latent nature of contamination (Dusseault and Jackson, 2014). In Alberta, approximately 4.6% of all wells exhibit either surface casing vent flow (SCVF) or near-well gas migration, though due to the latent nature of leaks this may not encapsulate all leaky gas wells (Dusseault and Jackson, 2014). Other estimates for western Canada show 7-19% of production wells completed between 2005-2007 exhibit gas migration along the casing annulus (Roy et al., 2016), although it is estimated that <4.5% of unconventional wells exhibit natural gas leakage (McIntosh et al., 2019).



Figure 1.1. Map of North American shale deposits. The largest Canadian deposits are located in Alberta and British Columbia, with smaller deposits in other provinces and territories (US EIA via CCA, 2014).

Releases of natural gas, consisting primarily of methane, have the potential to impact water quality. While methane itself is not toxic, increased methane concentrations can negatively impact water chemistry. Water quality impacts may include increased pH and alkalinity, production of sulfides, changes to cation concentrations and liberation of metals (Kelly et al., 1985; Roy et al., 2016; Woda et al., 2018). There is also speculation that increased levels of higher-order hydrocarbons such as ethane and propane, both of which are present at low levels in natural gas, could potentially mobilize heavy-metals such as arsenic (Rice et al., 2018; Wolfe and Wilkin, 2017). Stray gas migration also presents explosive risks when gas concentrations are high enough to reach lower-explosive limits (Abboud et al., 2020; Gorody, 2012; Soeder, 2018). Site investigations for stray

gas migration remain challenging due to the complex behaviour of gases in the subsurface, and limited understanding of the mechanisms of gas releases (Soeder, 2018).

1.1.1 Well Design and Causes of Gas Migration

Shale gas wells traverse three zones: the shallow zone, the intermediate zone and the deep zone (Dusseault and Jackson, 2014; Vengosh et al., 2014). The shallow zone is defined by the presence of potable groundwater or brackish water usable in agriculture (Dusseault and Jackson, 2014). The intermediate zone exists between the shallow and deep zones, consisting of various strata and formation fluids which may contact the production or surface casing (Dusseault and Jackson, 2014). The deep zone contains the target formation, the zone affected by hydraulic fracturing and any formations that can be hydraulically connected to the fracturing zone (Dusseault and Jackson, 2014). Wells typically have a production casing, a surface casing, and intermediate casings depending on the depth of the well (Dusseault and Jackson, 2014; Watson and Bachu, 2009) (Figure 1.2). The conductor casing (not shown in Figure 1.2) is a short casing (10-15 m) outside of the surface casing used during drilling to prevent cave-in (Dusseault and Jackson, 2014; Nowamooz et al., 2015). Each steel casing is typically separated by cement, which may extend the length of the casing until the bottom of the casing, known as the casing shoe (BCOGC, 2020). Stray gas migration typically follows leakage pathways including those created by casing failure, poorly cemented casing annulus and abandonment failure (Watson and Bachu, 2009). Casing failure is typically the result of corrosion on the external wall of the casing, due to either poor cement jobs or lack of cement (Watson and Bachu, 2009). While casing failure is possible, it remains a rarer source of gas migration (Dusseault and Jackson, 2014; Hammond et al., 2020).

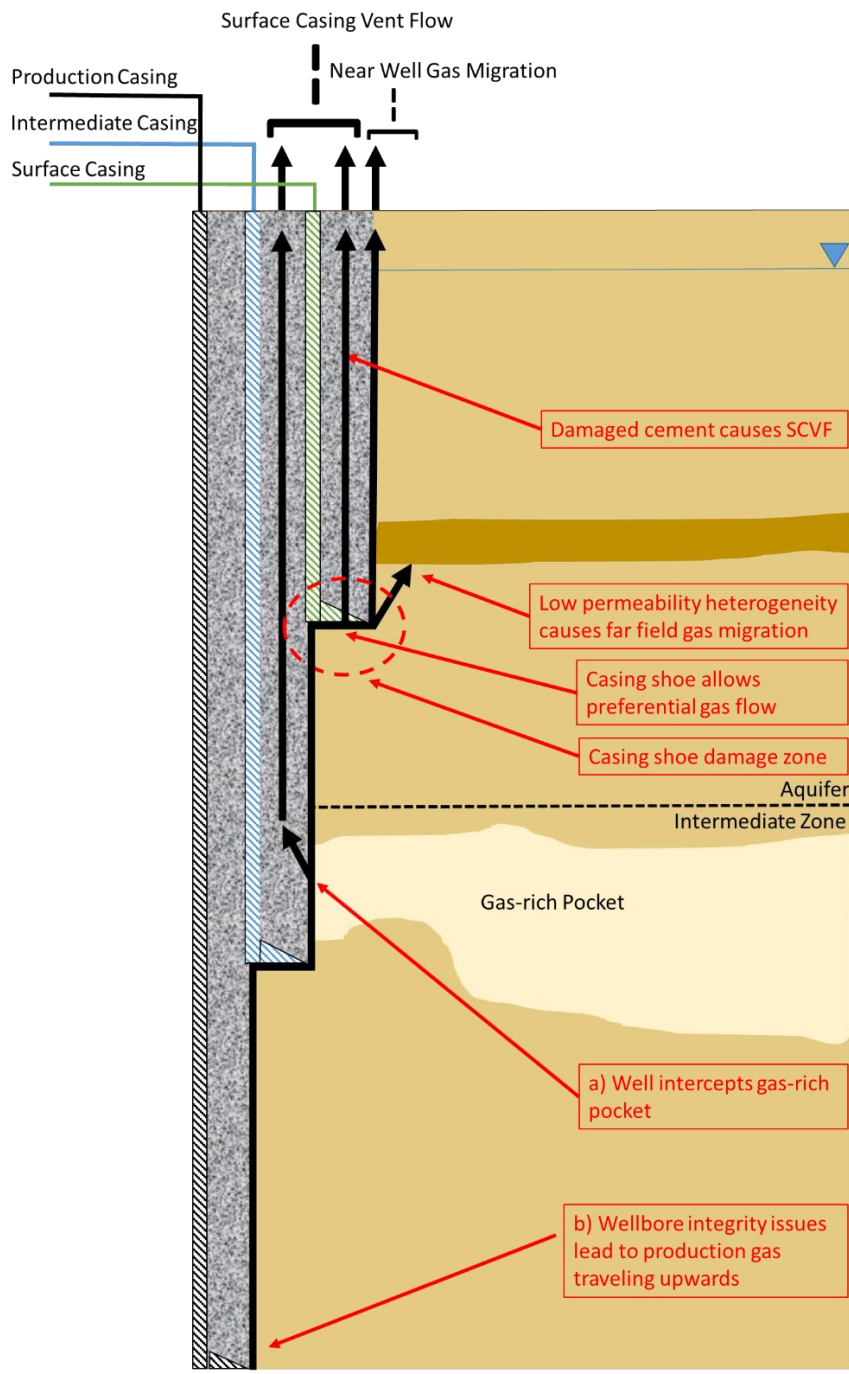


Figure 1.2. Conceptual sketch of potential gas sources and failure mechanisms leading to gas migration. Text labeled a) and b) indicate potential gas sources. Stray gas can travel through multiple different pathways (black lines) and be expressed at the well head as surface casing vent flow or near well gas migration, or gas may enter the aquifer leading to far field gas migration.

Pathways for gas migration through the casing annulus either exist between the outer casing and the cement sheath, or more commonly the cement sheath and the borehole rock wall, as the cement sheath becomes debonded from the borehole (Dusseault and Jackson, 2014; Watson and Bachu, 2009). The cement paste can shrink as it sets, reducing radial stress and allowing the formation of a gas column between the cement and the borehole rock (Bachu, 2017). Non-target gas deposits in the intermediate zone often acts as the source for gas migration, allowing gas to migrate from this zone up between the cement and the borehole rock (Dusseault and Jackson, 2014; Roy et al., 2016; Vengosh et al., 2014). Lastly, improper abandonment of wells is a significant source of gas migration, and in some regions (e.g., Alberta) accounts for the majority of gas migration when compared to suspended or active wells (Bachu, 2017; Watson and Bachu, 2009). Abandoned wells that exhibit gas migration are typically older wells, and may have been constructed prior to regulations for the proper abandonment of wells (Bachu, 2017; Kang et al., 2014). Moreover, the seals or plugs used to complete an abandoned well are also liable to fail such that leaks can occur as both atmospheric emissions and gas migration (Kang et al., 2014; Watson and Bachu, 2009). Regardless of the exact cause of a stray gas migration event, it has been shown that gas that leaks from wells can both emit to the atmosphere and migrate laterally to impact water sources (Figure 1.2) (Bachu, 2017; Forde et al., 2019; Gorody, 2012; Kang et al., 2014; Sherwood et al., 2016).

1.1.2 Gas Migration Dynamics

Early characterizations of the invasion of non-wetting fluids in porous media typically deemed NAPL and gases to be similar enough in both invasion and dissolution to be considered analogous (Geistlinger et al., 2005; Glass et al., 2001, 2000). The non-wetting fluid invades to create a structure of ‘pools’ and ‘fingers’ (Glass et al., 2000). Pools develop behind finer-grained (lower permeability, lower capillary entry pressure) heterogeneities, while fingers travel through the coarser materials, connecting pools (Glass et al., 2000). While the general invasion patterns are similar, gas and NAPL invasions have distinct behaviours due to differences in viscous forces, and

a greater density difference for gas-water systems than for NAPL-water systems (Geistlinger et al., 2005). Most notably, the invasion of gas tends to be led by the growth of a single finger rather than through multiple fingers as in NAPL systems (Glass et al., 2001, 2000; Glass and Yarrington, 2003). Importantly, these conclusions were drawn from systems with low gas injection rates ($1.7 \text{ m}^3/\text{day}$) at which discontinuous flow dominates (Glass et al., 2000). This is at the low end of surface casing vent flow rates, which typically range from $10^{-2} \text{ m}^3/\text{day}$ to $10 \text{ m}^3/\text{day}$, but can reach up to $5000 \text{ m}^3/\text{day}$ in severe cases (Nowamooz et al., 2015). As such, the influence of higher injection rates must be considered. The injection of gas in homogenous materials has been shown to fall within one of three flow regimes: discontinuous, transitional, and continuous (Geistlinger et al., 2006; Ji et al., 1993; Reddy and Adams, 2001; Selker et al., 2007; Van De Ven and Mumford, 2019). Discontinuous flow regimes show disconnected fingers of gas, periods of pressure variations resulting in fragmentation and mobilization of gas, and an asymmetric gas distribution (Geistlinger et al., 2006; Van De Ven and Mumford, 2019). Continuous flow regimes show continuous gas channels, and typically occur in a symmetric parabolic shape in homogenous material once steady state is reached (Geistlinger et al., 2006; Ji et al., 1993; Selker et al., 2007; Van De Ven and Mumford, 2019, 2018). Transitional flow regimes show characteristics of both discontinuous flow and continuous flow, with both fragmentation behaviour and continuous channel development (Geistlinger et al., 2006; Van De Ven and Mumford, 2019).

In heterogeneous systems with active stray gas leaks, it is expected that the source architecture will consist of a series of pools and parabolic-shaped gas patterns (Figure 1.3) (Van De Ven and Mumford, 2020a). Gas will migrate upwards in a parabolic pattern from a release point until it reaches a low permeability lens at which gas pooling occurs (Van De Ven and Mumford, 2020a). The gas then migrates laterally to the edge of the lens, at which point gas begins to migrate upwards in the same continuous parabolic pattern (Van De Ven and Mumford, 2020a). The result of this source architecture is significant lateral migration of stray gas due to small-scale heterogeneities

(Cahill et al., 2018, 2017; Forde et al., 2019; Klazinga et al., 2019; Llewellyn et al., 2015; Schout et al., 2020).

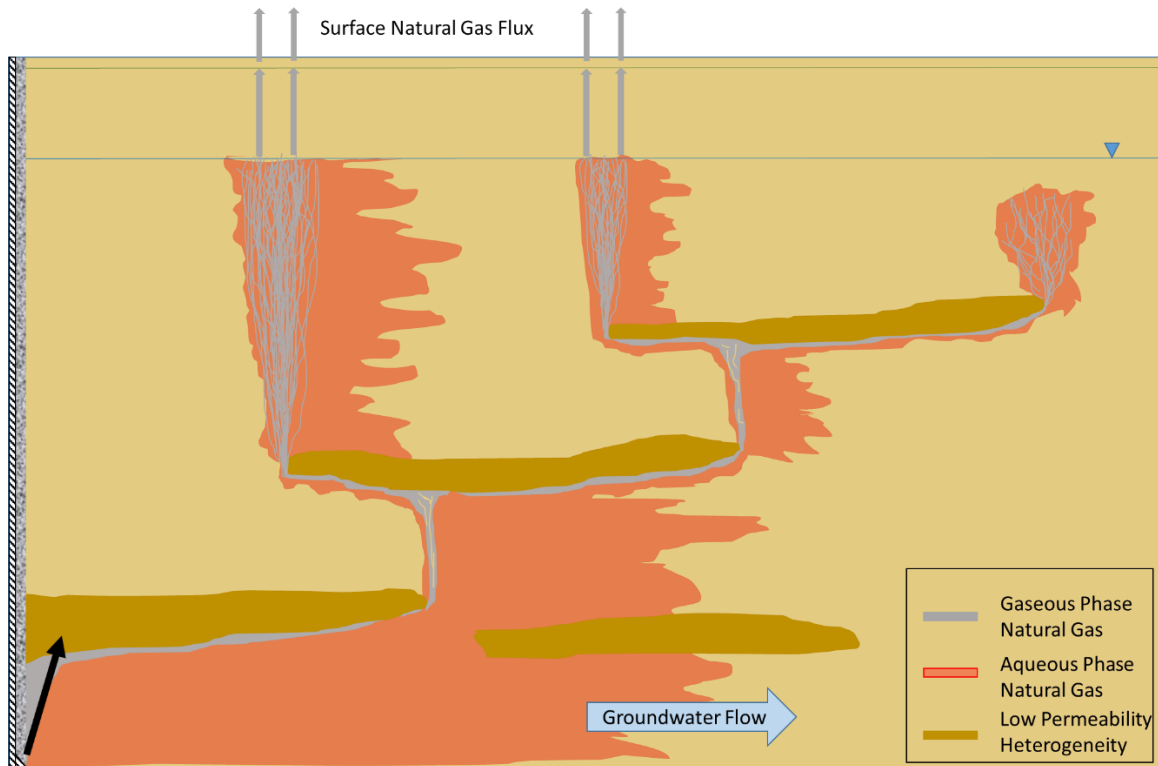


Figure 1.3. Conceptual sketch of stray gas migration in shallow aquifers. Gas pools under low permeability regions, and flows upwards at the edge of the low permeable region as a point source release. In homogenous regions, continuous gas channels form in a parabolic pattern from the release point. Stray gas is then expressed as either an aqueous expression after dissolution (red), or as a surface expression emitted to the atmosphere (grey arrows).

Furthermore, this leads to the development of dissolved concentration ‘hot spots’ both laterally and with depth, as gas saturations directly below a low-permeability layer will be high, while no gas may be detected above the same layer (Cahill et al., 2018). This presents challenges for site investigations as gas can travel well beyond the well pad and dissolved methane may not be detected unless multilevel sampling is conducted (Barth-Naftilan et al., 2018; McIntosh et al., 2019). When a leak is no longer active (post-repair) the continuous gas channels will ‘snap off’ due

to decreased gas pressure, and collapse to form discontinuous channels and ganglia (Geistlinger et al., 2005). This is referred to as a period of relaxation in which gas clusters can mobilize, increasing the number of ganglia (Van De Ven et al., 2020; Van De Ven and Mumford, 2020b). Following channel collapse and relaxation, the gas becomes trapped in the subsurface. Trapped gas in the subsurface has been shown to be highly persistent, leading to high concentrations of natural gas components in the subsurface long after a leak has stopped (Cahill et al., 2018; Klazinga et al., 2019).

Stray gas can be expressed as either a surface expression or an aqueous expression (Forde et al., 2019; Schout et al., 2020; Van De Ven and Mumford, 2020b). Surface expressions occur when gas pressures are sufficient for gas to reach the surface and emit to the atmosphere (Forde et al., 2019). Typically, surface expressions are detected either as methane efflux through shallow gas surveys, or by visual observations of distressed vegetation or bubbling at a wellhead (BCOGC, 2020; Forde et al., 2019). Methane efflux can occur beyond the well pad, and be highly variable both spatially and temporally (Forde et al., 2019). Heterogeneities in the subsurface can lead to substantial horizontal migration of gas such that methane efflux may not occur, or may be undetected as it extends beyond the vicinity of the well (Cahill et al., 2017; Forde et al., 2019). The vertical gas flow must also be substantial compared to horizontal groundwater flow, as dissolution of gases can arrest a plume and prevent gas from reaching the surface (Van De Ven and Mumford, 2020b). Aqueous expression refers to stray gas which dissolves in groundwater, as natural gas partitions into the aqueous phase, and dissolved gases partition into the gaseous phase (Van De Ven and Mumford, 2020a). During an active leak, both surface and aqueous expressions occur (Cahill et al., 2017; Van De Ven and Mumford, 2020a). Concentrations of methane will increase as gas migrates through the subsurface, until a steady state is reached at which the source architecture remains steady and only small variations of dissolved gas concentrations occur (Van De Ven and Mumford, 2020a). Post-repair, after relaxation of the source architecture, stray gas is only expressed in the

aqueous phase (Van De Ven and Mumford, 2020a). While the gas is no longer replenished, the trapped gas continues to dissolve into the aqueous phase. Conversely, dissolved background gases will partition into the gaseous phase, maintaining the source architecture despite a decreasing volume of natural gas (Van De Ven and Mumford, 2020a). In field settings, this relaxation and dissolution has resulted in higher dissolved methane concentrations after a leak has been stopped, indicating increased mass transfer post-repair (Cahill et al., 2018; Van De Ven and Mumford, 2020a). These high concentrations of hydrocarbons are persistent, and can take years to attenuate (Cahill et al., 2018; Roy et al., 2016).

1.1.3 Leak detection

The complexities of stray gas site monitoring coupled with the potential for both surface and aqueous expression has led to varying approaches for the regulation of stray gas migration sites. The majority of oil and gas operations in Canada occur in Alberta (Alberta Energy Regulator, AER), British Columbia (BC Oil and Gas Commission, BCOGC) and Saskatchewan (Saskatchewan Energy Regulation, SER). While drilling has also occurred in Quebec, New Brunswick and Nova Scotia, these provinces have implemented moratoriums on shale gas development, preventing further hydraulic fracturing operations (Becklumb et al., 2015). Regulations for the identification of stray gas migration from AER, BCOGC and SER all center on the use of shallow gas surveys to detect surface efflux, identification of stressed vegetation, high surface casing vent flows (i.e., greater than 300 m³/day as defined by AER) or bubbling at a wellhead (Alberta Energy Regulator, 2018; BCOGC, 2020; Government of Saskatchewan, 2015). Shallow gas surveys are typically conducted in a circular pattern around the wellbore 1-2 m apart (BCOGC, 2020; Government of Saskatchewan, 2018). Aqueous sampling is also used to identify impacts on groundwater resources typically as a result of high methane concentrations detected in a water supply well, though there is no concentration threshold at which this occurs (BCOGC, 2020). In the United States, dissolved methane concentrations are often used as action level

indicators, and concentrations greater than 10 mg/L are considered high enough to report, though this threshold varies between states (Mathes and White, 2006). When elevated concentrations of methane are detected in a water supply well, the gas fingerprinting process begins.

1.1.4 Source Identification

Debate often surrounds the origins of methane in shallow aquifers as it can occur from both natural and anthropogenic sources (Nicot et al., 2017). Natural sources of methane in shallow aquifers are typically the result of bacterial and environmental factors and the methane is commonly classified as biogenic. Anthropogenic sources in shallow aquifers are releases of methane because of human activities such as natural gas extraction. As such, anthropogenic methane is generally classified as thermogenic, as it originates from deep in the subsurface as a result of high temperature and pressure. The distinction between biogenic and thermogenic methane is used to distinguish naturally occurring methane from anthropogenically-released methane. Baldassare et al. (2014) describes a standard process for gas fingerprinting consisting of five steps: 1. Define and characterize the stray gas at the receptor (manner of manifestation, concentration, and gas and groundwater geochemistry), 2. Identify the potential source(s) of the stray gas, 3. Define the molecular and isotopic characteristics that distinguish the potential gas sources, 4. Evaluate stray gas geochemistry for potential secondary effects, and 5. Identify the best match between the stray gas and potential source(s).

Crucial to this process is the molecular and isotopic characterization of both the stray gas at the receptor and from potential sources. Most commonly, gas fingerprints consist of the hydrocarbon composition of the gas and stable carbon isotopic signature for methane (Baldassare et al., 2014; Gorody, 2012; Molofsky et al., 2016) Thermogenic gas is often identified by a $C1/(C2+C3)$ ratio of 100 or lower, and a stable carbon isotopic signature less than $-50\text{‰ } \delta C13-CH_4$ (where C1, C2 and C3 represent methane, ethane and propane, respectively). Biogenic gas is identified by a $C1/(C2+C3)$ ratio of 1000 or higher, and a stable carbon isotopic signature greater than $-50\text{‰ } \delta C13-$

CH₄. The values that define thermogenic and biogenic signatures are empirical, and often vary between studies (Cahill et al., 2018; Etiope et al., 2009; McIntosh et al., 2019; Molofsky et al., 2016). Gas fingerprints are typically plotted on ‘Bernard’ plots (Bernard et al., 1978), which can vary between studies (Figure 1.4).

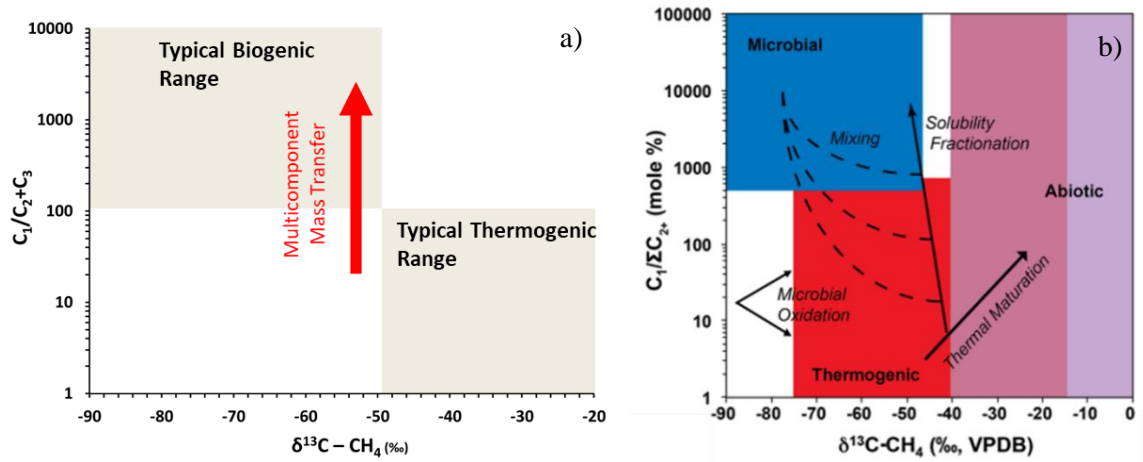


Figure 1.4. Bernard plots with varying levels of complexity (a) Simplified Bernard diagram adapted from Cahill et al. (2018). Multicomponent mass transfer (added in the current study) is shown by the red arrow, and is a proposed mechanism that increases the hydrocarbon ratio due to multicomponent mass transfer. (b) More complex Bernard diagram used in hydrocarbon fingerprinting. Post genetic processes are shown with black arrows, which cause transition between zones. Differences in biogenic (or microbial) and thermogenic delineations between (a) and (b) highlight the empirical nature of gas fingerprinting using hydrocarbon composition and isotopic signature.

Gas fingerprinting is not limited to the hydrocarbon composition and carbon isotopic signature of methane, and other tracers are increasingly used as additional lines of evidence. The non-reactive nature of noble gases make them suitable as both a compositional and isotopic tracer (Darrah et al., 2014). ²⁰Ne and ³⁶Ar are typically markers of air-saturated water, and are not subject to microbial degradation. When paired with ⁴He and ⁴⁰Ar, and hydrocarbon compositions and isotopic signatures, the origins of gas in the subsurface can be determined (Darrah et al., 2014). Deuterium

($\delta\text{D-CH}_4$) isotopes of methane can also be used as an indicator of gas origin (Humez et al., 2019). The abundance of nitrogen in natural gas reservoirs has also led to uses of dissolved nitrogen as a potential natural gas tracer (Larson et al., 2018). A distinct nitrogen $\delta^{15}\text{N-N}_2$ signature coupled with low nitrogen concentrations in stray gas relative to air-saturated water allows for the use of nitrogen as an additional tracer when coupled with hydrocarbon data (Larson et al., 2018). These techniques remain relatively uncommon, due to the complexities of analysis, but will likely increase in application as sampling procedures improve and analytical costs decrease (McIntosh et al., 2019).

Hydrocarbon composition and isotopic signature for gas sources are typically based on the analysis of a gas sample. However, for stray gas receptors they are typically based on the analysis of an aqueous sample. Baseline characterization of groundwater geochemistry in the region near a wellhead provides additional insight to the impacts of natural gas (Baldassare et al., 2014; Gorody, 2012; Humez et al., 2019). Unfortunately, gas migration sites often lack baseline sampling data and timelines for gas releases (Brantley et al., 2014). Attempts to create large-scale baseline data available for stray gas investigations have largely been unsuccessful due to inconsistencies in measurements between agencies and a lack of baseline sampling regulations and standard procedures (Soeder, 2018).

Once analyses of gaseous and aqueous samples are complete, secondary effects (post-genetic processes) must be considered for accurate source identification (Baldassare et al., 2014). Both the hydrocarbon composition and isotopic signature can vary as a result of multiple processes. Microbial oxidation of methane (aerobic and anaerobic) can lead to a decrease in hydrocarbon ratio as a result of the consumption of methane (Whiticar, 1999). Microbial oxidation will also lead to increases in $\delta^{13}\text{C-CH}_4$ as the result of preferential consumption of $\text{C}^{13}\text{-CH}_4$ by microorganisms (Etiopie et al., 2009; Whiticar, 1999; Wolfe and Wilkin, 2017). The solubilities of methane, ethane and propane are all different, and vary as a function of temperature and pressure (Humez et al.,

2019). As gases migrate upwards, hydrocarbons will exsolve at different rates, leading to changes in hydrocarbon ratios (Humez et al., 2019). This process is coupled with different adsorption properties of hydrocarbons and the preferential dissolution of higher solubility hydrocarbons, and is known generally as solubility fractionation (Figure 1.4) (Cahill et al., 2018; Etiope et al., 2009; McIntosh et al., 2019). This process is still not well understood and requires further research (Cahill et al., 2018; Etiope et al., 2009). There is also evidence of isotopic fractionation by diffusion causing depletion of C13-CH₄ (Etiope et al., 2009; Pape et al., 2010). This process is generally limited to migration between reservoirs rather than during stray gas migration, so while it is unlikely to impact aqueous samples, it can still impact the initial source gas composition (Etiope et al., 2009; Prinzhofer and Pernaton, 1997). Mixing is also commonly represented in gas fingerprinting, as the mixing of both thermogenic and biogenic gas sources results in a gas fingerprint which falls along a mixing line between thermogenic and biogenic (Harkness et al., 2017). All of these processes must be considered when applying fingerprinting techniques in any hydrogeological setting (McIntosh et al., 2019). However, these post-genetic processes are limited to changes that may occur either before a leak or during an active leak, and do not consider changes that may occur after a leak has been stopped.

1.1.5 Mass Transfer

As is the case with gas migration dynamics, studies of mass transfer in the context of trapped NAPL has informed the understanding of mass transfer of trapped gases. Early work on mass transfer kinetics focused on mass-flux through a thin, stagnant boundary layer of fluid surrounding a solid particle, a model credited to Nernst (Miller et al., 1990). The general mass flux equation is related to the stagnant film model as:

$$J = k_l(c_s - c) = \frac{D_w}{\delta}(c_s - c) \quad (1.1)$$

where J is mass flux, k_l is the mass transfer coefficient, c_s is the aqueous phase concentration of the immiscible fluid, c is the aqueous phase solute concentration in bulk solution, D_w is the free diffusion coefficient in water and δ is the stagnant film thickness (Miller et al., 1990). While functional as a conceptual model for mass transfer, the value of δ has been found to be a function of D_w , and thus the usefulness as a model for mass transfer in multiphase systems is limited (Miller et al., 1990). Therefore, empirical mass transfer coefficients are derived, often based on the dimensionless Sherwood number, as a function of the flow regime and the molecular diffusion of NAPL components (Miller et al., 1990; Sale and McWhorter, 2001). The mass transfer of NAPL has been shown to be sensitive to its configuration in the subsurface, with higher dissolution rates in fingers than in pools due to a greater interfacial area (Sale and McWhorter, 2001). Challenges associated with identifying the source architecture motivated the use of upscaled mass transfer coefficients, which can average the mass transfer over a domain (Christ et al., 2010, 2006). However, while this conceptual model can be applied to both trapped NAPL and trapped gas, differences in the properties of these fluids leads to differences in their multicomponent mass transfer (Geistlinger et al., 2005).

As an example of mass transfer, partitioning tracer tests have been successfully applied to quantify NAPL saturations (Cirpka and Kitanidis, 2001). The partitioning tracer will move into and out of the NAPL phase, leading to its delayed arrival relative to a non-partitioning tracer, and the period of lag is a function of NAPL saturation (Jin et al., 1995). As an extension of this principle, the effects of trapped gas presence in the subsurface on the transport of dissolved gases were first studied to determine whether dissolved gases could be reasonably used as tracers of groundwater flow (Donaldson et al., 1998, 1997; Fry et al., 1995). Fry et al. (1995) demonstrated through a series of column experiments that the partitioning of dissolved gases from the aqueous to the gaseous phase led to the retardation of dissolved gas as a function of trapped gas saturation. Donaldson et al. (1997, 1998) expanded upon this principle and proposed a kinetic model, which was able to

accurately describe the breakthrough and elution of oxygen. However, notably, the volume of trapped gas varied greatly in experiments when using helium, in some cases changing by 50% (Donaldson et al., 1997). Both Fry et al. (1995) and Donaldson et al. (1997) considered trapped gas saturations to be constant, and thus were not able to capture changes in gas volume as a result of gas partitioning.

Noting the lack of gas saturation changes in the Donaldson et al. (1997) model, Cirpka and Kitanidis (2001) developed a model to analyze the transport of volatile compounds in porous media using multicomponent multiphase mass transfer theory, while neglecting dispersive transport and mass transfer kinetics. The use of multicomponent equations is important, as the partitioning behaviour of one component will be impacted by the presence of other components, such that mass transfer can be considered to be ‘competitive’ (Cirpka and Kitanidis, 2001). Additionally, the gas saturation depends on the total mass of volatile compounds, such that changing the concentration of a compound will change the gas saturation, and thus the retardation factor of the competing components (Cirpka and Kitanidis, 2001). This is particularly applicable when using volatile tracers, as the assumption of a constant gas saturation is no longer valid as the tracer approaches its solubility (Cirpka and Kitanidis, 2001).

The Cirpka and Kitanidis (2001) model demonstrated that gas dissolution can produce non-monotonic behaviour, such that concentrations and gas saturations may increase or decrease with time. The presence of multiple components in both the trapped gas and the background gas will influence the dissolution behaviour of each component (Cirpka and Kitanidis, 2001). This set of equations has been applied in several instances including the mobilization and expansion of gases above DNAPL pools (Mumford et al., 2010), gas bubble formation from methanogenic aquifers (Amos and Ulrich Mayer, 2006) and the volatilization of crude oil spills (Molins et al., 2010).

This set of equations is limited in its application due to the assumption of local equilibrium. The local equilibrium assumption (LEA) is commonly applied in mass transfer dynamics in porous media as a simplification for long periods of contact time (15 mins or more) (Miller et al., 1990). The LEA treats mass transfer (or sorption or reactions) as “fast enough” with respect to the bulk flow rate, such that it is in a state of local chemical equilibrium and kinetics at the microscopic level can be neglected (Valocchi, 1985). As the description of microscopic kinetics can be neglected, the mathematical relationships are significantly simplified, though this assumption must be used under the proper conditions so as to not mischaracterize the mass transfer impacts. The LEA is an effective modeling tool used in many studies because of its ability to accurately describe mass transfer with high computational efficiency (Cirpka and Kitanidis, 2001; Miller et al., 1990).

Holocher et al. (2003) extended this approach and outlined a set of equations to describe the kinetic multicomponent dissolution of trapped gases with variable volume to predict the composition of excess air in the subsurface. This model was expanded upon by Geistlinger et al. (2005) to consider the effective gas-water interface as the bubble expands and contracts as a function of volumetric gas content. This kinetic model was validated against oxygen elution curves and compared to local equilibrium models. Figure 1.5 shows low flow (pore water velocity = 4 m/d) and high flow (pore water velocity = 17 m/d) regimes, to illustrate the discrepancies between the LEA and kinetic models at varying velocities. While the local equilibrium model does not precisely describe the elution of O₂ by Geistlinger et al (2005), it does correctly predict the dissolution process, predicting the changing gas volume and the correct partial pressures, and as such is still useful to characterize dissolution processes, particularly at low velocities (Geistlinger et al., 2005). This is important as it is rare in groundwater systems to encounter velocities as fast as those in the experimental range of Geistlinger et al. (2005) and thus LEA is useful in the context of shallow aquifer contamination.

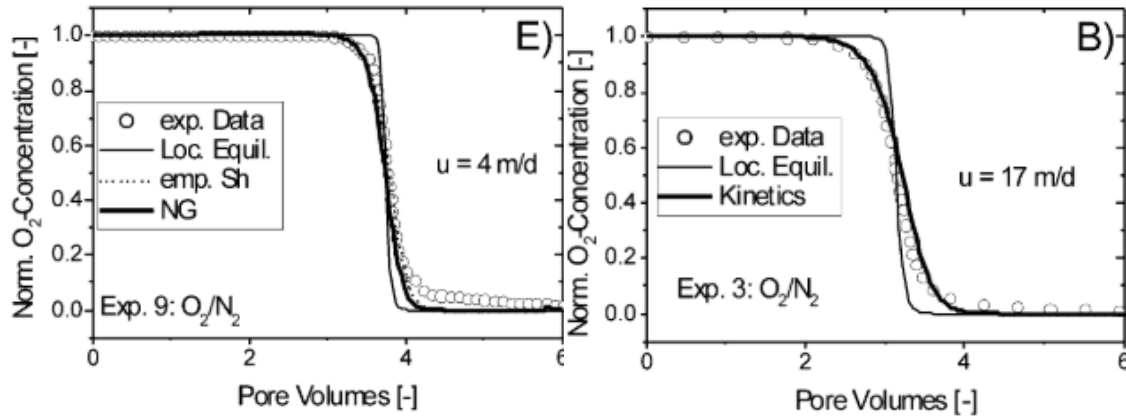


Figure 1.5. O₂ elution curves, with comparison between the experimental data (circles), kinetic theory (thick black line), local equilibrium assumption (thin black line) and a Sherwood correlation (dotted line) for two flow velocities (Geistlinger et al., 2005).

1.2 Research Need

Increased development of natural gas reserves presents potential for increased incidents of stray gas migration. To understand the impacts of these releases we must understand the processes that control the dissolution and persistence of stray gas. Furthermore, when concerns of stray gas migration are raised it is important to identify the gas source with confidence. As such, the processes that control gas dissolution in the subsurface must be well understood to properly monitor, regulate, and remediate stray gas migration incidents. It is expected that multicomponent mass transfer will be important in this understanding because of the mixture of components present in natural gas, as well as the other dissolved gases present in the groundwater.

1.3 Research Objectives

The goal of this research was to investigate the effects of multicomponent mass transfer on the dissolution and persistence of stray gas in the subsurface to improve gas migration investigation techniques. This goal was achieved using both bench-scale laboratory experiments and numerical modeling simulations to determine the key factors that affect natural gas dissolution, the dissolved concentrations of natural gas components, and their impacts on source identification techniques.

The specific research objectives were to:

- Understand the dissolution of single- and multicomponent source trapped gases in porous media. This objective was addressed using bench-scale column experiments in which gas was trapped in sand and dissolved, and dissolved gas concentrations were monitored over time (Chapter 2). The experiments were then simulated using the reactive transport code MIN3P (Chapter 2).
- Understand the impacts of background gases on the persistence and dissolution of trapped natural gas. This objective was addressed primarily by numerical modeling of the dissolution of methane subject to varying background gas concentrations, and investigating changes in dissolved gas concentrations and gas saturations over time (Chapter 2).
- Identify factors affecting the use of hydrocarbon ratios for source identification. This objective was addressed with bench-scale experiments, numerical modeling (Chapter 2) and partitioning calculations (Chapter 3) to identify both physical processes (Chapter 2) and differences in interpretation (Chapter 3) that can impact the use of hydrocarbon ratios in practice.

Ultimately this research aims to improve the conceptual model of stray gas migration such that the impacts of gas migration on the environment can be better understood, and the tools to identify gas migration incidents can be improved.

1.4 Thesis Organization

The following thesis has been organized in a manuscript format. The results chapters (Chapters 2 and 3) have been prepared with the intent for submission to peer-reviewed academic journals. Each chapter includes a separate Introduction section such that the objectives and results are supported

by previous literature. Chapter 2 presents laboratory experiments and numerical simulations of the dissolution of natural gas in porous media. Chapter 3 presents the calculation of hydrocarbon ratios for the purpose of source identification. Chapter 4 presents overall conclusions and recommendations for applications of the work and further research. The appendix includes additional laboratory results and model simulations. Due to the nature of the manuscript format, some material from the introduction in Chapter 1 will overlap with the introduction sections in Chapter 2 and Chapter 3.

1.5 References

- Abboud, J.M., Watson, T.L., Ryan, M.C., 2020. Fugitive methane gas migration around Alberta's petroleum wells. *Greenh. Gases Sci. Technol.* 15, 1–15. <https://doi.org/10.1002/ghg.2029>
- Alberta Energy Regulator, 2018. Directive 020 - Well Abandonment.
- Amos, R.T., Ulrich Mayer, K., 2006. Investigating the role of gas bubble formation and entrapment in contaminated aquifers: Reactive transport modelling. *J. Contam. Hydrol.* 87, 123-154. <https://doi.org/10.1016/j.jconhyd.2006.04.008>
- Bachu, S., 2017. GHG perspective – Gas migration outside well casing. *Int. J. Greenh. Gas Control* 61, 146–154. <https://doi.org/10.1016/j.ijggc.2017.04.003>
- Baldassare, F.J., McCaffrey, M.A., Harper, J.A., 2014. A geochemical context for stray gas investigations in the northern Appalachian Basin: Implications of analyses of natural gases from Neogene-through Devonian-age strata. *Am. Assoc. Pet. Geol. Bull.* 98, 341–372. <https://doi.org/10.1306/06111312178>
- Barth-Naftilan, E., Sohng, J., Saiers, J.E., 2018. Methane in groundwater before, during, and after hydraulic fracturing of the Marcellus Shale. *Proc. Natl. Acad. Sci. U. S. A.* 115, 6970–6975. <https://doi.org/10.1073/pnas.1720898115>
- BC Oil and Gas Commission, 2020. Oil and Gas Activity Operations Manual - December 2020. <https://www.bcogc.ca/files/operations-documentation/Oil-and-Gas-Operations-Manual/oil-and-gas-activity-operations-manual.pdf>
- Becklumb, P., Chong, J., Williams, T., 2015. Shale Gas in Canada: Environmental Risks and Regulation. Parliament of Canada, Library of Parliament, No. 2015-18-E.
- Bernard, B.B., Brooks, J.M., Sackett, W.M., 1978. Light Hydrocarbons in Recent Texas Continental Shelf and Slope Sediments. *J. Geophys. Res.* 83, 4053–4061. <https://doi.org/10.1029/JC083iC08p04053>

- Brantley, S.L., Yoxtheimer, D., Arjmand, S., Grieve, P., Vidic, R., Pollak, J., Llewellyn, G.T., Abad, J., Simon, C., 2014. Water resource impacts during unconventional shale gas development: The Pennsylvania experience. *Int. J. Coal Geol.* 126, 140–156. <https://doi.org/10.1016/j.coal.2013.12.017>
- Cahill, A.G., Beckie, R., Ladd, B., Sandl, E., Goetz, M., Chao, J., Soares, J., Manning, C., Chopra, C., Finke, N., Hawthorne, I., Black, A., Ulrich Mayer, K., Crowe, S., Cary, T., Lauer, R., Mayer, B., Allen, A., Kirste, D., Welch, L., 2019. Advancing knowledge of gas migration and fugitive gas from energy wells in northeast British Columbia, Canada. *Greenh. Gases Sci. Technol.* 9, 134–151. <https://doi.org/10.1002/ghg.1856>
- Cahill, A.G., Parker, B.L., Mayer, B., Mayer, K.U., Cherry, J.A., 2018. High resolution spatial and temporal evolution of dissolved gases in groundwater during a controlled natural gas release experiment. *Sci. Total Environ.* 622-623, 1178-1192. <https://doi.org/10.1016/j.scitotenv.2017.12.049>
- Cahill, A.G., Steelman, C.M., Forde, O., Kuloyo, O., Emil Ruff, S., Mayer, B., Ulrich Mayer, K., Strous, M., Cathryn Ryan, M., Cherry, J.A., Parker, B.L., 2017. Mobility and persistence of methane in groundwater in a controlled-release field experiment. *Nat. Geosci.* 10, 289-293. <https://doi.org/10.1038/ngeo2919>
- Christ, J.A., Ramsburg, C.A., Pennell, K.D., Abriola, L.M., 2010. Predicting DNAPL mass discharge from pool-dominated source zones. *J. Contam. Hydrol.* 114, 18–34. <https://doi.org/10.1016/j.jconhyd.2010.02.005>
- Christ, J.A., Ramsburg, C.A., Pennell, K.D., Abriola, L.M., 2006. Estimating mass discharge from dense nonaqueous phase liquid source zones using upscaled mass transfer coefficients: An evaluation using multiphase numerical simulations. *Water Resour. Res.* 42, 1–13. <https://doi.org/10.1029/2006WR004886>
- Cirpka, O.A., Kitanidis, P.K., 2001. Transport of volatile compounds in porous media in the presence of a trapped gas phase. *J. Contam. Hydrol.* 49, 263-285. [https://doi.org/10.1016/S0169-7722\(00\)00196-0](https://doi.org/10.1016/S0169-7722(00)00196-0)
- Council of Canadian Academies, 2014. Environmental Impacts of Shale Gas Extraction in Canada. Ottawa. <https://cca-reports.ca/reports/environmental-impacts-of-shale-gas-extraction-in-canada/>
- Darrah, T.H., Vengosh, A., Jackson, R.B., Warner, N.R., Poreda, R.J., 2014. Noble gases identify the mechanisms of fugitive gas contamination in drinking-water wells overlying the Marcellus and Barnett Shales. *Proc Natl Acad Sci U S A* 111, 14076–14081. <https://doi.org/10.1073/pnas.1322107111>
- Donaldson, J.H., Istok, J.D., Humphrey, M.D., O'Reilly, K.T., Hawelka, C.A., Mohr, D.H., 1997. Development and Testing of a Kinetic Model for Oxygen Transport in Porous Media in the Presence of Trapped Gas. *Ground Water.* 35, 270-279. <https://doi.org/10.1111/j.1745-6584.1997.tb00084.x>

- Donaldson, J.H., Istok, J.D., O'Reilly, K.T., 1998. Dissolved gas transport in the presence of a trapped gas phase: Experimental evaluation of a two-dimensional kinetic model. *Ground Water* 36, 133–142. <https://doi.org/10.1111/j.1745-6584.1998.tb01073.x>
- Dusseault, M., Jackson, R., 2014. Seepage pathway assessment for natural gas to shallow groundwater during well stimulation, in production, and after abandonment. *Environ. Geosci.* 21, 107–126. <https://doi.org/10.1306/eg.04231414004>
- Etiopie, G., Feyzullayev, A., Milkov, A. V., Waseda, A., Mizobe, K., Sun, C.H., 2009. Evidence of subsurface anaerobic biodegradation of hydrocarbons and potential secondary methanogenesis in terrestrial mud volcanoes. *Mar. Pet. Geol.* 26, 1692–1703. <https://doi.org/10.1016/j.marpetgeo.2008.12.002>
- Forde, O.N., Mayer, K.U., Hunkeler, D., 2019. Identification, spatial extent and distribution of fugitive gas migration on the well pad scale. *Sci. Total Environ.* 652, 356–366. <https://doi.org/10.1016/j.scitotenv.2018.10.217>
- Fry, V.A., Istok, J.D., Semprini, L., O'Reilly, K.T., Buscheck, T.E., 1995. Retardation of Dissolved Oxygen Due to a Trapped Gas Phase in Porous Media. *Groundwater* 33, 391–398. <https://doi.org/10.1111/j.1745-6584.1995.tb00295.x>
- Geistlinger, H., Beckmann, A., Lazik, D., 2005. Mass transfer between a multicomponent trapped gas phase and a mobile water phase: Experiment and theory. *Water Resour. Res.* 41, 1–15. <https://doi.org/10.1029/2004WR003885>
- Geistlinger, H., Krauss, G., Lazik, D., Luckner, L., 2006. Direct gas injection into saturated glass beads: Transition from incoherent to coherent gas flow pattern. *Water Resour. Res.* 42, 1–12. <https://doi.org/10.1029/2005WR004451>
- Glass, R.J., Conrad, S.H., Peplinski, W., 2000. Gravity-destabilized nonwetting phase invasion in macroheterogeneous porous media: Experimental observations of invasion dynamics and scale analysis. *Water Resour. Res.* 36, 3121–3137. <https://doi.org/10.1029/2000WR900152>
- Glass, R.J., Conrad, S.H., Yarrington, L., 2001. Gravity-destabilized nonwetting phase invasion in macroheterogeneous porous media: Near-pore-scale macro modified invasion percolation simulation of experiments. *Water Resour. Res.* 37, 1197–1207. <https://doi.org/10.1029/2000WR900294>
- Glass, R.J., Yarrington, L., 2003. Mechanistic modeling of fingering, nonmonotonicity, fragmentation, and pulsation within gravity/buoyant destabilized two-phase/unsaturated flow. *Water Resour. Res.* 39, 1058. <https://doi.org/10.1029/2002wr001542>
- Gorody, A.W., 2012. Factors affecting the variability of stray gas concentration and composition in groundwater. *Environ. Geosci.* 19, 17–31. <https://doi.org/10.1306/eg.12081111013>
- Government of Saskatchewan, 2018. Gas migration and surface casing vent flow (SCVF) issues and prevention. <https://www.saskatchewan.ca/business/agriculture-natural-resources-and->

industry/oil-and-gas/environmental-protection/gas-migration-and-surface-casing-vent-flow-reporting

- Government of Saskatchewan, 2015. Gas Migration - Guideline PNG026. <https://publications.saskatchewan.ca/api/v1/products/75531/formats/84462/download>
- Hammond, P.A., Wen, T., Brantley, S.L., Engelder, T., 2020. Gas well integrity and methane migration: evaluation of published evidence during shale-gas development in the USA. *Hydrogeol. J.* 28, 1481–1502. <https://doi.org/10.1007/s10040-020-02116-y>
- Harkness, J.S., Darrah, T.H., Warner, N.R., Whyte, C.J., Moore, M.T., Millot, R., Kloppmann, W., Jackson, R.B., Vengosh, A., 2017. The geochemistry of naturally occurring methane and saline groundwater in an area of unconventional shale gas development. *Geochim. Cosmochim. Acta* 208, 302–334. <https://doi.org/10.1016/j.gca.2017.03.039>
- Holocher, J., Peeters, F., Aeschbach-Hertig, W., Kinzelbach, W., Kipfer, R., 2003. Kinetic model of gas bubble dissolution in groundwater and its implications for the dissolved gas composition. *Environ. Sci. Technol.* 37, 1337–1343. <https://doi.org/10.1021/es025712z>
- Humez, P., Osselin, F., Wilson, L.J., Nightingale, M., Kloppmann, W., Mayer, B., 2019. A Probabilistic Approach for Predicting Methane Occurrence in Groundwater. *Environ. Sci. Technol.* 53, 12914–12922. <https://doi.org/10.1021/acs.est.9b03981>
- Jackson, R.B., Vengosh, A., Darrah, T.H., Warner, N.R., Down, A., Poreda, R.J., Oshborn, S.G., Zhao, K., Karr, J.D., 2013. Increased stray gas abundance in a subset of drkng water wells. *Proc. Natl. Acad. Sci. U. S. A.* 110, 11250–11255. <https://doi.org/10.1073/pnas.1221635110>
- Ji, W., Dahmani, A., Ahlfeld, D.P., Lin, J.D., Hill, E., 1993. Laboratory Study of Air Sparging: Air Flow Visualization. *Ground Water Monit. Remediat.* 13, 115–126. <https://doi.org/10.1111/j.1745-6592.1993.tb00455.x>
- Jin, M., Delshad, M., Varadarajan, D., McKinney, D.C., Pope, G.A., Sepehrnoori, K., Tilburg, C.E., 1995. Partitioning tracer test for detection, estimation, and remediation performance assessment of subsurface nonaqueous phase liquids. *Water Resour. Res.* 31, 1201–1211.
- Kang, M., Kanno, C.M., Reid, M.C., Zhang, X., Mauzerall, D.L., Celia, M.A., Chen, Y., Onstott, T.C., 2014. Direct measurements of methane emissions from abandoned oil and gas wells in Pennsylvania. *Proc. Natl. Acad. Sci.* 111, 18173–18177. <https://doi.org/10.1073/pnas.1408315111>
- Kelly, W.R., Matisoff, G., Fisher, J.B., 1985. The effects of a gas well blow out on groundwater chemistry. *Environ. Geol. Water Sci.* 7, 205–213. <https://doi.org/10.1007/BF02509921>
- Klazinga, D.R., Steelman, C.M., Cahill, A.G., Walton, K.M., Endres, A.L., Parker, B.L., 2019. Methane gas transport in unconfined aquifers: A numerical sensitivity study of a controlled release experiment at CFB Borden. *J. Contam. Hydrol.* 225, 103506. <https://doi.org/10.1016/j.jconhyd.2019.103506>

- Larson, T.E., Nicot, J.P., Mickler, P., Castro, M.C., Darvari, R., Wen, T., Hall, C.M., 2018. Monitoring Stray Natural Gas in Groundwater With Dissolved Nitrogen. An Example From Parker County, Texas. *Water Resour. Res.* 54, 6024–6041. <https://doi.org/10.1029/2018WR022612>
- Llewellyn, G.T., Dorman, F., Westland, J.L., Yoxtheimer, D., Grieve, P., Sowers, T., Humston-Fulmer, E., Brantley, S.L., 2015. Evaluating a groundwater supply contamination incident attributed to Marcellus Shale gas development. *Proc. Natl. Acad. Sci.* 112, 6325–6330. <https://doi.org/10.1073/pnas.1420279112>
- Mathes, M., White, J., 2006. Methane in West Virginia ground water. US Geol. Surv. Fact Sheet.
- McIntosh, J.C., Hendry, M.J., Ballentine, C., Haszeldine, R.S., Mayer, B., Etiope, G., Elsner, M., Darrah, T.H., Prinzhofer, A., Osborn, S., Stalker, L., Kuloyo, O., Lu, Z.T., Martini, A., Lollar, B.S., 2019. A Critical Review of State-of-the-Art and Emerging Approaches to Identify Fracking-Derived Gases and Associated Contaminants in Aquifers. *Environ. Sci. Technol.* 53, 1063–1077. <https://doi.org/10.1021/acs.est.8b05807>
- Miller, C.T., Poirier-McNeil, M.M., Mayer, A.S., 1990. Dissolution of Trapped Nonaqueous Phase Liquids: Mass Transfer Characteristics. *Water Resour. Res.* 26, 2783–2796 <https://doi.org/10.1029/WR026i011p02783>
- Molins, S., Mayer, K.U., Amos, R.T., Bekins, B.A., 2010. Vadose zone attenuation of organic compounds at a crude oil spill site - Interactions between biogeochemical reactions and multicomponent gas transport. *J. Contam. Hydrol.* 112, 15–29. <https://doi.org/10.1016/j.jconhyd.2009.09.002>
- Molofsky, L.J., Connor, J.A., McHugh, T.E., Richardson, S.D., Woroszylo, C., Alvarez, P.J., 2016. Environmental Factors Associated With Natural Methane Occurrence in the Appalachian Basin. *Groundwater* 54, 656–668. <https://doi.org/10.1111/gwat.12401>
- Mumford, K.G., Smith, J.E., Dickson, S.E., 2010. The effect of spontaneous gas expansion and mobilization on the aqueous-phase concentrations above a dense non-aqueous phase liquid pool. *Adv. Water Resour.* 33, 504–513. <https://doi.org/10.1016/j.advwatres.2010.02.002>
- National Energy Board of Canada, 2013. Canada's Energy Future 2013 - Energy supply and demand projections to 2035. Ottawa, ON.
- Nicot, J.P., Larson, T., Darvari, R., Mickler, P., Slotten, M., Aldridge, J., Uhlman, K., Costley, R., 2017. Controls on Methane Occurrences in Shallow Aquifers Overlying the Haynesville Shale Gas Field, East Texas. *Groundwater* 55, 443–454. <https://doi.org/10.1111/gwat.12500>
- Nowamooz, A., Lemieux, J.M., Molson, J., Therrien, R., 2015. Numerical investigation of methane and formation fluid leakage along the casing of a decommissioned shale gas well. *Water Resour. Res.* 51, 4592–4622. <https://doi.org/10.1002/2014WR016146>
- Pape, T., Bahr, A., Rethemeyer, J., Kessler, J.D., Sahling, H., Hinrichs, K.U., Klapp, S.A., Reeburgh, W.S., Bohrmann, G., 2010. Molecular and isotopic partitioning of low-

- molecular-weight hydrocarbons during migration and gas hydrate precipitation in deposits of a high-flux seepage site. *Chem. Geol.* 269, 350–363. <https://doi.org/10.1016/j.chemgeo.2009.10.009>
- Prinzhofer, A., Pernaton, É., 1997. Isotopically light methane in natural gas: Bacterial imprint or diffusive fractionation? *Chem. Geol.* 142, 193–200. [https://doi.org/10.1016/S0009-2541\(97\)00082-X](https://doi.org/10.1016/S0009-2541(97)00082-X)
- Reddy, K.R., Adams, J.A., 2001. Effects of Soil Heterogeneity on Airflow Patterns and Hydrocarbon Removal During In Situ Air Sparging. *J. Geotech. Geoenvironmental Eng.* 127, 234–247.
- Rice, A.K., Lackey, G., Proctor, J., Singha, K., 2018. Groundwater-quality hazards of methane leakage from hydrocarbon wells: A review of observational and numerical studies and four testable hypotheses. *Wiley Interdiscip. Rev. Water.* 5, e1283. <https://doi.org/10.1002/wat2.1283>
- Roy, N., Molson, J., Lemieux, J.M., Van Stempvoort, D., Nowamooz, A., 2016. Three-dimensional numerical simulations of methane gas migration from decommissioned hydrocarbon production wells into shallow aquifers. *Water Resour. Res.* 52, 5598–5618. <https://doi.org/10.1002/2016WR018686>
- Sale, T.C., McWhorter, D.B., 2001. Steady state mass transfer from single-component dense nonaqueous phase liquids in uniform flow fields. *Water Resour. Res.* 37, 393–404. <https://doi.org/10.1029/2000WR900236>
- Schout, G., Hartog, N., Hassanizadeh, S.M., Helmig, R., Griffioen, J., 2020. Impact of groundwater flow on methane gas migration and retention in unconsolidated aquifers. *J. Contam. Hydrol.* 230. <https://doi.org/10.1016/j.jconhyd.2020.103619>
- Selker, J.S., Niemet, M., Mcduffie, N.G., Gorelick, S.M., Parlange, J.Y., 2007. The local geometry of gas injection into saturated homogeneous porous media. *Transp. Porous Media* 68, 107–127. <https://doi.org/10.1007/s11242-006-0005-0>
- Sherwood, O.A., Rogers, J.D., Lackey, G., Burke, T.L., Osborn, S.G., Ryan, J.N., 2016. Groundwater methane in relation to oil and gas development and shallow coal seams in the Denver-Julesburg Basin of Colorado. *Proc. Natl. Acad. Sci. U. S. A.* 113, 8391–8396. <https://doi.org/10.1073/pnas.1523267113>
- Soeder, D.J., 2018. Groundwater Quality and Hydraulic Fracturing: Current Understanding and Science Needs. *Groundwater* 56, 852–858. <https://doi.org/10.1111/gwat.12810>
- U.S. Energy Information Administration, 2020. Annual Energy Outlook 2020. Washington, DC. www.eia.gov/aeo.
- U.S. Energy Information Administration, 2019. International Energy Outlook 2019. Washington, DC. www.eia.gov/aeo.

- US Environmental Protection Agency - US EPA, 2016. Hydraulic Fracturing for Oil and Gas: Impacts from the Hydraulic Fracturing Water Cycle on Drinking Water Resources in the United States (Main Report - EPA/600/R-16/236fa).
- Valocchi, A.J., 1985. Validity of the Local Equilibrium Assumption for Modeling Sorbing Solute Transport Through Homogeneous Soils. *Water Resour. Res.* 21, 808–820. <https://doi.org/10.1029/WR021i006p00808>
- Van De Ven, C.J.C., Abraham, J.E.F., Mumford, K.G., 2020. Laboratory investigation of free-phase stray gas migration in shallow aquifers using modified light transmission. *Adv. Water Resour.* 139, 103543. <https://doi.org/10.1016/j.advwatres.2020.103543>
- Van De Ven, C.J.C., Mumford, K.G., 2020a. Intermediate-Scale Laboratory Investigation of Stray Gas Migration Impacts: Methane Source Architecture and Dissolution. *Environ. Sci. Technol.* 54, 6299–6307. <https://doi.org/10.1021/acs.est.0c00456>
- Van De Ven, C.J.C., Mumford, K.G., 2020b. Aqueous and surface expression of subsurface GHGs: Subsurface mass transfer effects. *Water Res.* 170, 115327. <https://doi.org/10.1016/j.watres.2019.115327>
- Van De Ven, C.J.C., Mumford, K.G., 2019. Characterization of Gas Injection Flow Patterns Subject to Gravity and Viscous Forces. *Vadose Zo. J.* 18, 1–11. <https://doi.org/10.2136/vzj2019.02.0014>
- Van De Ven, C.J.C., Mumford, K.G., 2018. Visualization of gas dissolution following upward gas migration in porous media: Technique and implications for stray gas. *Adv. Water Resour.* 115, 33–43. <https://doi.org/10.1016/j.advwatres.2018.02.015>
- Vengosh, A., Jackson, R.B., Warner, N., Darrah, T.H., Kondash, A., 2014. A critical review of the risks to water resources from unconventional shale gas development and hydraulic fracturing in the United States. *Environ. Sci. Technol.* 48, 8334–8348. <https://doi.org/10.1021/es405118y>
- Watson, T., Bachu, S., 2009. Evaluation of the Potential for Gas and CO. *SPE Drill. Complet.* 24, 115–126. <https://doi.org/10.2118/106817-PA>
- Whiticar, M.J., 1999. Carbon and hydrogen isotope systematics of bacterial formation and oxidation of methane. *Chem. Geol.* 161, 291–314. [https://doi.org/10.1016/s0009-2541\(99\)00092-3](https://doi.org/10.1016/s0009-2541(99)00092-3)
- Woda, J., Wen, T., Oakley, D., Yoxtheimer, D., Engelder, T., Clara Castro, M., Brantley, S.L., 2018. Detecting and explaining why aquifers occasionally become degraded near hydraulically fractured shale gas wells. *Proc. Natl. Acad. Sci. U. S. A.* 115, 12349–12358. <https://doi.org/10.1073/pnas.1809013115>
- Wolfe, A.L., Wilkin, R.T., 2017. Evidence of Sulfate-Dependent Anaerobic Methane Oxidation within an Area Impacted by Coalbed Methane-Related Gas Migration. *Environ. Sci. Technol.* 51, 1901–1909. <https://doi.org/10.1021/acs.est.6b03709>

Chapter 2

Multicomponent mass transfer effects on the dissolution of stray gas: gas persistence and interpretation of hydrocarbon ratios

2.1 Introduction

Increases in natural gas extraction from deep geological reserves, both conventional and unconventional, has led to heightened environmental concern. Stray gas migration associated with leaky wells has emerged as a principal concern, as gas originating from deep in the subsurface can migrate upwards, impacting groundwater and surface water resources, and emitting to the atmosphere as a greenhouse gas (Bachu, 2017; CCA, 2014; Roy et al., 2016; US EPA, 2016). The presence of leaked natural gas in the subsurface, consisting primarily of methane with a smaller proportion of higher hydrocarbon chains such as ethane and propane, can contaminate drinking water resources and, in more severe cases, present risk of explosion or water well blowout from degassing (Kelly et al., 1985; McMahon et al., 2017).

Potential failure mechanisms that can lead to leaky wells include improper bondage of cement paste with the surrounding geological unit during well completion, well abandonment, casing degradation and interception of intermediate gas formations (Darrah et al., 2014). For example, achieving proper density and fill rates of cement slurry and ensuring proper bondage with intruded geological units is challenging. Pure cement paste can shrink after setting, and even a very small amount of shrinking can reduce the radial stress around the casing, allowing a narrow gas column to form between the cement and adjacent formation (Dusseault and Jackson, 2014). As the gas continues to form, the pressure difference between the water in the formation and the gas column increases. The longer the column that develops, the greater the pressure difference and the stronger the driving buoyant force, allowing the gas to rise along the well bore. Gas seepage may also occur

at the shoe of the surface casing under high shut-in pressure, which is of particular concern as the resulting gas leak would be closer to the surface (Dusseault and Jackson, 2014).

Gas in the gap between the cement and the formation will continue to migrate upwards in that gap so long as the gas pressure does not exceed the entry pressure of the formation. As gas continues to travel upwards and becomes adjacent to an aquifer, the low entry pressure of that aquifer, coupled with either the high pressure buildup at a capped surface-casing vent or a low permeability heterogeneity in the subsurface, causes gas migration into the adjacent aquifer (Dusseault and Jackson, 2014; Klazinga et al., 2019). During active leaks, the gas in the aquifer migrates vertically and forms continuous and discontinuous gas channels (Geistlinger et al., 2005; Van De Ven and Mumford, 2020a). In homogenous regions, the gas patterns form a parabolic shape, widening with increased height (Van De Ven et al., 2020). However, the distribution of gas will be substantially affected by heterogeneity and anisotropy, as gas pools form below low permeability lenses, leading to lateral migration (Glass et al., 2001; Van De Ven and Mumford, 2020a). This lateral gas migration has been shown to extend far beyond the well pad with gas most concentrated under lower-permeability zones in the subsurface (Cahill et al., 2018; Klazinga et al., 2019; Schout et al., 2020). After an active leak has stopped (inactive, repaired), the gas structure relaxes, causing gas channels to break up and form trapped blobs and ganglia (Geistlinger et al., 2005; Van De Ven et al., 2020).

During an active leak (Figure 2.1a), stray gas can be expressed in one of two ways: i) surface expression, where gas reaches the surface and emits as an efflux to the atmosphere (Forde et al., 2019; Schout et al., 2020; Van De Ven and Mumford, 2020b), and ii) aqueous expression, where gas in the subsurface dissolves in groundwater (Cahill et al., 2018; Schout et al., 2020; Van De Ven and Mumford, 2020b). Surface expressions are typically detected through bubbling at the well head or vegetation stress, and often serves as the first line of evidence of stray gas migration (Forde et

al., 2019). However, a significant amount of stray gas will also be expressed in the aqueous phase, leaving many leaks undetected until water resources have been impacted.

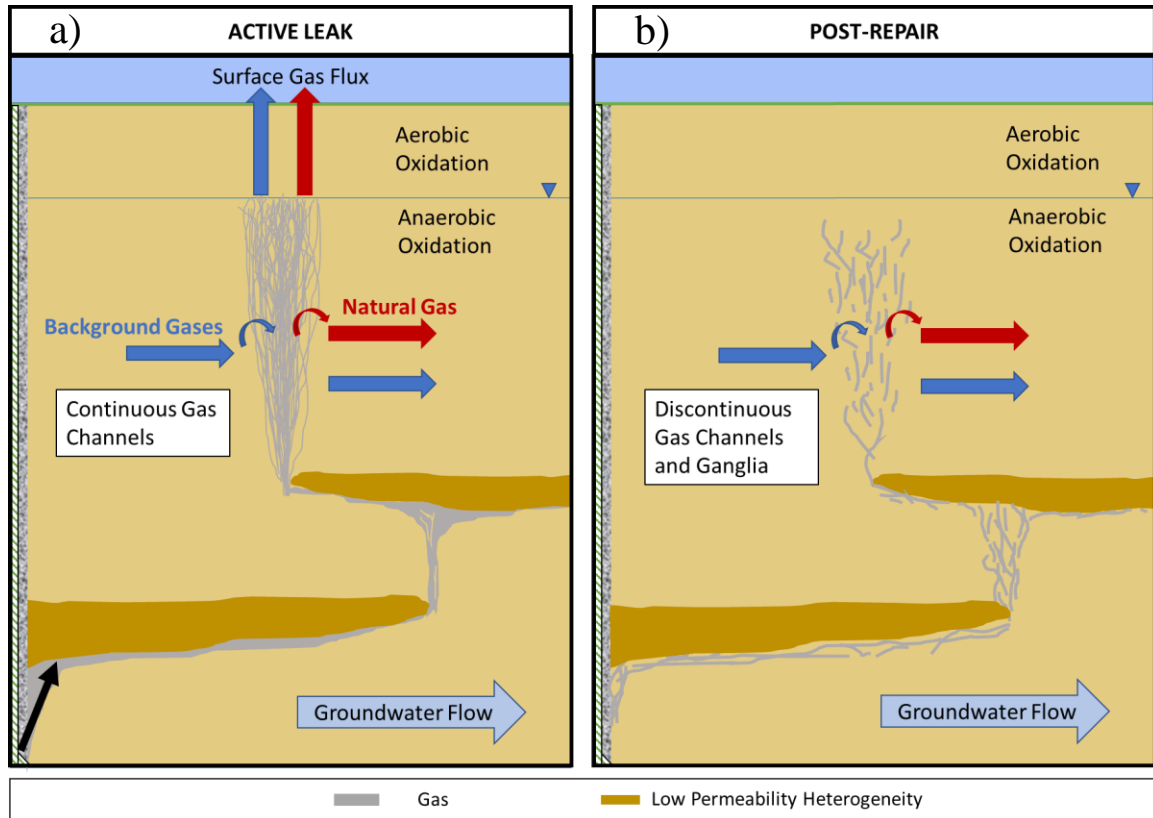


Figure 2.1. Conceptual model for a natural gas leak in the subsurface (a) during active leak when gas pools below low permeability heterogeneities as it travels upwards and becomes trapped in the subsurface, an aqueous phase natural gas plume develops as groundwater dissolves the trapped gaseous phase, and gas is emitted as a surface flux, and (b) post-repair when dissolution continues, but trapped gas becomes disconnected and surface emission stops. Curved arrows indicate partitioning, as background gases partition into the gas phase, and natural gas partitions into the aqueous phase. At the left side of each diagram, the hashed line and grey fill represent a well casing and cement respectively.

During active leaks, aqueous hydrocarbon concentrations increase as stray gas migrates through the subsurface (Cahill et al., 2018, 2017; Van De Ven and Mumford, 2020a). Dissolved background gases in groundwater partition into the gaseous phase as stray gas partitions to the aqueous phase

(Van De Ven and Mumford, 2020b). A steady state will be reached in which the gas source architecture remains steady and dissolved gas concentrations show only small fluctuations (Van De Ven and Mumford, 2020a). Post-repair (Figure 2.1b) and following a period of relaxation and redistribution, however, stray gas is expressed only in the aqueous phase. The gas in the aquifer is no longer being replenished by the leak and no gas is emitted, but trapped gas continues to dissolve and act as a source of dissolved methane and other hydrocarbon gases to the groundwater. As the gas channels are broken up, partitioning of background gases into the gaseous phase maintains the source architecture while natural gas partitions to the aqueous phase and is no longer replenished by the leak (Van De Ven and Mumford, 2020a). Both gaseous and aqueous phase stray gas will persist in the subsurface, and can take years to attenuate depending on the magnitude of the leak, presenting a long-term water quality concern (Cahill et al., 2018; Roy et al., 2016). In addition to affecting groundwater quality, dissolved gas concentrations are also used in combination with isotopic signatures for investigation and monitoring, including source identification and analysis of trends over time for gas fingerprinting.

The source of methane in the subsurface at suspected stray gas migration sites is often unclear, and can be produced from both natural and anthropogenic sources (Nicot et al., 2017). Naturally occurring methane is the product of bacterial and environmental factors and is commonly known as biogenic-source methane. Methane from natural gas extraction is referred to as thermogenic-source methane, and originates from deep in the subsurface as a result of high temperature and pressure. Thermogenic- and biogenic-source gases are commonly delineated by their fingerprint, based on their hydrocarbon composition and isotopic signature. Hydrocarbon composition is typically classified by the ratio of methane (C1) to higher hydrocarbon chains, most commonly ethane (C2) and propane (C3). Thermogenic is often identified by a $C1/(C2+C3)$ ratio of 100 or lower, and a stable carbon isotopic signature less than $-50\text{‰ } \delta^{13}\text{C-CH}_4$. Biogenic is identified by a $C1/(C2+C3)$ ratio of 1000 or higher, and a stable carbon isotopic signature greater than -50‰

$\delta^{13}\text{C}-\text{CH}_4$. However, the values that are used to define thermogenic and biogenic vary between studies (Cahill et al., 2018; Larson et al., 2018; Milkov and Etiope, 2018; Molofsky et al., 2016). Both hydrocarbon composition and isotopic signatures are important tools for practitioners and regulators to identify leaking wells when more apparent indicators such as surface casing vent flow or bubbling in water pools on the well pad are not present. The relative ease of collection and analysis of aqueous samples for hydrocarbons facilitates the source identification process for methane presence in groundwater.

Hydrocarbon composition and isotopic signature are typically plotted in combination on ‘Bernard diagrams’ (Figure 2.2), which delineate zones of biogenic and thermogenic source gases (Bernard et al., 1976). Gas fingerprinting delineations are based on empirical data, and the relatively limited number of basins and near-surface environments from which signatures have been derived may not apply to all geographic and geological contexts (McIntosh et al., 2019). Moreover, both the hydrocarbon composition and isotopic signature are not static and can be impacted by multiple processes. For example, atmospheric and hydrostatic water pressure changes, water pumping and post-genetic processes such as gas mixing and oxidation can change the fingerprint of a gas. The advection of gases can cause an increase in hydrocarbon ratio, attributed to differential solubility and adsorption of gas (Cahill et al., 2018; Etiope et al., 2009; McIntosh et al., 2019). Additionally, changes in isotopic signature can occur due to diffusive isotopic fractionation (Etiope et al., 2009; Hendry et al., 2016; McIntosh et al., 2019; Prinzhofer and Battani, 2003). Differences between hydrocarbon compositions from gas sources and groundwater samples have been noted in the field, and mixing and oxidation are typically determined to be the cause (Darrah et al., 2014; Molofsky et al., 2013; Moritz et al., 2015). This broad set of post-genetic processes can affect hydrocarbon composition and isotopic signatures, and must be interpreted appropriately considering the hydrogeological setting of the gas release (McIntosh et al., 2019). However, these processes largely center on active leaks in which the gas leak is at steady state, and do not consider the effect of

trapped gas dissolution on the composition of dissolved gases in the aqueous phase after a leak has stopped.

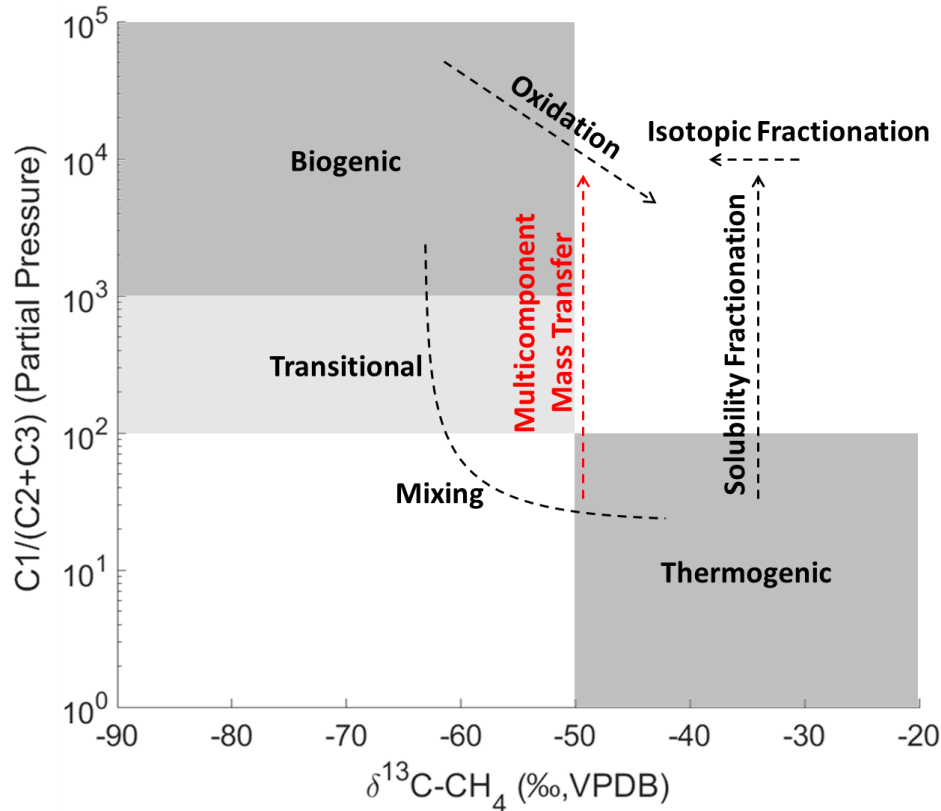


Figure 2.2. Adapted Bernard diagram (Bernard et al., 1976; Cahill et al., 2018; Etiope et al., 2009; McIntosh et al., 2019; Whiticar, 1999). Change due to multicomponent mass transfer is shown by the red arrow, and is a proposed mechanism of increases in hydrocarbon ratio due to competitive multicomponent mass transfer. Post genetic processes are shown by black arrows, which cause transition between zones. Delineations vary between studies due to the empirical nature of gas fingerprinting.

The dissolution of trapped gas is affected by both dissolved gases in the surrounding groundwater and the components in the trapped gas. For example, previous studies of multicomponent mass transfer showed that the presence of trapped gases can retard the breakthrough of dissolved gases (Donaldson et al., 1998, 1997; Fry et al., 1995). While early models assumed a constant gas

saturation, Donaldson et al. (1997) noted significant changes in gas saturation in their experiments. Cirpka and Kitanidis (2001) presented a set of equations to model the mass transfer between aqueous and gaseous phases during transport considering variable gas saturation and assuming local equilibrium, which has been used to simulate multiple applications (Amos and Mayer, 2006; Molins and Mayer, 2007; Mumford et al., 2010). A similar variable-volume approach has also been used to describe mass transfer under rate-limited conditions (Geistlinger et al., 2005; Holocher et al., 2003). The competitive nature of multicomponent gas dissolution will alter the concentrations of components principally as a function of their Henry's Law coefficients and Dalton's Law of partial pressures (Cirpka and Kitanidis, 2001). This suggests that the ratio of methane to other higher chain hydrocarbons could change as some components more readily partition into or out of the aqueous phase. Simulations that considered variable-volume multicomponent dissolution have demonstrated non-monotonic behaviour, during which aqueous and gaseous concentrations, as well as gas saturations, can increase and decrease during the dissolution of a trapped gas. This behaviour cannot be reproduced if only a single gas component is considered. Additionally, the presence of multiple components in a trapped gas will also decrease the solubility of each component, as solubility is determined by the partial pressure of each component and its respective Henry's Law coefficient. By extension, the dissolution behaviour is a product of both the trapped gas and the background dissolved gases. Geistlinger et al. (2005) confirmed that variable gas saturations must be considered to describe the dissolution of trapped gas, particularly when the composition of the trapped gas is significantly different than that of the background gases. This is the case for stray gas migration, where the composition of gas from deeper zones consists mostly of hydrocarbons and is much different than the dissolved atmospheric gases in shallow aquifers. Therefore, it is expected that the dissolution behaviour of the hydrocarbons in stray gas will be greatly impacted by the dissolved gases present in the surrounding groundwater.

Evidence of transient changes in hydrocarbon composition have been observed in a controlled-release field experiment (Cahill et al., 2018) of natural gas that was monitored over a year-long period, including 246 days after the release was stopped. During the active injection period the ratio of C1/C2 decreased with time, while after injection the ratio of C1/C2 increased with time. The change was attributed to the differential solubility of natural gas components, although Cahill et al. (2018) note that this effect is not yet well understood. In addition, there is a need to consider the mass transfer of background dissolved gases and their effect on gas persistence and changing hydrocarbon ratios. For example, laboratory studies have shown that multicomponent mass transfer effects can alter the concentrations of dissolved gases and the surface expression of gases, such that the surface expression of gas and trapped gases at late time may be different than the source gas (Van De Ven and Mumford, 2020b, 2020a). A change in the composition of trapped gas may impact the interpretation of gas detection using geophysical techniques such as ground-penetrating radar (Cahill et al., 2017; Lassen et al., 2015), as gas detection would not definitively indicate the continued presence of hydrocarbon gases.

In this study, a set of multicomponent gas dissolution experiments was conducted to investigate the persistence and composition of stray gas in the subsurface. These experiments were then simulated using a mass transfer model implemented in MIN3P (Amos and Mayer, 2006; Mayer et al., 2002) to match dissolved hydrocarbon concentrations and provide insight into the role of background dissolved gases. The objectives of this study were to: 1) determine the effect of multicomponent mass transfer on changes to the hydrocarbon ratio over time, and 2) investigate the parameters that lead to gas persistence in the subsurface and the relationship between aqueous and gaseous hydrocarbon concentrations. The overall goal was to improve the interpretation of hydrocarbon ratios in stray gas investigations such that appropriate mitigation and remediation measures can be taken.

2.2 Lab-Scale Experiments

2.2.1 Experimental Design

The experiments were designed to simulate the dissolution of trapped gas after a stray gas leak has been stopped (Figure 2.1b). Each experiment was conducted in a 5.3 cm-tall stainless steel column with a 7.2 cm inner diameter. This scale is a representative elementary volume for the coarse uniform sand used in the experiments, and the use of column with a small pore volume allowed gas emplacement and aqueous sampling to occur on the same day and capture changes in aqueous dissolved gas concentration over time. Filter paper (20 μm , Fisherbrand 09-795C) was placed at the bottom of the column between the sand and the bottom fitting, to prevent sand from entering the tubing and allow drainage to a uniform residual water saturation at higher gas pressures for the purpose of gas emplacement. A uniform, coarse sand (20/30 Accusand, $d_{50} = 0.72$ mm) (Schroth et al., 1996) was emplaced using a wet-packing method in which a sand-water slurry was poured continuously into the column to ensure a homogeneous pack. Deionized (DI) water was used in all experiments such that the impact of dissolved gases alone could be studied. The top and bottom port of the column were then attached with Swagelok gas tight fittings to the experimental setup shown in Figure 2.3. Each experiment consisted of two phases: gas emplacement and gas dissolution. Before gas emplacement, the valves were oriented for water flow from the pump reservoir to the outflow and 10 pore volumes of water (700 mL) were pumped (Masterflex L/S 1-100RPM) through the column. The water in the reservoir was sparged with gas (methane or a mix of methane, ethane and propane) to prevent dissolution of gas during emplacement. During gas emplacement, the valves were oriented such that the bottom of the column was connected to the drainage outlet, and the top of the column was connected to the gas cylinder. Gas emplacement consisted of a drainage and an imbibition stage. During drainage, a mass flow controller (Cole-Parmer 32907-63) was used to increase the gas pressure at the top of the column in 345 Pa increments, and the outflow was monitored until the sand pack reached residual water saturation.

Saturations were calculated by measuring the mass of water leaving the column after each pressure increase.

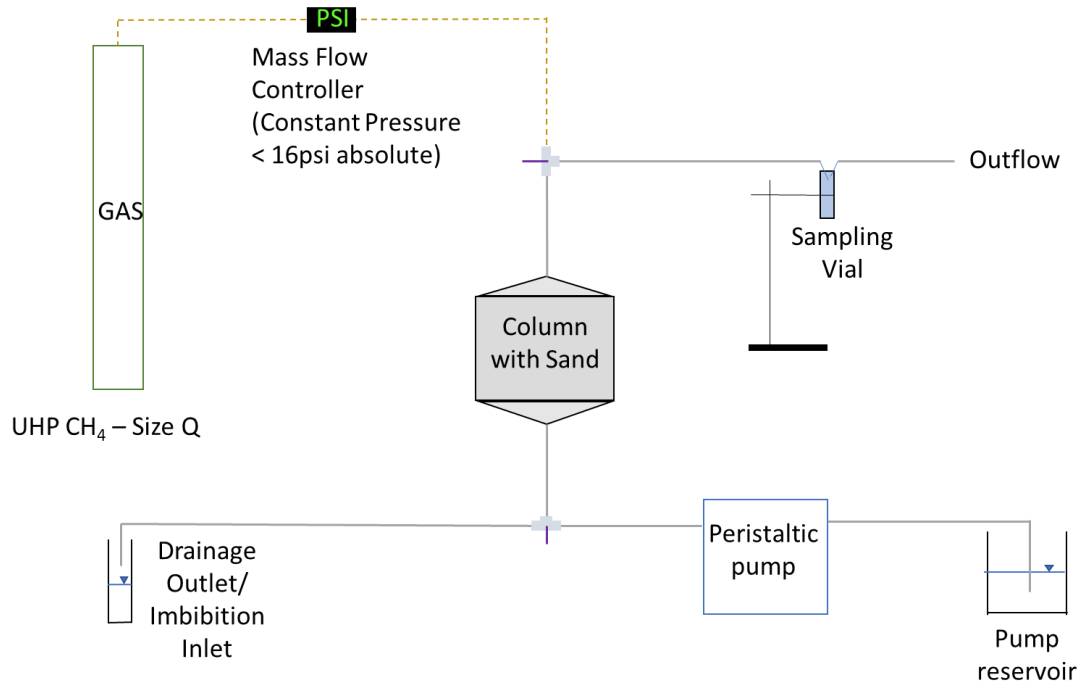


Figure 2.3. Diagram of experimental equipment used to conduct gas emplacement and dissolution experiments. Valves at tubing intersections allowed changes in water flow direction between the gas emplacement and dissolution phases of each experiment. Tubing in grey is 1/8” ID flexible PTFE tubing, and tubing in dashed yellow lines is 1/8” ID copper pipe used for gas transport. Images of lab equipment appear in Appendix D.

Capillary pressure-saturation drainage curves agreed with results obtained using the hanging column method for the same column (Appendix C), and were consistent with those reported by others for this sand (Schroth et al., 1996). In the imbibition stage, the valves were closed and the mass flow controller was shut off. The drainage outlet beaker was then filled with sparged water and raised to be level with the center of the column. The valves were then opened and sparged water imbibed the column, trapping gas as a non-wetting residual. The gas saturation was calculated from the mass of imbibed water and an estimate of porosity based on the mass of dry sand.

During the gas dissolution phase, the valves were oriented for water to flow from the pump reservoir to the outflow. DI water, which had been left to equilibrate with the atmosphere for 24 hours, was then pumped through the column at 2.5 mL/min, equivalent to a 2.7 m/day pore water velocity. This flow rate was selected as it is within the reasonable limits for local equilibrium modeling (Geistlinger et al., 2005). At the outflow, 10 or 15 mL sample vials were filled with column effluent by piercing the vial septa with two 21-gauge needles, one for inflow and one for outflow, and flowing 50 mL of water through each vial. Samples were analyzed for dissolved hydrocarbon concentrations. Background dissolved gases (N₂, O₂) were not measured because the collection of the required 120 mL sample volume would prevent accurate measurement of more rapidly changing hydrocarbon gas concentrations. Two sets of experiments were conducted: four single-component experiments (SC1-4) using 100% methane and four multicomponent experiments (MC1-4) using a mixture of 85% methane, 10% ethane and 5% propane (by volume) (Table 2.1). This gas mixture was selected to be representative of Montney gas and similar to the gas injected by Cahill et al. (2019).

Table 2.1. Summary of column experiments

Experiment	Porosity	Residual Water Saturation (After Drainage)	Initial Trapped Gas Saturation	Final Gas Saturation	Gas Composition
SC1	0.34	0.03	0.21	nm	100% methane
SC2	0.33	0.05	0.18	nm	
SC3	0.33	0.08	0.15	nm	
SC4	0.33	0.08	0.17	nm	
MC1	0.34	0.06	0.19	0.11	85% methane, 10% ethane, 5% propane
MC2	0.33	0.09	0.17	0.093	
MC3	0.34	0.08	0.17	0.086	
MC4	0.34	0.10	0.16	0.093	

nm: not measured

Influent dissolved gas concentrations were 0.373 mmol/L (11.94 mg/L) O₂ and 0.778 mmol/L (21.79 mg/L) N₂. At the end of each multicomponent experiment, the valves were oriented for

water to flow from the outflow to the drainage outlet, and the mass of water drained from the column was measured to calculate the final gas saturation. The dispersivity of both the saturated and unsaturated column was measured to be 4.5 mm using separate bromide tracer tests (Appendix B).

2.2.2 Dissolved Gas Quantification

Analysis of dissolved methane concentrations in SC1-3 was conducted at the Analytical Services Unit at Queen's University. The samples were collected in 10 mL glass headspace vials sealed with PTFE septa with magnetic screw-caps. PTFE septa are suitable for short sample holding times (Eby et al., 2015), and all samples were refrigerated immediately after collection and analyzed within 24 hours. Prior to analysis, 5 mL of pure nitrogen was injected into each vial to create a headspace, and the samples were sonicated for 15 minutes to ensure equilibration with the aqueous phase. Analysis was conducted by gas chromatography (Agilent 7890B with Agilent 80 PAL autosampler) using a PoraBOND Q16 column (50 m, 0.530 mm diameter, 10 µm film), hydrogen carrier gas and a flame-ionization detector (FID). Calibration was performed before every experiment with triplicate measurements using 0.1%, 1%, 4.8%, and 10% methane balanced with nitrogen. Calibration data was used to determine the 95% confidence interval for each sample (Miller and Miller, 2005). Calculations of dissolved gas concentration were done using the Kampbell and Vandegrift method (1998).

Analysis of dissolved methane concentrations in SC4 and MC1-4 was conducted at the Aqueous Geochemistry and Isotope Science Laboratory at the University of Calgary. The samples were collected in 15 mL glass serum bottles with grey bromobutyl (GB) stoppers, which are suitable for holding times up to 6 months (Eby et al., 2015). Headspace was created in each bottle by replacing 3.0 mL of water with ultrapure helium. Samples were then shaken for 5 minutes and allowed to equilibrate at 20°C for approximately 12 hours. Immediately prior to analysis, a 0.5 mL aliquot of headspace was removed from each vial and diluted with 2.0 mL of ultrapure helium. 2.5mL of each

diluted gas was analyzed by gas chromatography (Bruker-450) using a Bruker BR-1 capillary column (10 m, 0.15 mm diameter, 2 μm film), hydrogen carrier gas and FID. Certified gas standards (Praxair Distribution) were used to calibrate the GC immediately prior to the analysis. The lower detection limit for methane, ethane and propane was 1 ppm in the headspace, equivalent to 0.023 $\mu\text{g/L}$, 0.058 $\mu\text{g/L}$ and 0.067 $\mu\text{g/L}$ in the aqueous phase, respectively. Analytical precision and accuracy for gas composition analysis is typically better than $\pm 2.5\%$ of the reported concentrations.

2.3 Numerical Modeling

2.3.1 Model Description

MIN3P (Amos and Mayer, 2006; Mayer et al., 2002) is a multicomponent reactive transport model for variably-saturated media and was used to model the dissolution of methane and natural gas. The finite volume method (equivalent to block-centered finite difference for regular geometries) was used for spatial discretization, and a fully implicit time scheme is used for temporal discretization (Mayer et al., 2002). The model can simulate bubble growth and dissolution as a function of the partial pressures of dissolved gases, based on principals for gas partitioning outlined by Cirpka and Kitanidis (2001). Partitioning of volatile compounds is according to Henry's Law:

$$p_i = C_i^w H_i \quad (2.1)$$

where p_i is the partial pressure of component i and C_i^w is the aqueous concentration of component i , and H_i is the Henry's constant of component i . Assuming ideal gas behaviour, the gaseous phase concentrations are related to their partial pressures by:

$$C_i^g = \frac{p_i}{RT} \quad (2.2)$$

where C_i^g is the gaseous concentration of component i , R is the ideal gas constant and T is temperature. Dalton's law states that the total gas pressure is equal to the sum of the gaseous phase

pressures. Consistent with Cirpka and Kitanidis (2001), it is assumed that the total gas pressure is constant and equal to the water pressure. As the volatile compounds compete to be present in the gaseous phase, non-linear mass transfer behaviour arises because the sum of the partial pressures is fixed, causing the gas saturation and the aqueous phase concentrations to change to satisfy Henry's Law and Dalton's Law (Cirpka and Kitanidis, 2001). The partial pressures at this scale can then be related to the total pressure such that

$$P = \sum_{i=1}^N p_i \quad (2.3)$$

where P is the total gas pressure. The total concentration is the saturation-weighted sum of the gaseous and aqueous concentrations:

$$C_i^T = (1 - S_g)C_i^w + S_g C_i^g \quad (2.4)$$

where C_i^T is the total concentration and S_g is the gas saturation. The partial pressure of each component can then be expressed in terms of total concentration:

$$p_i = \frac{C_i^T H_i}{1 + \left(\frac{H_i}{RT} - 1\right) S_g} \quad (2.5)$$

The change in the total concentration, representing mass in both the aqueous and gaseous phases, over time subject to advection and dispersion, and neglecting molecular diffusion, is:

$$\frac{\partial C_i^T}{\partial t} = -\frac{q}{\theta} \frac{\partial C_i^w}{\partial x} + \frac{q\alpha}{\theta} \frac{\partial^2 C_i^w}{\partial x^2} \quad (2.6)$$

where θ is the porosity, q is the specific discharge, and α is the longitudinal dispersivity. Equation 2.6 assumes that any change in the total concentration is due only to transport in the aqueous phase, and the gaseous phase remains trapped (Cirpka and Kitanidis, 2001). Once C_i^T is calculated, a value of S_g is calculated that satisfies both Equations 2.3 and 2.5. MIN3P has been verified against Cirpka

& Kitanidis (2001) and the capability to model dispersion effects in a small column made it viable to model the experimental system (Amos and Mayer, 2006).

Hydrocarbon ratios are calculated using an equivalent gas phase partial pressure based on aqueous concentrations. Comparing a ratio of partial pressures, rather than a ratio of aqueous concentrations, is important for comparing to ratios determined for an original source gas. The hydrocarbon ratio of a source gas is typically based on the fraction of each component in a gas sample, which is different than the composition of the aqueous phase in equilibrium with a gas:

$$\frac{C_1}{C_2+C_3} = \frac{C_{C_1}^w H_{C_1}}{C_{C_2}^w H_{C_2} + C_{C_3}^w H_{C_3}} \quad (2.7)$$

2.3.2 Model Implementation

MIN3P was used to simulate the mass transfer and transport of dissolved gases in a region that contains trapped methane or natural gas, representative of conditions after a leak has been stopped (Figure 2.1b). An initial gas saturation was applied throughout the domain, which was a 1D column made of 53 1 mm control volumes. The initial gas saturation is equal in volume and composition to the experiments (Table 2.1). The aqueous phase was assumed to be initially in equilibrium with the gas phase. The influent boundary condition was a constant concentration of dissolved gas, and the effluent boundary was a Neumann type boundary to match experimental conditions.

Five sets of simulations were conducted and are summarized in Table 2.2 and include single-component (SC) and multicomponent (MC) simulations. The first set, SC-Sim simulated methane dissolution for comparison to the single-component (methane) column experiments SC1-4. The second set, SC-BG simulated methane dissolution under conditions similar to the experiments but for a variety of dissolved gas concentration to determine the effects of the dissolved background gases on the methane dissolution behaviour and gas persistence. The background dissolved gas concentration can be expressed as a fraction of the water pressure, neglecting capillary pressure:

$$f = \frac{\sum C_i^w H_i}{P_w} \quad (2.8)$$

where P_w is the water pressure and f is the fraction of total gas pressure in the background (influent) to the total hydrostatic pressure. The background gas composition was assumed to be 79% nitrogen and 21% oxygen, and was varied such that f ranged from 0 to 1, where $f = 0$ has no dissolved background gases, and $f = 1$ has dissolved background gases at solubility. Varying values of f were investigated over 23 simulations. The third set of simulations, MC-BG, varied f over the same range as the SC-BG simulations, but using a multicomponent source gas (highly thermogenic). The fourth set, MC-Sim simulated the multicomponent column experiments MC1-4. The fifth set, MC-Sources, included four simulations of multicomponent dissolution behaviour similar to the experiments but for different source gas mixtures. Source mixtures were varied from 50% methane to 99.9% methane, with the balance being 2/3 ethane and 1/3 propane. The model parameters used in every MIN3P simulation are shown in Table 2.3. The physicochemical properties for each gas component including Henry's constants are shown in Table 2.4. No fitting parameters were used to match the SC-Sim and MC-Sim simulations to the experiments. The dispersivity value was determined by fitting the breakthrough curve from an independent bromide tracer test with MIN3P (Appendix B). The tracer test was conducted in the same experimental setup as the gas dissolution experiments, and as such the dispersivity value is representative of the entire system including dispersion in tubing and end caps. Some variability is expected between experiments, and measured dispersivity values serve primarily as an estimate of apparent dispersion in the experimental apparatus.

Table 2.2. Simulations

Simulation	Source gas composition (fraction)			Source Gas Hydrocarbon Ratio	Background dissolved gas fraction (f)*
	C1	C2	C3		
SC-Sim	1	0	0	N/A	1
SC-BG	1	0	0	N/A	0 to 1
MC-BG	0.5	0.33	0.17	1	0 to 1
MC-Sim	0.85	0.1	0.05	5.67	1
MC-Sources	0.75	0.17	0.083	3	1
	0.85	0.1	0.05	5.67	1
	0.99	0.067	0.033	100	1
	0.999	0.0067	0.0033	1000	1

*All background gases considered to be 79% N₂ and 21% O₂.

Table 2.3. Model Parameters

Parameter	Symbol	Value	Units
Column length	L	52.9×10^{-3}	m
Column diameter	d	72.3×10^{-3}	m
Longitudinal dispersivity	α	$4.5E \times 10^{-3}$	m
Water pressure	P_w	101325	Pa
Darcy flux	q	1.014×10^{-5}	m/s
Pore water velocity	v	3.121×10^{-5}	m/s
Porosity	θ	0.335	-
Gas saturation	S_g	0.1738	-
Free diffusion coefficient in water	D_w	1.0×10^{-9}	m ² /s
Free diffusion coefficient in gas	D_g	1.0×10^{-5}	m ² /s

Table 2.4. Physicochemical properties of volatile compounds

Name	Formula	Henry's Law coefficient at 298K (Pa m ³ mol ⁻¹)*
Oxygen	O ₂	8.04×10^4
Nitrogen	N ₂	1.53×10^5
Methane	CH ₄	7.14×10^4
Ethane	C ₂ H ₆	5.26×10^4
Propane	C ₃ H ₈	6.66×10^4

*From Sander (2015)

2.4 Results and Discussion

2.4.1 Single-component (Methane) Dissolution

Figure 2.4a shows the results of experiments SC1-4 and simulation SC-Sim. Methane concentrations are initially at or above the theoretical solubility of methane at STP (22.7 mg/L). Samples with concentrations higher than solubility are likely due to excess gas as small bubbles entering the first sample vials, as a result of residual gas in the lines and top of the column. Concentrations return below solubility after 1 pore volume.

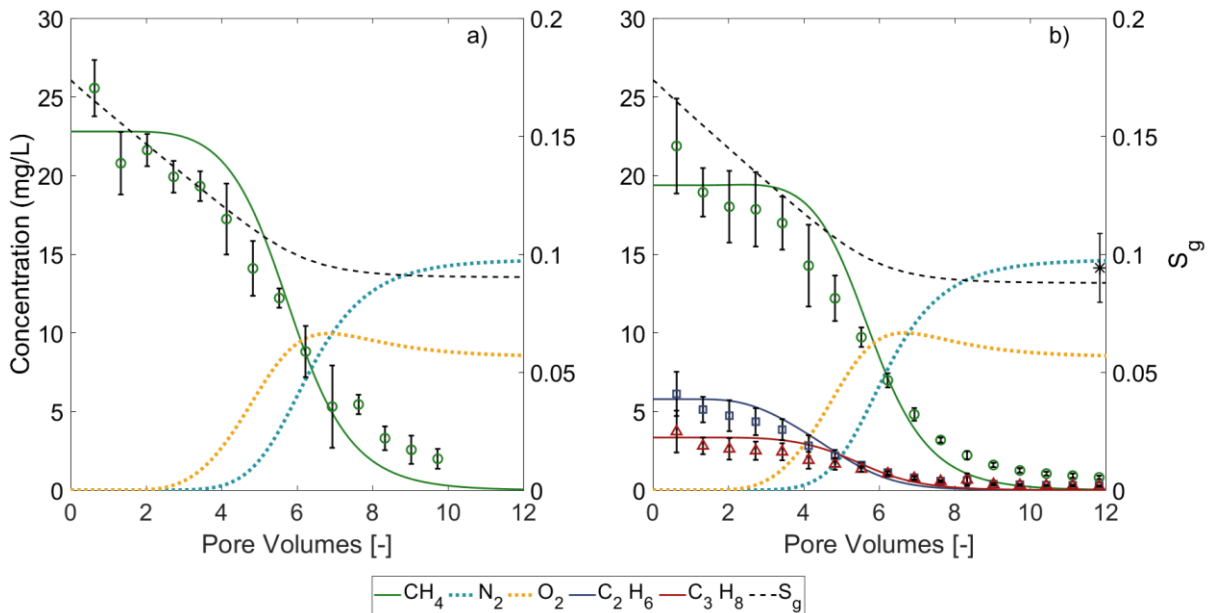


Figure 2.4. Measured (symbols) and simulated (lines) aqueous effluent concentrations for the (a) single-component (methane) and (b) multicomponent experiments. Experimental data points match the colours of the simulated data. Concentrations that are only simulated (no experimental data) are shown as dotted lines. Simulated average gas saturations throughout the column are shown as a dashed line. Asterisk symbol plotted on right axis at 12 pore volumes is the mean experimental final gas saturation. Error bars indicate 95% confidence interval on the mean for both measured concentrations and final gas saturation based on four experiments. Data from individual experiments appears in Appendix A.

Concentrations decrease gradually until 3.5 pore volumes, at which point concentrations begin to decrease more quickly as methane leaves the system. The rate of dissolution decreases at 8 pore volumes as the source is largely depleted, although a small quantity of methane persists in the column after 10 pore volumes.

The SC-Sim simulation agrees well with the measured concentrations, but does overestimate methane concentrations at early time (2-4 pore volumes) and underestimate methane concentrations at late time (8-12 pore volumes). These differences are attributed to the local equilibrium assumption. Geistlinger et al. (2005) demonstrated that local equilibrium models of partitioning will overestimate at early time as concentrations begin to decrease, and underestimate concentrations at late time. However, they also conclude that local equilibrium remains a reasonable assumption at low velocities (below 4 m/day). The simulated concentration plateau until 3.5 pore volumes was not observed in the experimental data, which may be caused by incomplete mixing across the cross section of the column, that is not represented by the 1D simulations. The simulations accurately predicted the dissolution of trapped gas, including both the significant decrease in methane concentration beginning at 3.5 pore volumes and the depletion of methane in the system after 10 pore volumes. The model provides additional insight into the nature of the mass transfer in the system. As methane concentrations begin to decrease, a front of dissolved oxygen (concentration > 1 mg/L) appears at 3.3 pore volumes, followed by a front of dissolved nitrogen at 4.7 pore volumes. Oxygen arrives first due to its higher solubility. The oxygen concentration is non-monotonic; it first increases up to 10 mg/L before decreasing to 8 mg/L. This is due to the competitive nature of gas dissolution resulting from adherence to Henry's Law and Dalton's Law as the gas dissolves. Notably, the dissolved methane concentration is nearly zero (0.09 mg/L) at 12 pore volumes, and yet a gas phase remains. The average simulated gas saturation plateaus at 0.09 at 12 pore volumes.

Figure 2.5a shows the mole fractions in the gas phase for SC-Sim. The persistent gas phase consists of nitrogen and oxygen, originally introduced as dissolved gases in the influent. At 12 pore volumes, the composition in the gas phase is 79% nitrogen and 21% oxygen which matches the background dissolved gas composition used in the simulations (Table 2.2).

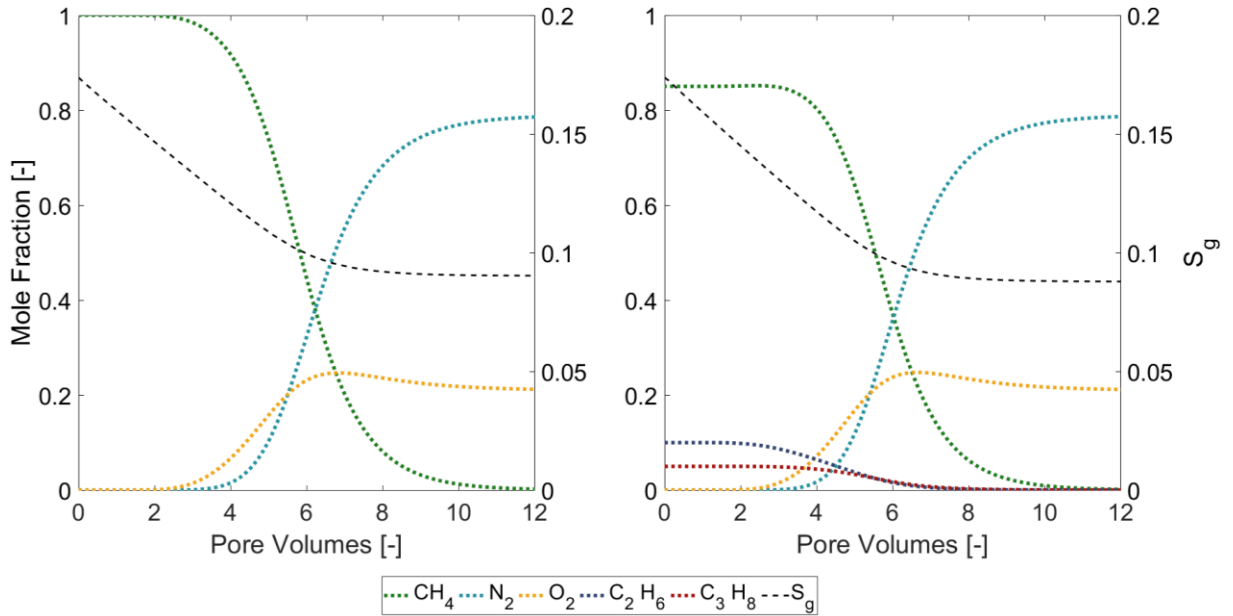


Figure 2.5. Mole fractions in the gas phase for the (a) single-component (methane) and (b) multicomponent simulations SC-Sim and MC-Sim. Mole fractions are those in the trapped gas adjacent to the column’s effluent edge. Simulated average gas saturations throughout the column are shown as a dashed black line.

The persistence of gas is consistent with the observations of Van de Ven and Mumford (2020a), as the source gas has partitioned into the aqueous phase, but background dissolved gases have partitioned into the gaseous phase, sustaining the gas saturation after the source gas is depleted. Similar considerations have been identified in studies of CO₂ geological storage, which have shown that gases such as CH₄ and H₂S present in deep brines will compete with injected CO₂, leading to the exsolution of dissolved gases not present in the injected gas (Ghaderi et al., 2011; Soltanian et al., 2018). These results emphasize the importance of considering multicomponent effects on

dissolution, as even a single-component source becomes multicomponent because of the mass transfer of background dissolved gases.

2.4.2 Impact of Dissolved Background Gases

Results from the methane dissolution experiments and simulation show that the presence of trapped gas does not necessarily indicate a hydrocarbon source that is currently dissolving. However, high trapped gas saturations in combination with low dissolved hydrocarbon concentrations may indicate that natural gas was there at a previous time. After a leak is stopped, the composition of the trapped gas depends on the time of sampling. The source architecture of trapped gas may remain long after the source gas has dissolved away, and consist of background gases at lower gas saturations. Figure 2.6 shows select results from the SC-BG simulations for different background gas concentrations, represented by their f values. Apart from a significantly sharp front associated with no dissolved gases present ($f = 0$), the methane concentration trends during dissolution are largely unaffected by the influent dissolved gas concentration. The timing of concentration decrease (4-8 pore volumes) and extinction (10 pore volumes) are very similar. Thus with very low dissolved gas concentrations ($f \leq 0.2$), the source gas will dissolve very quickly, however for $f \geq 0.4$ the dissolution curve is largely insensitive to the background dissolved gas concentrations. However, gas persistence is highly sensitive to the background dissolved gas concentrations (Figure 2.6b). From $f = 0$ to $f = 0.4$, quick extinction behaviour occurs, with gas saturations decreasing to zero at the same time that methane concentrations reach zero (~10 pore volumes). Under these conditions, the sum of the potential partial pressures (i.e., partial pressures in equilibrium to the aqueous concentrations according to Henry's Law) is insufficient to sustain the required gas pressure. The

time to gas extinction increases as the background dissolved gas concentrations increase.

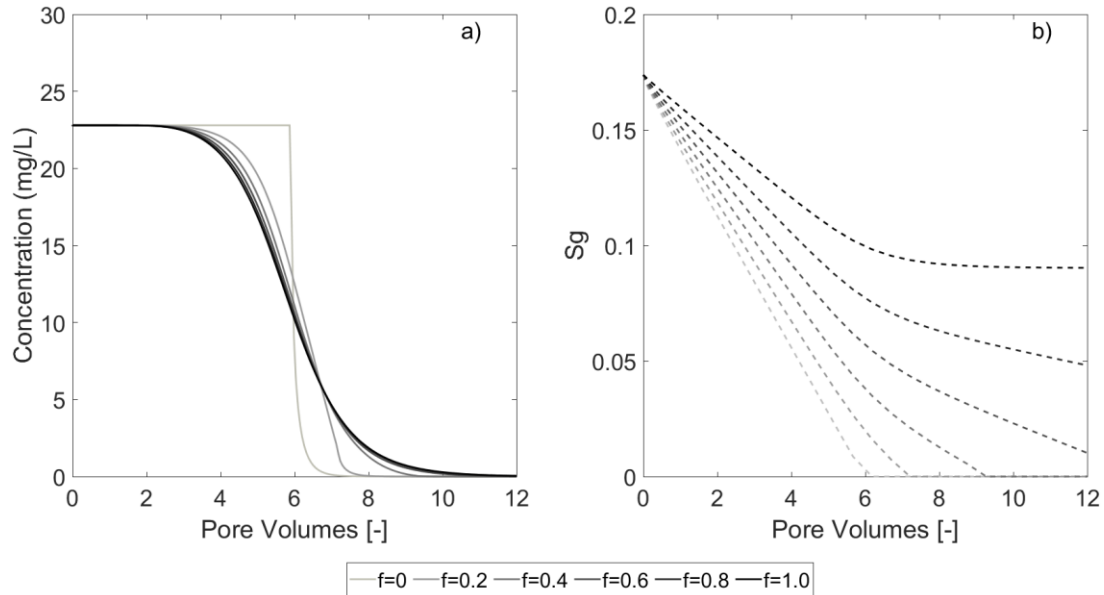


Figure 2.6. Simulated effluent concentrations (a, solid lines) and gas saturations (b, dashed lines) for methane dissolution for a range of background dissolved gas concentration from the SC-Sim simulations.

For $f \geq 0.6$, persistent gas behaviour occurs, as the trapped gas persists past 12 pore volumes because sufficient oxygen and nitrogen are present to sustain the gas phase. It is important to note that the background dissolved gas concentrations required to sustain the gas phase depends strongly on the surrounding water pressure, with higher concentrations required for higher water (and, therefore, gas) pressure. However, simulations conducted for a range of f values but at a higher water pressure (results not shown) indicate that persistence depends on f . Therefore, persistence will increase with more volatile gases (larger H_i), higher concentrations (C_i^w) or lower water (gas) pressure (P_w) (Equation 2.8).

Figure 2.7 highlights the role of f on gas persistence based on results from simulation sets SC-BG and MC-BG. Gas persistence can be classified here in three categories: quick extinction, persistent, and highly persistent. Quick extinction exists for $f < 0.4$, and the gas is extinct at the same time as

the source gas aqueous concentration reaches zero. Persistent behaviour exists for $0.4 < f < 0.95$, as the gas is extinct after the source gas has dissipated, and remains for up to 100 pore volumes. Highly persistent behaviour exists for $f > 0.95$, as gas persists beyond 100 pore volumes. For the groundwater velocity expected at many stray gas migration sites, this could represent a substantial period of time. For example, at a groundwater velocity of 1 cm/day, and a source zone of 10 m length, 100 pore volumes equates to 274 years. These simulations were conducted for water pressures of 0 m and 30 m of water, and the persistence behaviour is identical for the same f . In field conditions there will be added gas sinks and sources that will impact gas persistence, but regardless the notion of an f value demonstrates that increased background dissolved gas concentrations will increase gas persistence.

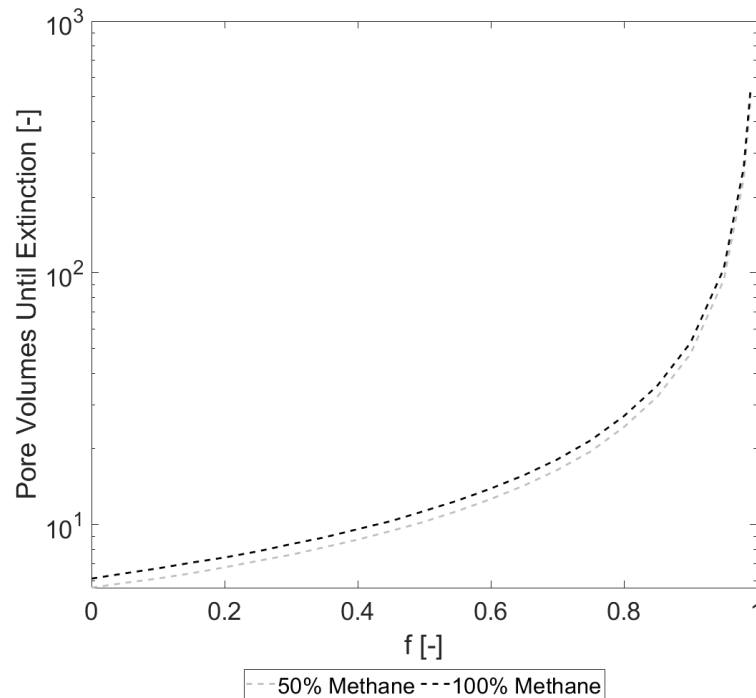


Figure 2.7. Pore volumes until extinction for a highly thermogenic multicomponent source and a source entirely composed of methane (MC-BG and SC-BG). Pore volumes until extinction ($S_g = 0$) is plotted on the y-axis in pore volumes for corresponding relative background gas concentrations (f).

2.4.3 Multicomponent Source Dissolution

Figure 2.4b shows the results of experiments MC1-4 and simulation MC-Sim. Methane concentrations are initially at or above the theoretical solubility of methane at STP for this gas mixture (19.3 mg/L), consistent with a reduction in solubility with a reduced mole fraction of methane in the gas phase. Samples with concentrations higher than solubility are likely the result of small gas bubbles entering the first vial collected after dissolution has begun. Concentrations then return below solubility after 1 pore volume. Methane concentrations show a decreasing trend, though the data is more sporadic until 4 pore volumes, at which point concentrations are less scattered and begin to decrease significantly as methane leaves the system. Similar to the SC1-4 experiments, the rate of dissolution decreases at 8 pore volumes as the source is largely depleted, although a small quantity of methane persists in the column after 12 pore volumes. Concentrations of both ethane and propane also exhibit higher than solubility concentrations until 1 pore volume. Ethane and propane concentrations decrease gradually after 1 pore volume, with the most significant decreases coming between 4 and 8 pore volumes. Notably, while ethane is at a higher concentration in the source gas, the two have nearly identical aqueous concentrations by 6 pore volumes. As with methane, low concentrations are maintained for ethane and propane up until 12 pore volumes. The MC-Sim simulation overestimates the concentrations of all three components at early time (2-4 pore volumes), but the overestimation is most apparent for methane, and is minor for ethane and propane. Concentrations are accurately predicted to decrease between 4 and 8 pore volumes. Concentrations at late time (8-12) pore volumes are underestimated, with concentrations of all three components near 1 mg/L despite predictions near zero. Similar to the SC-Sim simulation, the simulated concentration plateau at early time was not observed.

The behaviour for nitrogen and oxygen concentrations is the same in MC-Sim as SC-Sim. Oxygen breaks through first at 3.3 pore volumes due to its higher solubility, with nitrogen breaking through at 4.7 pore volumes. The behaviour of oxygen is non-monotonic as concentrations increase to 10

mg/L before decreasing to 8 mg/L. Both nitrogen and oxygen plateau at 12 pore volumes, at concentrations equal to the influent dissolved gas concentrations. Methane concentrations decrease by 1 mg/L at 3.94 pore volumes, ethane concentrations decrease by 1 mg/L at 3.25 pore volumes and propane concentrations decrease by 1 mg/L at 4.86 pore volumes. The timing of concentration decreases is again dictated by the Henry's constant of each component and their partial pressures. In comparison to SC-Sim, methane concentrations decrease 0.54 pore volumes later in MC-Sim. Gas saturation in MC-Sim follows a very similar trend as in SC-Sim, with a final gas saturation of 0.088 compared to 0.09. The predicted S_g for MC-Sim matches the measured final measured S_g in MC1-4 of 0.094 ± 0.015 (95% confidence interval on the mean). Thus, trapped gas remains in the system despite all components of the initial gas mixture having left the system.

Figure 2.7 shows the time of extinction ($S_g = 0$) from the MC-BG simulations (50% methane). The time of extinction is lower than for the SC-BG simulations (100% methane) for low dissolved background gas concentrations. However, as f approaches 1, the time of extinction for both sources converge. Figure 2.7 shows that the persistence of gas in the subsurface is more sensitive to the background dissolved gas concentration than to the composition of the source gas.

The results from MC1-4 confirm that methane persists longer than ethane and propane due to its lower solubility. Therefore, the average $C1/(C2+C3)$ over experiments MC1-4 increased from 6.2 to 9.0, a 1.45 \times increase, after starting with a source gas ratio of 5.67 (Figure 2.8). An increase by the same relative amount would shift a gas signature from transitional to biogenic (e.g., 690 to 1000) despite the dissolved methane, ethane and propane concentrations in the original source gas not being clearly biogenic prior to dissolution.

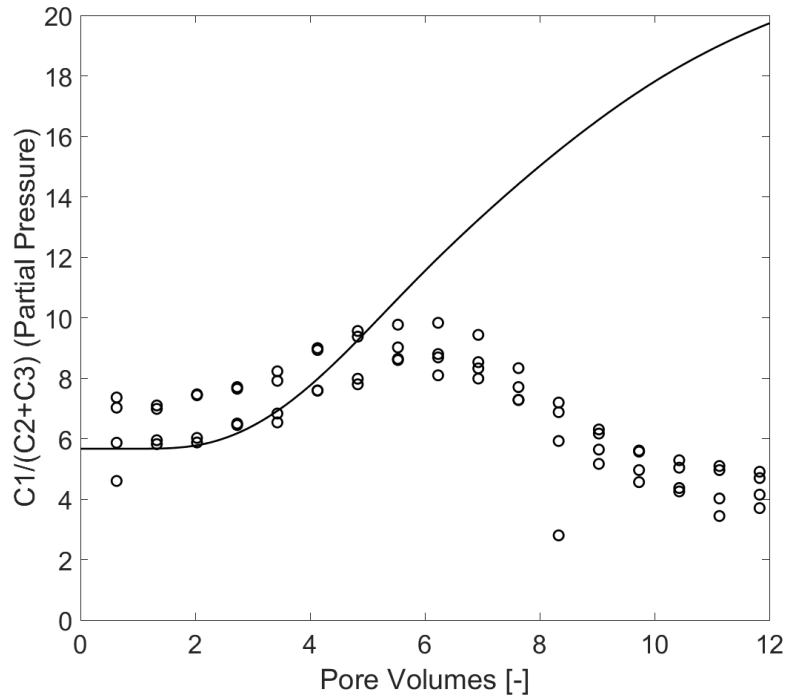


Figure 2.8. Hydrocarbon ratio over the duration of the multicomponent experiments (symbols) and MC-Sim simulations (line). Ratios are calculated in terms of partial pressure. The source gas has a hydrocarbon ratio of 5.67.

Results from MC-Sim showed increasing ratios with the decrease in all concentrations at early time, as ethane concentrations decreased earlier than methane and propane concentrations (Figure 2.8). However, at 5.5 pore volumes, the measured ratios of MC1-4 began to decrease until reaching an average of 4.36 at 12 pore volumes. This is lower than the source gas ratio of 5.67. At 5.5 pore volumes, the concentrations of ethane and propane began to level off at 1.5 mg/L, while methane concentrations continued to decrease. The concentrations of both ethane and propane plateau near 1.5 mg/L due primarily to rate-limited mass transfer, as the rate of mass transfer decreases when ethane and propane reach low concentrations. At 5.5 pore volumes, the average methane concentration was 9.72 mg/L, the average ethane concentration was 1.60 mg/L, and the average propane concentration was 1.34 mg/L. This leads to a decreasing ratio since methane concentrations are decreasing more than ethane and propane. At 12 pore volumes, all three components are at low

concentrations but still above the detection limit (1 ppm in the headspace), however ethane and propane remain in higher proportion than they would be at equilibrium with the source gas. This increase and subsequent decrease in hydrocarbon ratios shows that any analysis of transient ratios may become challenging when higher hydrocarbon chains are at low concentrations (< 1.5 mg/L).

The MC-Sim simulation agrees with the measured increase in hydrocarbon ratio until 5.5 pore volumes. The increase in ratio is a result of ethane's lower Henry's constant, and to a minor extent the slightly lower Henry's constant of propane, relative to methane. The concentrations of ethane and propane decrease before the methane concentrations, and the ratio increases. However, the simulations do not show a later decrease in ratio because the concentrations of each component continue to decrease to near zero according to the assumption of local equilibrium mass transfer. MIN3P does not consider the effects of rate-limited mass transfer observed in the experimental results, leading to continued decreases in ethane and propane concentrations and continued increases in hydrocarbon ratio. Therefore, while simulations may predict changes in hydrocarbon ratios at low concentrations, care must be taken when interpreting trends in low concentrations that are near detection limits.

The MC-Sources simulations were conducted to determine the change in ratio as a result of multicomponent source dissolution for a range of source compositions. Four different source gases were simulated, ranging from highly thermogenic to biogenic (Table 2). Figure 2.9 shows the results of these simulations, in which ratios are not longer calculated once any of the gases in the system is below the detection limit of 1 ppm in the headspace. The results of these simulations show an upward shift in hydrocarbon ratio regardless of the initial ratio. This shift would be observable in aqueous samples as concentrations of each component are above their detection limit. The ratio increases as methane is removed more slowly than ethane and propane.

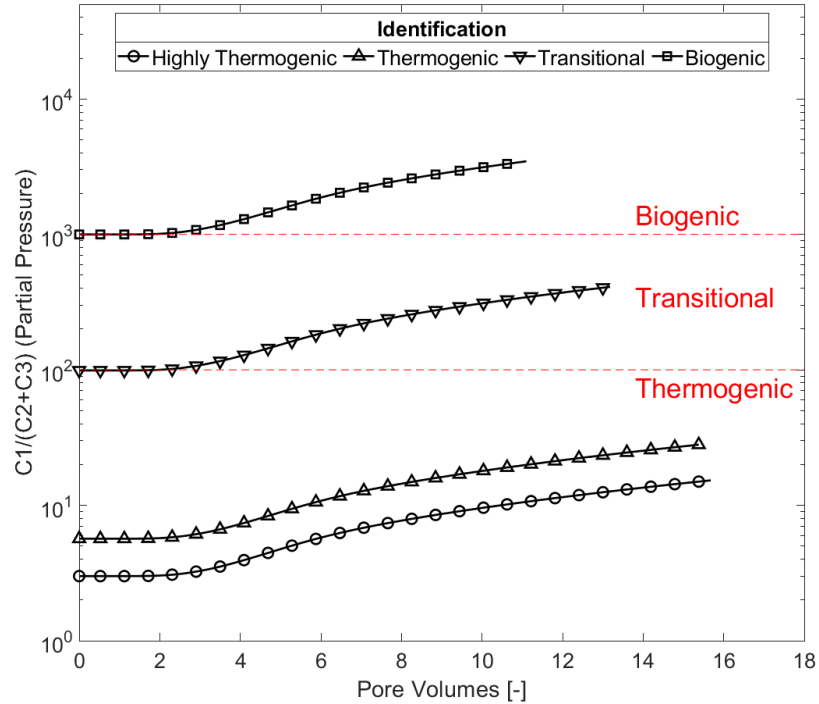


Figure 2.9. Hydrocarbon ratio during natural gas dissolution predicted in the MC-Sources simulations. Each line represents a different initial hydrocarbon ratio ranging from 3 (highly thermogenic - 75% methane) to 1000 (biogenic – 99.9% methane).

The severity of the increase is a function of dispersion in this system; a higher dispersivity will result in a lower change in ratio as the effects of different Henry's constants are 'smoothed', and these effects would need to be studied at larger scales. This finding further indicates the time-dependent nature of aqueous sampling for source identification. When using hydrocarbon ratios, the time between gas being trapped in the subsurface and a sample being collected can change the fingerprint of the gas. Further studies are required to determine whether the magnitude of the increase in ratio at the field scale will be sufficient to cause misidentification of thermogenic gas as either biogenic or transitional. Regardless, the observed variation of hydrocarbon ratios with time is further evidence that hydrocarbon ratio observations should be coupled with other fingerprinting techniques such as stable isotope characterization and the use of noble gases to provide additional lines of evidence.

2.5 Summary and Conclusions

Laboratory experiments and numerical modeling of the dissolution of trapped natural gas in porous media demonstrate that multicomponent mass transfer will impact hydrocarbon ratios (C_1/C_2+C_3) over time. The 1D dissolution experiments showed that hydrocarbon ratios can both increase and decrease with time. Increases in hydrocarbon ratio are due to differences in Henry's law constants for each component, with ethane and propane partitioning more readily to the aqueous phase and dissolving first. This increase was matched by simulations that assumed local equilibrium mass transfer. However, experimental data also showed a decrease in hydrocarbon ratios at later time as the concentration of ethane and propane remained above 1 mg/L rather decreased to zero while methane concentrations continued to decrease. Therefore, at low concentrations of each component, ratios may be less reliable for both trend analysis within a single well and source identification when compared to a gas sample. The decrease in hydrocarbon ratio was not matched by simulations, which predicted a constantly increasing hydrocarbon ratio. This discrepancy is likely due to the limitations of the local equilibrium assumption. Further work is required to understand the extent of hydrocarbon ratio changes in larger scale systems.

Importantly, these results demonstrate that the use of hydrocarbon ratios is time dependent, as hydrocarbon ratios are not constant as trapped gas dissolves. Simulations for a range of initial source gas compositions demonstrated that the increase in hydrocarbon ratio for a source gas depends on its composition. The magnitude of increase is greater for a biogenic or transitional source gas than for a thermogenic source. A transitional hydrocarbon signature could therefore be interpreted as biogenic if an adequate ratio shift occurred, and this should be explored in future work at the field scale. Additional lines of evidence are essential for the accurate identification of a source gas, particularly after a stray gas leak has stopped and gas compositions change during dissolution. Further work is needed in larger, heterogeneous systems to determine the impacts of dispersion on the magnitude of the change in ratios over time.

Experiments showed a rapid decrease in hydrocarbon concentrations during the dissolution of trapped gas at early time, followed by a slow decrease to low non-zero concentrations. Simulations accurately predicted the gas dissolution, though early time and late time predictions overestimated and underestimated concentrations, respectively, due to the local equilibrium assumption. Experiments showed that gas persisted despite low concentrations of the source gas due to multicomponent mass transfer effects. Simulations accurately predicted the final gas saturation measured in the experiments, and indicated that the gas remaining consisted of background gases dissolved in the influent water. As such, even for single-component gas sources, the presence of background dissolved gases impacts gas saturations, and multicomponent effects should be considered to understand the dissolution of stray gas. Simulations demonstrated that the dissolution of trapped gas is sensitive to dissolved background gases at low concentrations ($f < 0.4$). However, the dissolution behaviour becomes insensitive at higher dissolved background concentrations ($f > 0.4$). Gas persistence increases exponentially with dissolved gas concentrations. At low background gas concentrations, the gas is extinguished at the same time as the components of the source gas are removed. However, at high background gas concentrations, the gas can persist for hundreds of pore volumes. These conclusions are independent of the depth at which the gas dissolves. Therefore, the concentration of background dissolved gases relative to the water pressure will significantly impact the persistence of gas in the subsurface, and should be incorporated into numerical models of stray gas migration and dissolution. Furthermore, baseline sampling of dissolved gas concentrations will help to improve the understanding of gas dissolution for site investigations.

Multicomponent mass transfer effects should be considered for stray gas investigations to apply appropriate mitigation and remediations strategies. Caution should be taken when considering hydrocarbon ratios as they are both time and concentration dependent. The variation in ratios is an additional factor that indicates they should be coupled with other source identification techniques

such as isotopic signatures. Gas presence at a site, whether detected with a total dissolved gas probe or geophysical techniques, does not necessarily indicate that natural gas is present in the subsurface, as background dissolved gases can partition to the gaseous phase. Conversely, high gas saturations with low hydrocarbon concentrations may still indicate the presence of a leak at an earlier time. Importantly, multicomponent effects during dissolution must be considered even for a single-component source because gases in the background will impact gas persistence and dissolution of both single-component and multicomponent sources.

2.6 References

- Amos, R.T., Ulrich Mayer, K., 2006. Investigating the role of gas bubble formation and entrapment in contaminated aquifers: Reactive transport modelling. *J. Contam. Hydrol.* 87, 123-154. <https://doi.org/10.1016/j.jconhyd.2006.04.008>
- Bachu, S., 2017. GHG perspective – Gas migration outside well casing. *Int. J. Greenh. Gas Control* 61, 146–154. <https://doi.org/10.1016/j.ijggc.2017.04.003>
- Bernard, B.B., Brooks, J.M., Sackett, W.M., 1976. Natural gas seepage in the Gulf of Mexico. *Earth Planet. Sci. Lett.* 31, 48–54. [https://doi.org/10.1016/0012-821X\(76\)90095-9](https://doi.org/10.1016/0012-821X(76)90095-9)
- Cahill, A.G., Parker, B.L., Mayer, B., Mayer, K.U., Cherry, J.A., 2018. High resolution spatial and temporal evolution of dissolved gases in groundwater during a controlled natural gas release experiment. *Sci. Total Environ.* 622-623, 1178-1192. <https://doi.org/10.1016/j.scitotenv.2017.12.049>
- Cahill, A.G., Steelman, C.M., Forde, O., Kuloyo, O., Emil Ruff, S., Mayer, B., Ulrich Mayer, K., Strous, M., Cathryn Ryan, M., Cherry, J.A., Parker, B.L., 2017. Mobility and persistence of methane in groundwater in a controlled-release field experiment. *Nat. Geosci.* 10, 289-293. <https://doi.org/10.1038/ngeo2919>
- Cirpka, O.A., Kitanidis, P.K., 2001. Transport of volatile compounds in porous media in the presence of a trapped gas phase. *J. Contam. Hydrol.* 49, 263-285. [https://doi.org/10.1016/S0169-7722\(00\)00196-0](https://doi.org/10.1016/S0169-7722(00)00196-0)
- Council of Canadian Academies, 2014. Environmental Impacts of Shale Gas Extraction in Canada. Ottawa. <https://cca-reports.ca/reports/environmental-impacts-of-shale-gas-extraction-in-canada/>
- Darrah, T.H., Vengosh, A., Jackson, R.B., Warner, N.R., Poreda, R.J., 2014. Noble gases identify the mechanisms of fugitive gas contamination in drinking-water wells overlying the Marcellus and Barnett Shales. *Proc Natl Acad Sci U S A* 111, 14076–14081. <https://doi.org/10.1073/pnas.1322107111>

- Donaldson, J.H., Istok, J.D., Humphrey, M.D., O'Reilly, K.T., Hawelka, C.A., Mohr, D.H., 1997. Development and Testing of a Kinetic Model for Oxygen Transport in Porous Media in the Presence of Trapped Gas. *Ground Water*. 35, 270-279. <https://doi.org/10.1111/j.1745-6584.1997.tb00084.x>
- Donaldson, J.H., Istok, J.D., O'Reilly, K.T., 1998. Dissolved gas transport in the presence of a trapped gas phase: Experimental evaluation of a two-dimensional kinetic model. *Ground Water* 36, 133–142. <https://doi.org/10.1111/j.1745-6584.1998.tb01073.x>
- Dusseault, M., Jackson, R., 2014. Seepage pathway assessment for natural gas to shallow groundwater during well stimulation, in production, and after abandonment. *Environ. Geosci.* 21, 107–126. <https://doi.org/10.1306/eg.04231414004>
- Eby, P., Gibson, J.J., Yi, Y., 2015. Suitability of selected free-gas and dissolved-gas sampling containers for carbon isotopic analysis. *Rapid Commun. Mass Spectrom.* 29, 1215–1226. <https://doi.org/10.1002/rcm.7213>
- Etiopé, G., Feyzullayev, A., Milkov, A. V., Waseda, A., Mizobe, K., Sun, C.H., 2009. Evidence of subsurface anaerobic biodegradation of hydrocarbons and potential secondary methanogenesis in terrestrial mud volcanoes. *Mar. Pet. Geol.* 26, 1692–1703. <https://doi.org/10.1016/j.marpetgeo.2008.12.002>
- Forde, O.N., Mayer, K.U., Hunkeler, D., 2019. Identification, spatial extent and distribution of fugitive gas migration on the well pad scale. *Sci. Total Environ.* 652, 356–366. <https://doi.org/10.1016/j.scitotenv.2018.10.217>
- Fry, V.A., Istok, J.D., Semprini, L., O'Reilly, K.T., Buscheck, T.E., 1995. Retardation of Dissolved Oxygen Due to a Trapped Gas Phase in Porous Media. *Groundwater* 33, 391–398. <https://doi.org/10.1111/j.1745-6584.1995.tb00295.x>
- Geistlinger, H., Beckmann, A., Lazik, D., 2005. Mass transfer between a multicomponent trapped gas phase and a mobile water phase: Experiment and theory. *Water Resour. Res.* 41, 1-15. <https://doi.org/10.1029/2004WR003885>
- Ghaderi, S.M., Keith, D.W., Lavoie, R., Leonenko, Y., 2011. Evolution of hydrogen sulfide in sour saline aquifers during carbon dioxide sequestration. *Int. J. Greenh. Gas Control* 5, 347–355. <https://doi.org/10.1016/j.ijggc.2010.09.008>
- Glass, R.J., Conrad, S.H., Yarrington, L., 2001. Gravity-destabilized nonwetting phase invasion in macroheterogeneous porous media: Near-pore-scale macro modified invasion percolation simulation of experiments. *Water Resour. Res.* 37, 1197–1207. <https://doi.org/10.1029/2000WR900294>
- Hendry, J.M., Barbour, L.S., Schmeling, E.E., Mundle, S.O.C., Huang, M., 2016. Water Resources Research. *J. Am. Water Resour. Assoc.* 5, 6440-6450. <https://doi.org/10.1111/j.1752-1688.1969.tb04897.x>

- Holocher, J., Peeters, F., Aeschbach-Hertig, W., Kinzelbach, W., Kipfer, R., 2003. Kinetic model of gas bubble dissolution in groundwater and its implications for the dissolved gas composition. *Environ. Sci. Technol.* 37, 1337–1343. <https://doi.org/10.1021/es025712z>
- Kampbell, D.H., Vandegrift, S.A., 1998. Analysis of Dissolved Methane, Ethane, and Ethylene in Ground Water by a Standard Gas Chromatographic Technique. *J. Chromatogr. Sci.* 36, 253–256. <https://doi.org/10.1093/chromsci/36.5.253>
- Kelly, W.R., Matisoff, G., Fisher, J.B., 1985. The effects of a gas well blow out on groundwater chemistry. *Environ. Geol. Water Sci.* 7, 205–213. <https://doi.org/10.1007/BF02509921>
- Klazinga, D.R., Steelman, C.M., Cahill, A.G., Walton, K.M., Endres, A.L., Parker, B.L., 2019. Methane gas transport in unconfined aquifers: A numerical sensitivity study of a controlled release experiment at CFB Borden. *J. Contam. Hydrol.* 225, 103506. <https://doi.org/10.1016/j.jconhyd.2019.103506>
- Larson, T.E., Nicot, J.P., Mickler, P., Castro, M.C., Darvari, R., Wen, T., Hall, C.M., 2018. Monitoring Stray Natural Gas in Groundwater With Dissolved Nitrogen. An Example From Parker County, Texas. *Water Resour. Res.* 6024–6041. <https://doi.org/10.1029/2018WR022612>
- Lassen, R.N., Plampin, M., Sakaki, T., Illangasekare, T.H., Gudbjerg, J., Sonnenborg, T.O., Jensen, K.H., 2015. Effects of geologic heterogeneity on migration of gaseous CO₂ using laboratory and modeling investigations. *Int. J. Greenh. Gas Control* 43, 213–224. <https://doi.org/10.1016/j.ijggc.2015.10.015>
- Mayer, K.U., Frind, E.O., Blowes, D.W., 2002. Multicomponent reactive transport modeling in variably saturated porous media using a generalized formulation for kinetically controlled reactions. *Water Resour. Res.* 38, 1174–1195. <https://doi.org/10.1029/2001WR000862>
- McIntosh, J.C., Hendry, M.J., Ballentine, C., Haszeldine, R.S., Mayer, B., Etiope, G., Elsner, M., Darrah, T.H., Prinzhofer, A., Osborn, S., Stalker, L., Kuloyo, O., Lu, Z.T., Martini, A., Lollar, B.S., 2019. A Critical Review of State-of-the-Art and Emerging Approaches to Identify Fracking-Derived Gases and Associated Contaminants in Aquifers. *Environ. Sci. Technol.* 53, 1063–1077. <https://doi.org/10.1021/acs.est.8b05807>
- McMahon, P.B., Belitz, K., Barlow, J.R.B., Jurgens, B.C., 2017. Methane in aquifers used for public supply in the United States. *Appl. Geochemistry* 84, 337–347. <https://doi.org/10.1016/j.apgeochem.2017.07.014>
- Milkov, A. V., Etiope, G., 2018. Revised genetic diagrams for natural gases based on a global dataset of >20,000 samples. *Org. Geochem.* 125, 109–120. <https://doi.org/10.1016/j.orggeochem.2018.09.002>
- Miller, J.N., Miller, J.C., 2005. *Statistics and Chemometrics for Analytical Chemistry*, Fifth edit. ed. Pearson Education Limited.

- Molins, S., Mayer, K.U., 2007. Coupling between geochemical reactions and multicomponent gas and solute transport in unsaturated media: A reactive transport modeling study. *Water Resour. Res.* 43. <https://doi.org/10.1029/2006WR005206>
- Molofsky, L.J., Connor, J.A., McHugh, T.E., Richardson, S.D., Woroszylo, C., Alvarez, P.J., 2016. Environmental Factors Associated With Natural Methane Occurrence in the Appalachian Basin. *Groundwater* 54, 656–668. <https://doi.org/10.1111/gwat.12401>
- Molofsky, L.J., Connor, J.A., Wylie, A.S., Wagner, T., Farhat, S.K., 2013. Evaluation of Methane Sources in Groundwater in Northeastern Pennsylvania. *Groundwater*. 51, 333-349. <https://doi.org/10.1111/gwat.12056>
- Moritz, A., Hélie, J.F., Pinti, D.L., Larocque, M., Barnetche, D., Retailleau, S., Lefebvre, R., Gélinas, Y., 2015. Methane baseline concentrations and sources in shallow aquifers from the shale gas-prone region of the St. Lawrence lowlands (Quebec, Canada). *Environ. Sci. Technol.* 49, 4765–4771. <https://doi.org/10.1021/acs.est.5b00443>
- Mumford, K.G., Smith, J.E., Dickson, S.E., 2010. The effect of spontaneous gas expansion and mobilization on the aqueous-phase concentrations above a dense non-aqueous phase liquid pool. *Adv. Water Resour.* 33, 504-513. <https://doi.org/10.1016/j.advwatres.2010.02.002>
- Nicot, J.P., Larson, T., Darvari, R., Mickler, P., Slotten, M., Aldridge, J., Uhlman, K., Costley, R., 2017. Controls on Methane Occurrences in Shallow Aquifers Overlying the Haynesville Shale Gas Field, East Texas. *Groundwater* 55, 443–454. <https://doi.org/10.1111/gwat.12500>
- Prinzhofer, A., Battani, A., 2003. Gas isotopes tracing: An important tool for hydrocarbons exploration. *Oil Gas Sci. Technol.* 58, 299–311. <https://doi.org/10.2516/ogst:2003018>
- Roy, N., Molson, J., Lemieux, J.M., Van Stempvoort, D., Nowamooz, A., 2016. Three-dimensional numerical simulations of methane gas migration from decommissioned hydrocarbon production wells into shallow aquifers. *Water Resour. Res.* 52, 5598-5618. <https://doi.org/10.1002/2016WR018686>
- Schout, G., Hartog, N., Hassanizadeh, S.M., Helmig, R., Griffioen, J., 2020. Impact of groundwater flow on methane gas migration and retention in unconsolidated aquifers. *J. Contam. Hydrol.* 230. <https://doi.org/10.1016/j.jconhyd.2020.103619>
- Schroth, M.H., Istok, J.D., Ahearn, S.J., Selker, J.S., 1996. Characterization of Miller-Similar Silica Sands for Laboratory Hydrologic Studies. *Soil Sci. Soc. Am. J.* 60, 1331. <https://doi.org/10.2136/sssaj1996.03615995006000050007x>
- Soltanian, M.R., Amooie, M.A., Cole, D.R., Darrah, T.H., Graham, D.E., Pfiffner, S.M., Phelps, T.J., Moortgat, J., 2018. Impacts of Methane on Carbon Dioxide Storage in Brine Formations. *Groundwater* 56, 176–186. <https://doi.org/10.1111/gwat.12633>
- US Environmental Protection Agency - US EPA, 2016. Hydraulic Fracturing for Oil and Gas: Impacts from the Hydraulic Fracturing Water Cycle on Drinking Water Resources in the United States (Main Report - EPA/600/R-16/236fa).

- Van De Ven, C.J.C., Abraham, J.E.F., Mumford, K.G., 2020. Laboratory investigation of free-phase stray gas migration in shallow aquifers using modified light transmission. *Adv. Water Resour.* 139, 103543. <https://doi.org/10.1016/j.advwatres.2020.103543>
- Van De Ven, C.J.C., Mumford, K.G., 2020a. Intermediate-Scale Laboratory Investigation of Stray Gas Migration Impacts: Methane Source Architecture and Dissolution. *Environ. Sci. Technol.* 54, 6299–6307. <https://doi.org/10.1021/acs.est.0c00456>
- Van De Ven, C.J.C., Mumford, K.G., 2020b. Aqueous and surface expression of subsurface GHGs: Subsurface mass transfer effects. *Water Res.* 170, 115327. <https://doi.org/10.1016/j.watres.2019.115327>
- Whiticar, M.J., 1999. Carbon and hydrogen isotope systematics of bacterial formation and oxidation of methane. *Chem. Geol.* 161, 291–314. [https://doi.org/10.1016/s0009-2541\(99\)00092-3](https://doi.org/10.1016/s0009-2541(99)00092-3)

Chapter 3

Calculation of gas ratios for use in source identification for stray gas migration

3.1 Introduction

Advances in energy development of deep geologic formations has led to an increase in natural gas production in North America (Rice et al., 2018). An increased number of new wells, in addition to existing abandoned wells, has raised concerns of groundwater contamination resulting from stray gas migration. Energy wells can leak due to improper well completion, interception of intermediate gas formations, or casing degradation (Darrah et al., 2015; Dusseault and Jackson, 2014). Regardless of the failure mechanism, stray gas can migrate vertically along compromised wells and potentially be released into the surrounding formation, migrating laterally and potentially impacting shallow aquifers (Cahill et al., 2018; Klazinga et al., 2019). The natural gas released consists primarily of methane (C1), ethane (C2), and propane (C3).

Stray gas is expressed in two ways i) surface expression, in which stray gas reaches the surface and is emitted to the atmosphere, and/or ii) aqueous expression, in which stray gas dissolves into groundwater (Van De Ven and Mumford, 2020). Surface expression presents safety concerns, as high methane concentrations can lead to explosions or well blowout (Schout et al., 2017; USEPA, 2016). Surface expression can also contribute to atmospheric methane emissions and present an additional source of greenhouse gases to the atmosphere (Forde et al., 2019; Kang et al., 2014; Van De Ven and Mumford, 2020). Aqueous expression also presents concern, as high methane presence can degrade water quality including changes in pH, reduction of sulfate to hydrogen sulfide and production of alkalinity (Kelly et al., 1985; Vengosh et al., 2014). Stray gas investigations can be triggered by water quality concerns in domestic supply wells (Gorody, 2012) or by evidence of surface efflux such as bubbling at a well head, increased CH₄ in air measurements via LEL

monitoring in wells or surface flux chambers, or stressed vegetation (BCOGC, 2020; Forde et al., 2019). Upwards gas migration can be slowed by gas dissolution into groundwater and low permeability heterogeneities such that surface expression can take years to occur after a leak (Schout et al., 2020; Van De Ven and Mumford, 2020). As such, aqueous sampling remains a key component of stray gas migration investigations.

When a suspected leak is detected, the origin of the gas needs to be determined (Barth-Naftilan et al., 2018; McIntosh et al., 2019; Nicot et al., 2017). Methane in the subsurface is categorized as either biogenic or thermogenic. Biogenic methane is the result of microbial breakdown of organic material and thermogenic methane is the result of abiotic degradation of organic material at high temperatures deep in the subsurface (Molofsky et al., 2013). Natural gas production typically extracts thermogenic-source gas (Kang et al., 2014; Molofsky et al., 2016a; Whiticar, 1990). Biogenic- and thermogenic-source gases can be distinguished by both their isotopic signature and their hydrocarbon ratios ($C1/(C2+C3)$) (Cahill et al., 2018; Cesar et al., 2020; Molofsky et al., 2013). Biogenic sources typically have a hydrocarbon ratio greater than 1000 and a stable carbon isotopic signature greater than $-50\text{‰ } \delta C^{13}\text{-CH}_4$, and thermogenic sources typically have a hydrocarbon ratio less than 100 and a stable carbon isotopic signature less than $-50\text{‰ } \delta C^{13}\text{-CH}_4$ (Bernard et al., 1978; Cahill et al., 2018; Molofsky et al., 2013). These distinctions are empirical, and thus their suitability for any specific site investigation relies partly on their geological environment and the target formation (McIntosh et al., 2019). Additionally, non-hydrocarbon gases may be present in a target formation and can be used for source identification. For example, helium is used as a tracer for sources where the source gas contains a significant portion of helium, and sampling results can be classified based on ratios such as He/CH_4 (Darrah et al., 2015; Harkness et al., 2017).

While it makes a stronger case to identify the origin of stray gas by considering both the isotopic and compositional fingerprint of aqueous samples, some investigations rely primarily on compositional analysis, due to the low cost of dissolved gas analysis relative to isotopic analysis or due to multiple potential sources with similar isotopic signatures. However, the reliability of dissolved gas composition is subject to change due to post-genetic processes such as microbial oxidation and mixing (Cahill et al., 2018; Etiope et al., 2009; McIntosh et al., 2019). These processes alone call into question the suitability of hydrocarbon ratios as the primary identification technique and require appropriate interpretation and may require additional lines of evidence to properly identify a source. Regardless of other processes that affect gas composition, it is important that in cases where these ratios are used, the ratios are calculated appropriately and consistently across studies. Hydrocarbon ratios are unitless, and as such, different studies may use different data to calculate the ratios, including aqueous concentration, mole fraction in the headspace, or equivalent gas pressure. So long as the calculation method is consistent, the use of any specific method will not impact the use of ratios for trend analysis within a single study or single well composition over time. This does however present challenges and the potential for misinterpretation for hydrocarbon ratios used for source identification or inter-comparison between studies. As more investigations are conducted, there will be more opportunity for comparison of dissolved gas ratios between sites and sources, and as such it is important that comparisons are made based on an equivalent basis.

Dissolved gas samples are typically groundwater samples collected in either flexible bags such as an IsoFlask, or in VOA vials (Molofsky et al., 2016b). The analysis for both containers relies on analysis of gas in the headspace of the container via gas chromatography to determine the composition of the aqueous sample, assuming equilibrium between the aqueous and gas phases. Laboratory results from dissolved gas samples are typically expressed as mole fraction in the headspace of each gas, or an equivalent aqueous concentration (mg/L or mol/L). This aqueous

concentration is calculated from the headspace composition, by assuming that all mass in the sample can be attributed to the aqueous phase through a mass balance and Henry's Law partitioning (Kampbell and Vandegrift, 1998). While the gas in the headspace used for analysis is at equilibrium with the water in the sample, dictated by the volume of water and gas, that does not mean that the fraction of each component in the headspace is the same as in the gas that initially dissolved into the water which was sampled, even if post-genetic changes are negligible. This is a result of differing temperature and pressure conditions during sample analysis compared to those during initial gas dissolution.

In this study, a set of calculations was conducted to determine the differences between dissolved gas ratios when calculated with different units, based on both headspace and total mass. The calculations analyze a hypothetical aqueous sample as it moves from the subsurface to the analytic lab, and the resulting changes in gas ratios. The objective was to establish the method to calculate the hydrocarbon ratio based on the analysis of an aqueous sample that would accurately match a source gas composition in the absence of post-genetic changes. This method could then serve as the standard method to calculate dissolved gas ratios such that data between stray gas site investigations can be compared more easily, and improve the accuracy of hydrocarbon ratios from aqueous samples used as a source identification technique.

3.2 Conceptual Model and Calculation Approach

3.2.1 Conceptual Model

The conceptual model for stray gas migration, sample collection, and sample analysis is shown in Figure 3.1. When a source gas migrates into a heterogeneous shallow aquifer, it may travel laterally beneath low permeability layers. The gas partitions into the aqueous phase and the dissolved gases are transported downgradient. This partitioning is assumed to occur under local equilibrium conditions for slow groundwater velocities at most sites (Geistlinger et al., 2005).

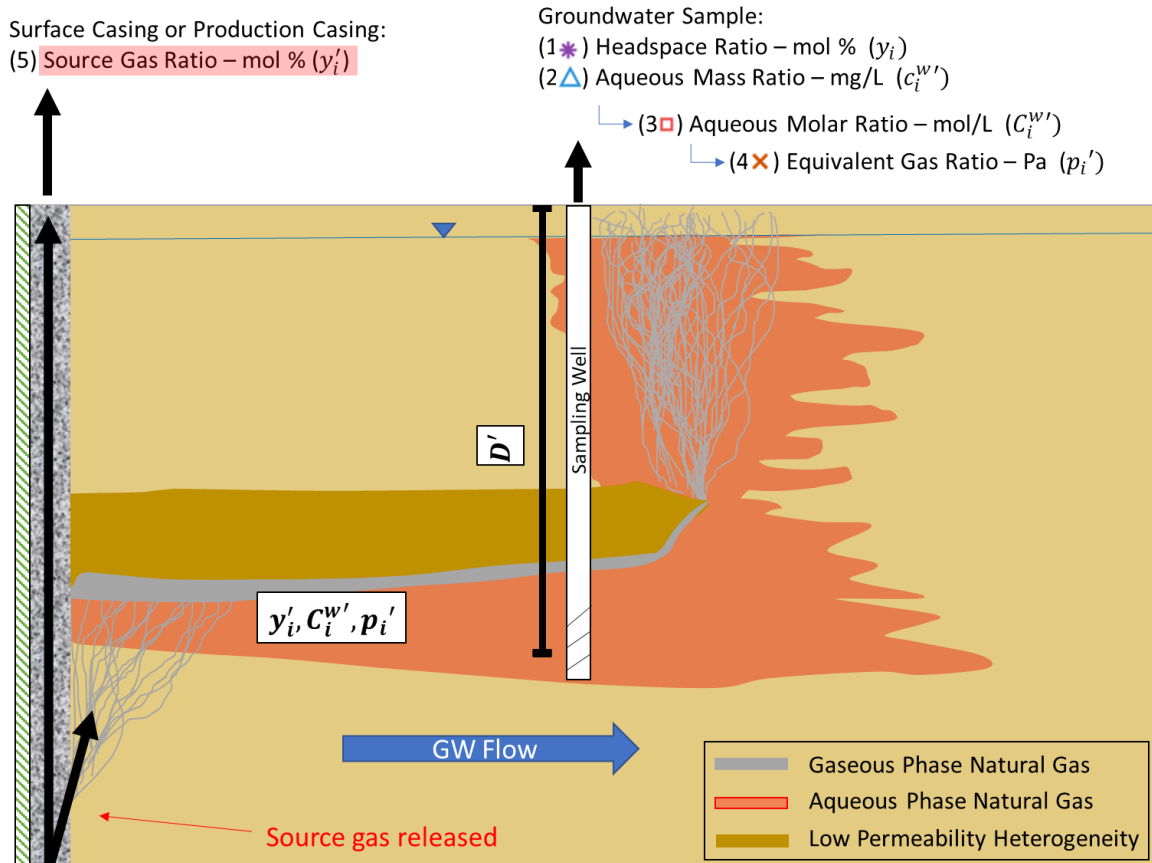


Figure 3.1. Conceptual model of a gas leak from an energy well that travels up along the outside of the well from either the production formation or an intermediate non-target formation. Source gas is collected from the surface casing and groundwater samples are collected downgradient of the leak.

The dissolved gas concentration in the aqueous phase is a function of the partial pressure of each component in the trapped gas phase at its in situ depth, dictated by the water and capillary pressures, and their respective Henry's Law coefficients. Samples of water containing the dissolved gases are collected at depth (D'), assumed to be collected in such a way that any exsolved gas created by bringing the sample to surface is captured in the sampling vessel. The depth of sample collection must be considered in the analysis because the gas pressure increases with hydrostatic pressure. As such, the deeper the sample the greater the potential for exsolution during sampling (Banks et al., 2017). For this study, the samples are assumed to be collected in an IsoFlask or similar vessel in

which the bag can expand such that a headspace can develop, and that headspace is at atmospheric pressure. Additionally, it is assumed that no degassing occurs outside the IsoFlask, and that there are no interactions with the atmosphere during sampling.

3.2.2 Ratio Definitions

Four different methods of calculating the hydrocarbon ratio ($C_1/(C_2+C_3)$) from an aqueous sample are described below, based on data commonly obtained during sample analysis: headspace ratio, aqueous mass ratio, aqueous molar ratio, and equivalent gas ratio. These were compared to the source gas ratio, which is representative of gas collected from a surface casing that has no contact with the surrounding groundwater. The headspace ratio is calculated using the mole fraction in the headspace:

$$HS = \frac{y_{C_1}}{y_{C_2} + y_{C_3}} \quad (3.1)$$

where HS is the headspace ratio, and y is the mole fraction in the headspace of the sampling vessel. The aqueous mass ratio is calculated based on the aqueous concentration of the dissolved gases, expressed as a mass concentration:

$$AMS = \frac{c_{C_1}^{w'}}{c_{C_2}^{w'} + c_{C_3}^{w'}} \quad (3.2)$$

where AMS is the aqueous mass ratio and c is concentration [mg L^{-1}]. The aqueous concentration assumes all gas in the sample was dissolved in the aqueous phase at the sample collection depth (D'). In all equations, ' indicates conditions at the sampling depth rather than the conditions under which sample analysis is conducted. The aqueous molar ratio is calculated using the same aqueous concentration of the dissolved gases but expressed as a molar concentration:

$$\text{AMO} = \frac{C_{C1}^{w'}}{C_{C2}^{w'} + C_{C3}^{w'}} \quad (3.3)$$

where AMO is the aqueous molar ratio and C is the concentration [mol L^{-1}]. All three of these ratios are derived from the values commonly reported by analytical laboratories. The equivalent gas ratio is calculated by converting the aqueous molar concentration of each component to a partial pressure according to Henry's Law. This is representative of the partial pressure of a gas in equilibrium with the water at the sampling depth:

$$\text{EQG} = \frac{p_{C1}'}{p_{C2}' + p_{C3}'} \quad (3.4)$$

where EQG is the equivalent gas ratio and p is the partial pressure [Pa]. Source gas samples are collected as gaseous samples:

$$\text{SG} = \frac{y'_{C1}}{y'_{C2} + y'_{C3}} \quad (3.5)$$

where SG is the source gas ratio and y' is the mole fraction in the gas sample. For source identification, SG is assumed to be the 'true' ratio, as the goal of source identification is to match the ratio of hydrocarbons in the aqueous sample to that of the source. Therefore, the most appropriate ratio to use when analyzing aqueous sample results is that which most accurately represents the gas origin.

3.2.3 Ratio Calculations

The following set of equations follows the evolution of a source gas as it partitions at depth to the aqueous phase and is then sampled, brought to surface and the headspace is then analyzed by gas chromatography (GC) (Figure 3.2). This was used to simulate sample collection and create a set of

hypothetical sample results with known composition from a known gas source, and was used to compare the accuracy of the HS, AMS, AMO and EQG ratios.

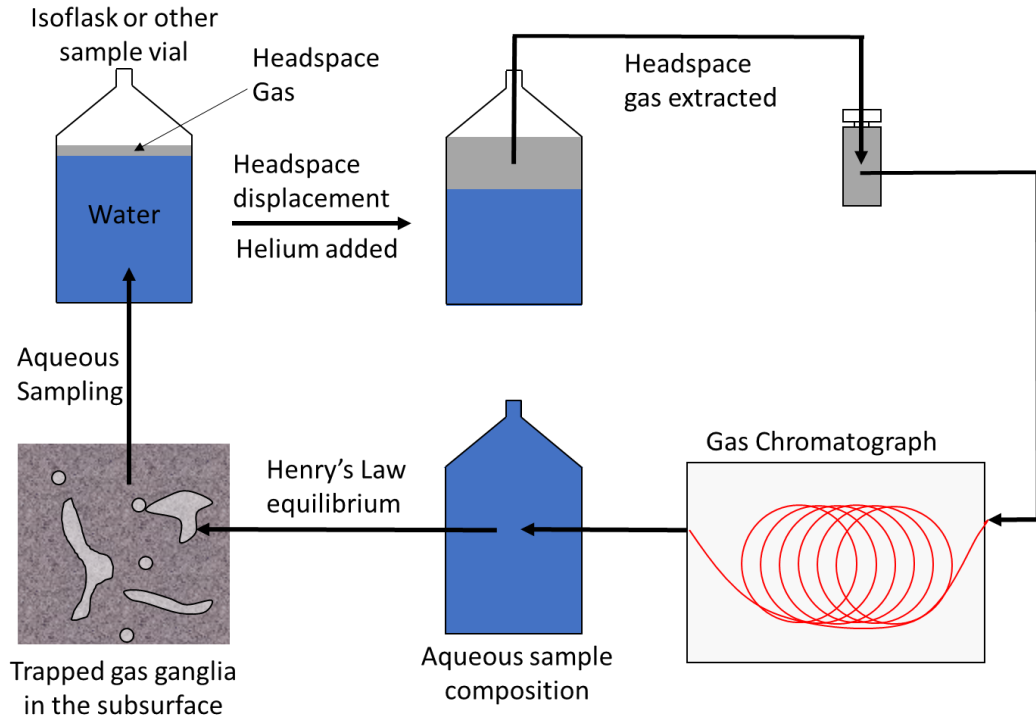


Figure 3.2. Analysis process for a dissolved gas sample beginning with a source gas partitioning to the aqueous phase. The dissolved gas is collected through aqueous sampling, and measured by headspace displacement. After the headspace gas is measured by GC analysis, mass balance calculations are used determine the dissolved gas composition. Through Henry's Law equilibrium calculations, the initial composition is determined based on the dissolved gas composition.

Assuming negligible capillary pressure, hydrostatic pressure is a reasonable approximation for the total gas pressure at depth:

$$P' = P + \rho g D' \quad (3.6)$$

where P' is the total gas pressure at depth [Pa], P is atmospheric pressure [Pa], ρ is the density of water [g m^{-3}] and g is gravitational acceleration [m s^{-2}]. The partial pressure of each gas component at depth is calculated based on the mole fraction of each component in the source gas:

$$p'_i = y_i' P' \quad (3.7)$$

where p'_i is the partial pressure of component i at depth [Pa]. The molar concentration in the water at depth is:

$$C_i^{w'} = \frac{p'_i}{H_i} \quad (3.8)$$

where H_i [$\text{Pa m}^3 \text{ mol}^{-1}$] is the Henry's law coefficient of component i . Note that increased temperature and pressure at depth is neglected for the Henry's Law constants used here. The number of moles in the water collected during sampling can then be calculated from the volume of water collected (either 250 mL or 500 mL in this study):

$$n_i^{w'} = C_i^{w'} V^w \quad (3.9)$$

where $n_i^{w'}$ is the number of moles of component i in the water at depth, and V^w is the volume of water collected [m^3]. The water is then brought to surface, and a new equilibrium is established within the sampling vessel while conserving the moles of each component ($n_i^{w'} = n_i^w + n_i^g$). The moles in the water are calculated as:

$$n_i^w = \frac{p_i V^w}{H_i} \quad (3.10)$$

where n_i^w is the moles of component i in the water at surface, and p_i is the partial pressure of component i at surface [Pa]. The moles in the gas are calculated as:

$$n_i^g = \frac{p_i V^g}{RT} \quad (3.11)$$

where n_i^g is the moles of component i in the water at surface, V^g is the volume of gas in the headspace, R is the ideal gas constant and T is temperature. The partial pressure of each component can therefore be written as:

$$p_i = \frac{n_i^{w'} H_i RT}{V^g H_i + V^w RT} \quad (3.12)$$

Applying Dalton's law, a set of equations is written to solve for the volume of gas V^g generated by exsolution when the sample bag is at atmospheric pressure:

$$P = \sum p_i = \sum \frac{n_i^{w'} H_i RT}{V^g H_i + V^w RT} \quad (3.13)$$

If the headspace volume was determined to greater than 30 mL based only on exsolution, it was assumed that there was enough gas for headspace analysis and the composition was defined by equation 3.12. If less than 30 mL, helium was added to create a 30 mL headspace before applying equation 3.12. The mole fraction in the headspace was then calculated as:

$$y_i = \frac{p_i}{P} \quad (3.14)$$

where y_i is the mole fraction in the headspace. Analytical results are typically reported as mole fraction in the headspace (y_i) or as an aqueous concentration ($C_i^{w''}$ or $c_i^{w''}$) calculated according to Kampbell and Vandegrift (1998).

3.2.4 Dissolved Gas Sampling Scenarios

Four scenarios were used to investigate the differences between ratios (equations 3.1 to 3.4) (Table 3.1). For all scenarios, it was assumed that the water sample volume was 500 mL except for selected calculations in Scenario 1, and that a minimum of 30 mL of headspace was present, either created

by exsolution or by additional helium. All scenarios consider a biogenic source gas with an initial $C1/(C2+C3) = 1000$. Scenario 1 is the base case in which a source gas is at local equilibrium with the aqueous phase, and is collected into an IsoFlask. In Scenario 2 the sample is subjected to dilution during collection, such that water in direct contact with the source gas was mixed with surrounding groundwater that contains no dissolved gases. Calculations were performed using a dilution factor to simulate the dilution process at a fixed depth of 30 m. Scenario 3 also considered dilution at depth during sample collection, but with air-saturated water (ASW), which results in a sample composed of 10% water with dissolved hydrocarbons and 90% air-saturated water. The number of moles in the water of each hydrocarbon component is calculated as:

$$n_i^{w'} = FC_i^{w'}V^w \quad (3.15)$$

where F is the dilution factor. Scenario 4 considered the use of He/CH₄ for source identification for a source gas with helium present. Table 3.2 shows the Henry's Law coefficients used in each scenario.

Table 3.1. Scenarios for gas sampling and analysis calculations

Scenario	Description	C1	C2	C3	Other Gases
1	Base case	99.9%	0.07%	0.03%	--
2	Dilution with gas-free water	99.9%	0.07%	0.03%	--
3	Dilution with ASW	99.9%	0.07%	0.03%	79% N ₂ , 21% O ₂
4	Helium in source gas	97.94%	0.068%	0.029%	1.96% He

Table 3.2. Henry’s Law coefficients for volatile compounds

Name	Formula	Henry’s Law (H) coefficient at 298K (Pa m ³ mol ⁻¹)*
Oxygen	O ₂	8.04×10^4
Nitrogen	N ₂	1.53×10^5
Methane	CH ₄	7.14×10^4
Ethane	C ₂ H ₆	5.26×10^4
Propane	C ₃ H ₈	6.66×10^4
Helium	He	2.56×10^5

*From Sander (2015)

3.3 Results and Discussion

3.3.1 Headspace Ratio

Scenario 1 is used to outline the differences in ratios for a base case (Figure 3.3).

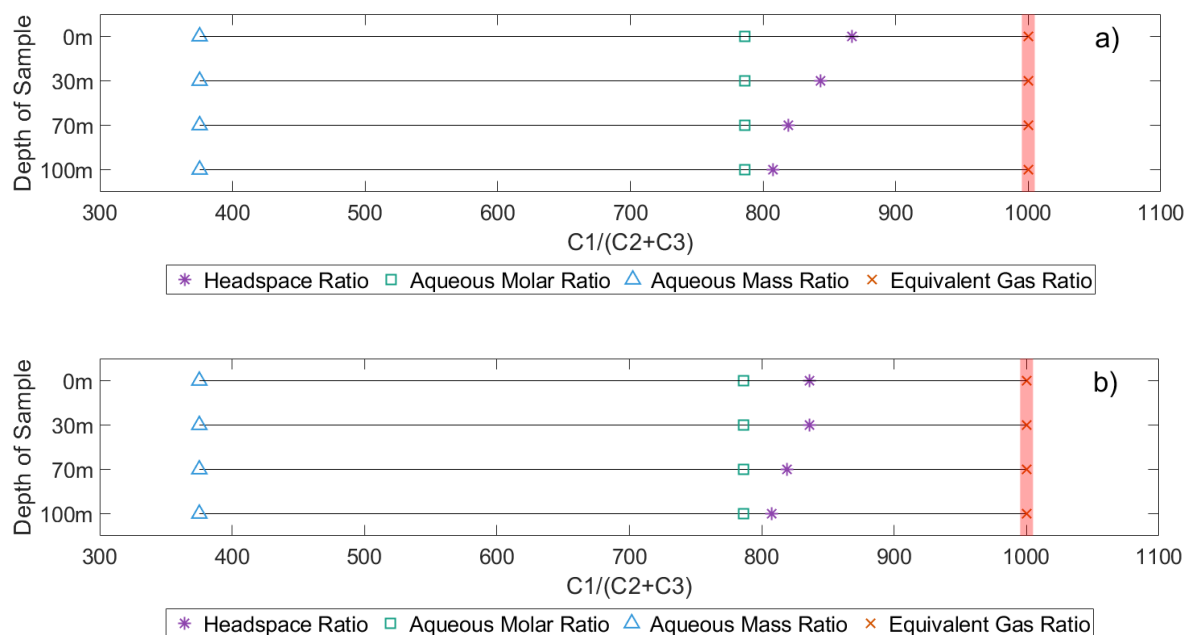


Figure 3.3. Different compositional ratios for an initial source gas with a hydrocarbon ratio of 1000 (highlighted in red). Each line represents a different depth of sample to simulate higher hydrostatic pressure and thus higher gas solubility for a) 500 mL of sample collected, and b) 250 mL of sample collected.

The headspace ratio (purple asterisks, Figure 3.3) is lower than the source gas ratio (red bar) by a factor of 1.15 (1000/867 at 0 m) to 1.24 (1000/807.4 at 100 m), depending on the depth at which the sample is collected. The magnitude of the difference between these ratios increases as depth increases. This is a result of increased gas solubility at greater depths; as the solubility increases, water in contact with the source gas will have greater concentrations of each component resulting in increased exsolution during sampling and a larger headspace in the sample bag. Both ethane and propane partition more readily to the aqueous phase than methane (a greater molar concentration for an equal partial pressure). Consequently, at depth, the mole fraction of ethane and propane in the aqueous phase is greater than in the source gas, resulting in an aqueous molar ratio that is less than the source gas ratio (Figure 3.3). At surface, a headspace develops, and methane partitions preferentially to the gaseous phase. However, with the large headspace that develops, the mole fraction of methane in the gas at surface is lower relative to its mole fraction in the gas at depth. Therefore, the use of mole fraction in the headspace of an aqueous sample does not accurately represent the composition of the original source gas. In the context of hydrocarbon ratios, using the headspace ratio will underestimate the source hydrocarbon ratio. The magnitude of the underestimation depends on the gas pressure at depth. If an infinitely small headspace developed and was sampled, $p_i = p'_i$ and the headspace ratio is equal to the source gas ratio. Conversely, for an infinitely deep sample which develops an infinitely large headspace, the headspace ratio will approach the ratio of moles in the water at depth, $n_i^{w'}$. This result also depends on the sample volume (Figure 3.3b). When a lower sample volume is collected, the volume of gas that partitions to the headspace is reduced. With 500 mL of water collected, only samples from 0 m depth require headspace displacement using helium, whereas with 250 mL of water, 0 m and 30 m depth samples require headspace displacement. The ratios for samples which require headspace displacement have a fixed error, whereas those which can exsolve enough gas to create a headspace vary with depth. This is due to the partial pressure of each component being calculated with a fixed gas volume.

When comparing samples that require headspace displacement in Figure 3.3a and Figure 3.3b, the error is greater in Figure 3.3b as V^w has been reduced. The dependence of headspace ratios on the solubility of gases in a sample due to depth and sample volume add error to ratio calculations.

3.3.2 Aqueous Mass and Molar Ratio

The aqueous mass ratio (blue triangles, Figure 3.3), has a fixed difference of $2.67\times$ lower than the source composition. This difference is sufficient to change the identification of a sample from likely biogenic ($C1/(C2+C3) = 1000$) to either thermogenic or in a transitional zone between thermogenic to biogenic ($C1/(C2+C3) = 375$), for which mixing would likely be the justification. When calculating the dissolved gas concentration for each component, the total mass of each component is based on its Henry's Law coefficient, its mole fraction in the headspace, and the volume of headspace and water in the sample vessel. The total mass is then attributed solely to the aqueous phase, because the mass of each gas in the sample would have initially been dissolved in the sample at depth prior to exsolution or helium headspace displacement. This process accounts for every variable that may affect the proportion of each gas in the headspace, and is thus independent of depth.

The aqueous molar ratio (green squares, Figure 3.3), has a fixed difference of $1.27\times$ lower than the source composition. The difference between the aqueous mass and aqueous molar ratios is simply a conversion from concentration in terms of mass to concentration in terms of moles. Since the heavier hydrocarbons are in the denominator, the aqueous mass ratio will always be a smaller value.

The discrepancy between the aqueous mass ratio and aqueous molar ratio to the source gas ratio is because they use aqueous concentrations to compare to a gas composition. In a gas sample, no partitioning between the aqueous phase and gaseous phase occurs. Other processes can change the gas signature in the sample, such as mixing or oxidation, but a gas sample will provide accurate compositional data of the source gas if those processes are negligible. Aqueous concentrations, by

contrast, are a product of gas partitioning, and therefore the proportion of each component that has partitioned into the water during the initial dissolution will not be identical to that of the initial source gas. Rather, they will be weighted by their respective Henry's Law coefficients. Therefore, the aqueous concentrations should be converted to equivalent gas units using Henry's Law for accurate comparison to the initial source.

3.3.3 Equivalent Gas Ratio

The equivalent gas ratio (red crosses, Figure 3.3), accurately portrays the hydrocarbon ratio in the source gas (red bar) by using the partial pressures of each component that would be in equilibrium with the concentrations in the aqueous sample at depth. This is achieved by converting the aqueous concentrations to partial pressures using Henry's Law. The equation for the conversion of $C_1/(C_2+C_3)$ from aqueous molar concentrations to partial pressures is:

$$EQG = \frac{C_{C1}^w H_{C1}}{C_{C2}^w H_{C2} + C_{C3}^w H_{C3}} \quad (3.16)$$

A similar ratio could be calculated using aqueous mass concentration using appropriate units of the Henry's Law constant. This conversion is not necessary if comparisons are being done within a study to analyse for trends in a well or between wells, so long as the ratio used is consistent between samples and the purpose is for trend analysis. The use of aqueous ratios will still show these trends. However, when comparing data sets between studies, it is important that a consistent ratio is used. Moreover, the comparison between a source gas and a dissolved gas sample for the purpose of source identification will be most accurate when using the equivalent gas ratio.

3.3.4 Effects of Dilution

In Scenario 2 (Figure 3.4), dilution occurs at depth, and thus the concentration of each component is reduced.

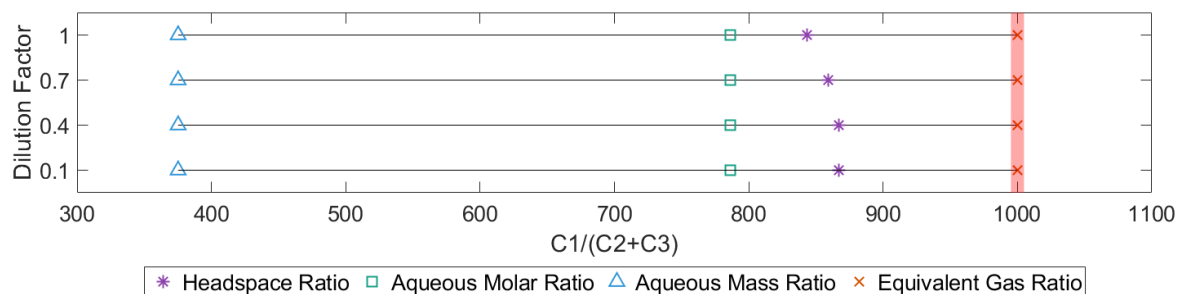


Figure 3.4. Calculated compositional ratios for varying dilution factor. The initial source gas has a ratio of 1000, and the sampling collection depth is 30 m. 500 mL of sample is collected, and a minimum of 30 mL of headspace is needed for each sample, with helium added when exsolution alone does not produce enough gas.

Both aqueous concentration ratios maintain the same difference to the SG ratio as shown in Figure 3.3. Therefore, dilution will not impact the error associated with using an aqueous concentration ratio. The EQG ratio is also not impacted by dilution and matches the source gas ratio. The difference between the SG and HS ratios decreases with dilution. This is again a result of the higher solubility of ethane and propane relative to methane, leading to a higher mole fraction of ethane and propane in the aqueous sample. As the solution becomes more dilute, the number of moles of gas which can exsolve in the sample is reduced. This further complicates the use of headspace ratios for source identification as dilution will alter the calculated headspace ratio.

Scenario 3 assumes dilution of the concentrations of C1, C2 and C3 with air-saturated water at a factor of 0.1 (10% dissolved natural gas, 90% air-saturated water). The relationship between ratios seen in Figure 3.3a will be unaffected by the presence of atmospheric nitrogen and oxygen despite a reduction in the total dissolved moles of C1, C2 and C3 in the sample (Figure 3.5)

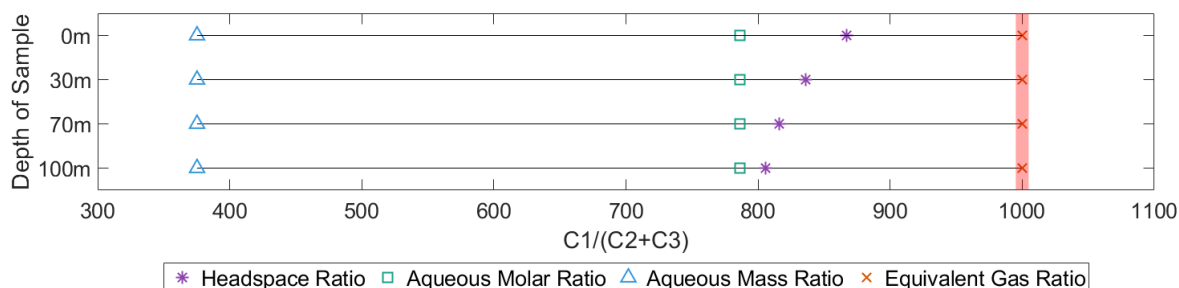


Figure 3.5. Different compositional ratios from an initially biogenic source gas with atmospheric nitrogen added.

Helium is added for headspace displacement for samples collected at 0 m, and at all other depths a headspace develops through exsolution. When comparing a dilution factor of 0.1 at 30 m with and without air-saturated water, the HS ratio with air-saturated water (836.2) is slightly lower than the HS ratio without air-saturated water (867.2). This is because a headspace is able to develop when oxygen and nitrogen are present in the sampled water, and the volume of gas is greater ($V^g = 59.9$ mL) than the case where helium is added ($V^g = 30$ mL). The addition of nitrogen and oxygen does not change the proportions of hydrocarbons; the relationships between ratios are maintained and are the same as those shown in Figure 3.3a.

3.3.5 Addition of non-hydrocarbon gases

Helium has been used as a tracer for stray gas site investigations where the source formation has a high proportion of helium, and He/CH₄ ratios are often reported. Helium has a higher Henry's Law constant, and thus will less-readily partition to the aqueous phase at depth. A set of calculations was performed for an initial gas containing 1.96% helium, balanced with C1, C2 and C3 and at a biogenic C1/(C2+C3) ratio of 1000. The source gas ratio of He/CH₄ is therefore 0.02. Figure 3.6 shows the results of these calculations; this set of results only includes samples from depths where 30 mL of headspace could form without additional helium added.

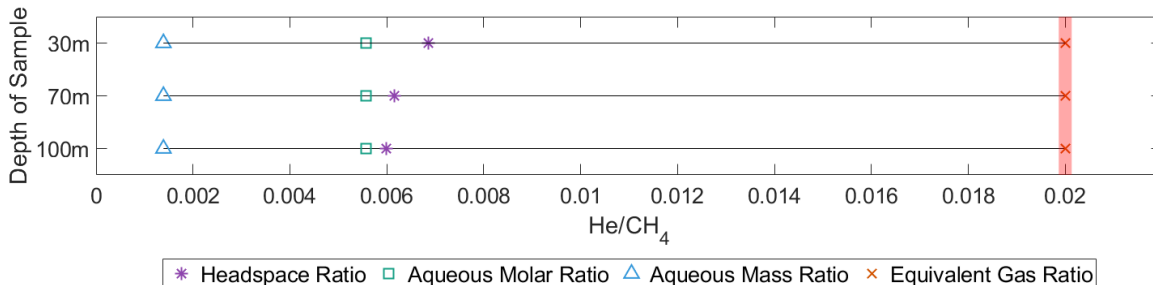


Figure 3.6. Different compositional ratios for an initial He/CH₄ ratio of 0.02. 500 mL of sample is collected, and a minimum of 30 mL of headspace is required. No additional helium is added to the system and as such a 0 m depth is neglected.

The same relative order is maintained for He/CH₄ as for C₁/(C₂+C₃) between all ratios, where the AMS ratio most underestimates the source gas ratio, followed by the AMO and HS ratio, but the magnitude of change is far increased due to the significant difference in gas solubility between helium and methane. The HS ratio is 2.92× (0.02/0.0068) to 3.34× (0.02/0.006) lower than the SG ratio, the aqueous molar ratio is 3.49× lower than the SG ratio, and the AMS ratio is 14.39× lower than the source gas ratio. These differences reach up to an order of magnitude and emphasize the importance of using the equivalent gas ratio as it is still equal to the source gas ratio even in the presence of helium. The reason for the greater magnitude of difference is the significantly higher Henry's Law constant of helium relative to methane. When investigating C₁/(C₂+C₃), the difference between the Henry's Law constants of each component is not nearly as large (Table 3.2), but the HS ratio will still be lower than the true ratio since the component in the numerator has a higher Henry's Law constant than the two components in the denominator.

3.4 Summary and Conclusions

Dissolved gas ratios are commonly used in stray gas migration site investigations due the relative ease of sampling and low cost of analysis. They are used both for source identification in comparing dissolved gas composition to a suspected source, and analysis of dissolved gas ratios in wells over time. The calculation of ratios using results from the analysis of dissolved gas samples is impacted

by the units used to calculate the ratios, which can be based on headspace composition or total mass in a sample expressed as an aqueous concentration. For source identification, this is particularly important as ratios vary for a single sample depending on the units used. The calculation of ratios for a set of hypothetical samples using different units and sample collection depths demonstrated that the equivalent gas ratio is most appropriate for source identification. The use of both headspace gas ratios and aqueous ratios lead to underestimation of the $C1/(C2+C3)$ ratio compared to an original source gas, and may lead to misidentification of a source. The error in headspace ratios is a function of depth, as gases dissolving at a greater depth will have a greater exsolved gas volume at surface. The difference applies not only to hydrocarbon gases but other dissolved gas ratios, and the magnitude of change is a function of the difference in Henry's Law constants. Moreover, the use of equivalent gas ratios is not impacted by the presence of other gases, as while the concentration of dissolved gas components may change, their proportions will not. The aqueous ratios will not be affected by depth, and as such can reasonably be used for trend analysis within a single well or single study. However, the equivalent gas ratio is also recommended for trend analysis to establish a common basis for comparison between current and future studies. It is also recommended that studies on stray gas migration report the units used to calculate ratios so that appropriate comparisons can be made.

3.5 References

- Banks, E.W., Smith, S.D., Hatch, M., Burk, L., Suckow, A., 2017. Sampling Dissolved Gases in Groundwater at in Situ Pressure: A Simple Method for Reducing Uncertainty in Hydrogeological Studies of Coal Seam Gas Exploration. *Environ. Sci. Technol. Lett.* 4, 535–539. <https://doi.org/10.1021/acs.estlett.7b00457>
- Barth-Naftilan, E., Sohng, J., Saiers, J.E., 2018. Methane in groundwater before, during, and after hydraulic fracturing of the Marcellus Shale. *Proc. Natl. Acad. Sci. U. S. A.* 115, 6970–6975. <https://doi.org/10.1073/pnas.1720898115>
- BCOGC, 2020. Oil and Gas Activity Operations Manual - December 2020. <https://www.bco.gc.ca/files/operations-documentation/Oil-and-Gas-Operations-Manual/oil-and-gas-activity-operations-manual.pdf>

- Bernard, B.B., Brooks, J.M., Sackett, W.M., 1978. Light Hydrocarbons in Recent Texas Continental Shelf and Slope Sediments. *J. Geophys. Res.* 83, 4053–4061. <https://doi.org/10.1029/JC083iC08p04053>
- Cahill, A.G., Parker, B.L., Mayer, B., Mayer, K.U., Cherry, J.A., 2018. High resolution spatial and temporal evolution of dissolved gases in groundwater during a controlled natural gas release experiment. *Sci. Total Environ.* 622-623, 1178-1192. <https://doi.org/10.1016/j.scitotenv.2017.12.049>
- Cesar, J., Nightingale, M., Becker, V., Mayer, B., 2020. Stable carbon isotope systematics of methane, ethane and propane from low-permeability hydrocarbon reservoirs. *Chem. Geol.* 558, 119907. <https://doi.org/10.1016/j.chemgeo.2020.119907>
- Darrah, T.H., Jackson, R.B., Vengosh, A., Warner, N.R., Whyte, C.J., Walsh, T.B., Kondash, A.J., Poreda, R.J., 2015. The evolution of Devonian hydrocarbon gases in shallow aquifers of the northern Appalachian Basin: Insights from integrating noble gas and hydrocarbon geochemistry. *Geochim. Cosmochim. Acta* 170, 321–355. <https://doi.org/10.1016/j.gca.2015.09.006>
- Dusseault, M., Jackson, R., 2014. Seepage pathway assessment for natural gas to shallow groundwater during well stimulation, in production, and after abandonment. *Environ. Geosci.* 21, 107–126. <https://doi.org/10.1306/eg.04231414004>
- Etiopie, G., Feyzullayev, A., Baci, C.L., 2009. Terrestrial methane seeps and mud volcanoes: A global perspective of gas origin. *Mar. Pet. Geol.* 26, 333–344. <https://doi.org/10.1016/j.marpetgeo.2008.03.001>
- Forde, O.N., Mayer, K.U., Hunkeler, D., 2019. Identification, spatial extent and distribution of fugitive gas migration on the well pad scale. *Sci. Total Environ.* 652, 356–366. <https://doi.org/10.1016/j.scitotenv.2018.10.217>
- Geistlinger, H., Beckmann, A., Lazik, D., 2005. Mass transfer between a multicomponent trapped gas phase and a mobile water phase: Experiment and theory. *Water Resour. Res.* 41, 1-15. <https://doi.org/10.1029/2004WR003885>
- Gorody, A.W., 2012. Factors affecting the variability of stray gas concentration and composition in groundwater. *Environ. Geosci.* 19, 17–31. <https://doi.org/10.1306/eg.12081111013>
- Harkness, J.S., Darrah, T.H., Warner, N.R., Whyte, C.J., Moore, M.T., Millot, R., Kloppmann, W., Jackson, R.B., Vengosh, A., 2017. The geochemistry of naturally occurring methane and saline groundwater in an area of unconventional shale gas development. *Geochim. Cosmochim. Acta* 208, 302–334. <https://doi.org/10.1016/j.gca.2017.03.039>
- Kampbell, D.H., Vandegrift, S.A., 1998. Analysis of Dissolved Methane, Ethane, and Ethylene in Ground Water by a Standard Gas Chromatographic Technique. *J. Chromatogr. Sci.* 36, 253–256. <https://doi.org/10.1093/chromsci/36.5.253>
- Kang, M., Kanno, C.M., Reid, M.C., Zhang, X., Mauzerall, D.L., Celia, M.A., Chen, Y., Onstott, T.C., 2014. Direct measurements of methane emissions from abandoned oil and gas wells

in Pennsylvania. *Proc. Natl. Acad. Sci.* 111, 18173–18177.
<https://doi.org/10.1073/pnas.1408315111>

Kelly, W.R., Matisoff, G., Fisher, J.B., 1985. The effects of a gas well blow out on groundwater chemistry. *Environ. Geol. Water Sci.* 7, 205–213. <https://doi.org/10.1007/BF02509921>

Klazinga, D.R., Steelman, C.M., Cahill, A.G., Walton, K.M., Endres, A.L., Parker, B.L., 2019. Methane gas transport in unconfined aquifers: A numerical sensitivity study of a controlled release experiment at CFB Borden. *J. Contam. Hydrol.* 225, 103506.
<https://doi.org/10.1016/j.jconhyd.2019.103506>

McIntosh, J.C., Hendry, M.J., Ballentine, C., Haszeldine, R.S., Mayer, B., Etiope, G., Elsner, M., Darrah, T.H., Prinzhofer, A., Osborn, S., Stalker, L., Kuloyo, O., Lu, Z.T., Martini, A., Lollar, B.S., 2019. A Critical Review of State-of-the-Art and Emerging Approaches to Identify Fracking-Derived Gases and Associated Contaminants in Aquifers. *Environ. Sci. Technol.* 53, 1063–1077. <https://doi.org/10.1021/acs.est.8b05807>

Molofsky, L.J., Connor, J.A., McHugh, T.E., Richardson, S.D., Woroszylo, C., Alvarez, P.J., 2016a. Environmental Factors Associated With Natural Methane Occurrence in the Appalachian Basin. *Groundwater* 54, 656–668. <https://doi.org/10.1111/gwat.12401>

Molofsky, L.J., Connor, J.A., Wylie, A.S., Wagner, T., Farhat, S.K., 2013. Evaluation of Methane Sources in Groundwater in Northeastern Pennsylvania. *Groundwater*. 51, 333-349.
<https://doi.org/10.1111/gwat.12056>

Molofsky, L.J., Richardson, S.D., Gorody, A.W., Baldassare, F., Black, J.A., McHugh, T.E., Connor, J.A., 2016b. Effect of Different Sampling Methodologies on Measured Methane Concentrations in Groundwater Samples. *Groundwater* 54, 669–680.
<https://doi.org/10.1111/gwat.12415>

Nicot, J.P., Larson, T., Darvari, R., Mickler, P., Slotten, M., Aldridge, J., Uhlman, K., Costley, R., 2017. Controls on Methane Occurrences in Shallow Aquifers Overlying the Haynesville Shale Gas Field, East Texas. *Groundwater* 55, 443–454.
<https://doi.org/10.1111/gwat.12500>

Rice, A.K., Lackey, G., Proctor, J., Singha, K., 2018. Groundwater-quality hazards of methane leakage from hydrocarbon wells: A review of observational and numerical studies and four testable hypotheses. *Wiley Interdiscip. Rev. Water.* 5, e1283.
<https://doi.org/10.1002/wat2.1283>

Sander, R., 2015. Compilation of Henry's law constants (version 4.0) for water as solvent. *Atmos. Chem. Phys.* 15, 4399–4981. <https://doi.org/10.5194/acp-15-4399-2015>

Schout, G., Hartog, N., Hassanizadeh, S.M., Griffioen, J., 2017. Impact of an historic underground gas well blowout on the current methane chemistry in a shallow groundwater system. *Proc. Natl. Acad. Sci. U. S. A.* 115, 296–301. <https://doi.org/10.1073/pnas.1711472115>

- Schout, G., Hartog, N., Hassanizadeh, S.M., Helmig, R., Griffioen, J., 2020. Impact of groundwater flow on methane gas migration and retention in unconsolidated aquifers. *J. Contam. Hydrol.* 230. <https://doi.org/10.1016/j.jconhyd.2020.103619>
- US Environmental Protection Agency - US EPA, 2016. Hydraulic Fracturing for Oil and Gas: Impacts from the Hydraulic Fracturing Water Cycle on Drinking Water Resources in the United States (Main Report - EPA/600/R-16/236fa).
- Van De Ven, C.J.C., Mumford, K.G., 2020. Aqueous and surface expression of subsurface GHGs: Subsurface mass transfer effects. *Water Res.* 170, 115327. <https://doi.org/10.1016/j.watres.2019.115327>
- Vengosh, A., Jackson, R.B., Warner, N., Darrah, T.H., Kondash, A., 2014. A critical review of the risks to water resources from unconventional shale gas development and hydraulic fracturing in the United States. *Environ. Sci. Technol.* 48, 8334–8348. <https://doi.org/10.1021/es405118y>
- Whiticar, M.J., 1990. A geochemical perspective of natural gas and atmospheric methane. *Org. Geochem.* 16, 531–547. [https://doi.org/10.1016/0146-6380\(90\)90068-B](https://doi.org/10.1016/0146-6380(90)90068-B)

Chapter 4

Conclusions and Recommendations

4.1 Summary and Conclusions

Increased development of deep natural gas deposits in North America requires consideration of the potential impacts on the environment in both the short and long term. Stray gas migration from leaking energy wells is a known risk of natural gas extraction, and can impact groundwater quality as well as emit greenhouse gases to the atmosphere. Therefore, the mechanisms controlling stray gas releases into the subsurface must be understood such that leaks can be identified, monitored and remediated. Understanding the dissolution of stray gas will allow for appropriate regulations and standards to be applied for natural gas extraction.

The dissolution of single- and multicomponent source gases trapped in porous media was studied. Bench-scale column experiments showed that with a single-component source, methane concentrations were initially at pure solubility, and decreased as methane dissolved into initially methane-free influent water. Effluent concentrations of methane were not reduced to zero over the period of data collection, which was attributed to dissolution kinetics. With a multicomponent source, the concentration of methane was lower than its pure solubility as a result of a reduced partial pressure in the gas source. The concentrations of all three components (methane, ethane, propane) decreased as the source gas dissolved. All three components were still present at the end of the data collection period. Simulations using MIN3P were able to accurately predict both the single- and multicomponent source dissolution data collected in the lab, with differences being attributed primarily to the local equilibrium assumption used in MIN3P.

Bench-scale experiments and MIN3P simulations demonstrated that background gases impact the persistence and dissolution of trapped natural gas. Experimental results showed that after 12 pore

volumes of water had flowed through the column, gas saturation had decreased from 0.18 to 0.09, but the aqueous concentrations of the original source gas components (methane only or methane, ethane and propane) had decreased to near 1 mg/L. This suggests that at the end of each experiment, the gas phase is composed primarily of influent dissolved background gases that have partitioned into the gaseous phase, sustaining the trapped gas phase. MIN3P simulations demonstrated that the shape of the aqueous concentration breakthrough during dissolution of the source gas will also be impacted by the presence of background dissolved gases, as extremely low background gas concentrations led to sharp dissolution fronts. However, as background gas concentrations increase, the dissolution behaviour of the source gas converges such that it is largely insensitive to background gas concentrations above a dissolved gas concentration equivalent to a sum of partial pressures that is 40% of the water pressure. Gas persistence was shown to be highly sensitive to background dissolved gas concentrations. At low background dissolved gas concentrations, gas will be extinguished once the source gas has dissolved into the aqueous phase. However, at high background dissolved gas concentrations, gas becomes highly persistent as the background gases can partition to the gaseous phase. This applies to the dissolution of both single-component and multicomponent source gases. As such, even single-component source dissolution should be considered a multicomponent problem, as the presence of other gases will impact the persistence of gas in the subsurface. It is important then that any conceptual or numerical model of stray gas leaks considers not only the source gas, but also the background gases.

Bench-scale and numerical simulations demonstrated that hydrocarbon ratios change over time due to dissolution. Methane, ethane, and propane each have different Henry's law coefficients, and as such partition to the aqueous phase at different rates. Bench-scale experiments showed that this ratio can both increase and decrease with time, and that hydrocarbon ratios are less reliable when each component's concentration is near its detection limit. Numerical simulations demonstrated that the increase in hydrocarbon ratio observed in the experiments is possible for any initial source gas

composition, as the ratio will always increase due to ethane and propane concentrations decreasing before methane concentrations. The increase in ratio presents the potential for misidentification of a source if the time-dependent nature of aqueous sampling for source identification is not considered, however the magnitude of ratio increases due to multicomponent mass transfer at field scales must be studied to fully understand the potential for classification changes.

Differences in interpretation can also impact the use of hydrocarbon ratios in practice. Proper sampling and analytical methods allows for a direct comparison to be made between an initial source gas composition and an aqueous sample. However, analytical results often present measurements in terms of mole fraction of a gas in the headspace of a sample, or the aqueous concentration of a dissolved gas. If these results are used directly to calculate the hydrocarbon ratio, significant error is introduced. When using mole fraction in the headspace the partitioning of gases to and from the aqueous sample, the volume of headspace and volume of water have not yet been accounted for, and as such the proportions of gas in the headspace are not representative of the initial source gas. The calculation of aqueous concentrations accounts for these variables, however a ratio calculated using aqueous concentrations is not equivalent to the ratio in the gas that was at equilibrium with the water at depth. The calculation of hydrocarbon ratios using mole fraction in the headspace, total concentrations on a mole basis and total concentrations on a mass basis resulted in the underestimation of the source gas ratio by a factor of 1.15 to 1.24, 1.27 and 2.67 respectively. An equivalent gas ratio must be calculated, in which aqueous concentrations are converted to their equivalent partial pressures such that comparisons can be made between aqueous sample hydrocarbon ratios and the original source gas. The combination of physical processes and interpretation challenges means that care must be taken when using any dissolved gas ratio for source identification. Furthermore, multiple lines of evidence should be used as additional sources or sinks of gas components in the subsurface may impact any one dissolved gas concentrations.

4.2 Recommendations for Future Work

Further work is required to understand the effects of multicomponent mass transfer on stray gas dissolution. The work conducted in this study is limited to the post-repair dissolution of trapped gas. However, stray gas field investigations may also be conducted on active leaks or leaks which release periodically. Changes in hydrocarbon ratio have been noted during active injection and post-repair in field-scale studies (Cahill et al., 2018), and further work should be conducted to understand compositional changes of multicomponent sources during both periods. The study of the effects of background gases on gas dissolution and persistence was limited to experimental gas saturation measurements and numerical simulations, however the aqueous concentrations of the background gases during experiments were not measured due to lab limitations. Similar experiments should be conducted to monitor both source and background gases. These experiments should be conducted with varied background gas concentrations and compositions to experimentally validate the numerical modeling results that demonstrate that gas persistence is highly dependent on background gas concentrations. Increases in scale to both large-scale column experiments or field scale experiments would allow for sampling of dissolved gases to expand to non-hydrocarbon gases. Additionally, small-scale column effects on dispersivity would be reduced. While baseline sampling is often limited at stray gas migration sites, a greater understanding of the dissolved gases present at a site before gas release may provide additional insight on the expected persistence of stray gas, and by consequence provide additional motivation for baseline sampling prior to drilling. To determine the importance of background gases at the field scale, the comparison of field injections of natural gas at sites with varying geochemistry would be valuable. Ultimately, a greater understanding of the effects of background gases will allow for better interpretation of field-scale gas migration such that the conceptual model of gas migration can be improved.

4.3 Contributions

This study contributed to the field of gas migration by providing further understanding of multicomponent mass transfer effects on the dissolution of gas in the subsurface. This study validated the use of MIN3P to model the dissolution of stray gas in the subsurface, for aqueous concentrations and gas saturation (Chapter 2). This work demonstrated the importance of considering the composition of both the source gas and the background dissolved gas for stray gas dissolution (Chapter 2). It is expected that demonstrating that hydrocarbon ratios are subject to change through both multicomponent mass transfer (Chapter 2) and interpretation techniques (Chapter 3) will help improve best practices when using hydrocarbon ratios and other dissolved gas ratios for source identification. Furthering the conceptual model of gas migration in the subsurface will allow for more appropriate regulations to be applied to stray gas releases.

4.4 References

Cahill, A.G., Parker, B.L., Mayer, B., Mayer, K.U., Cherry, J.A., 2018. High resolution spatial and temporal evolution of dissolved gases in groundwater during a controlled natural gas release experiment. *Sci. Total Environ.* 622-623, 1178-1192. <https://doi.org/10.1016/j.scitotenv.2017.12.049>

Appendix A

Supplemental Figures (Chapter 2)

Aqueous effluent concentrations for the single-component (methane, SC1-4) and multicomponent (MC1-4) experiments are plotted as average values in Figure 2.4. Figure A. 1. shows the data from each single-component experiment, and Figure A. 2. shows the data from each multicomponent experiment.

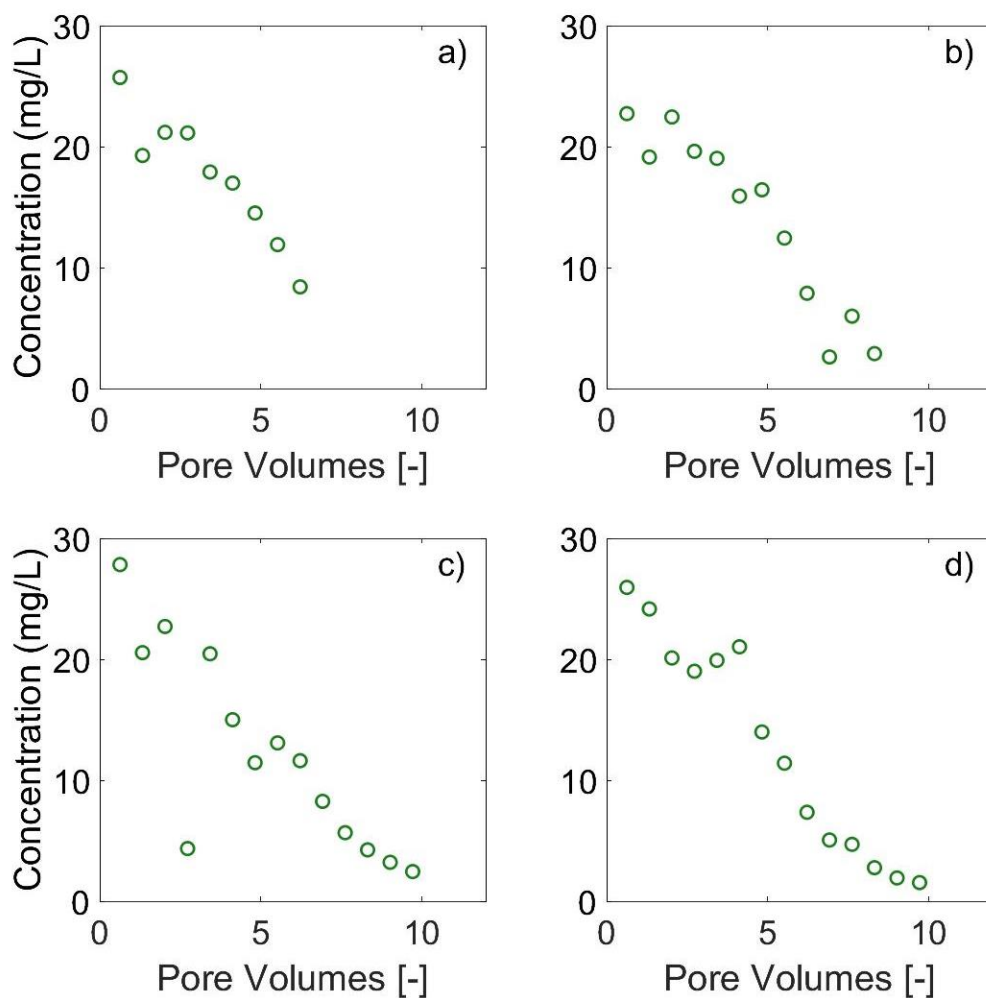


Figure A. 1. Measured aqueous effluent concentrations for the single-component (methane) experiments a) SC1 b) SC2 c) SC3 d) SC4.

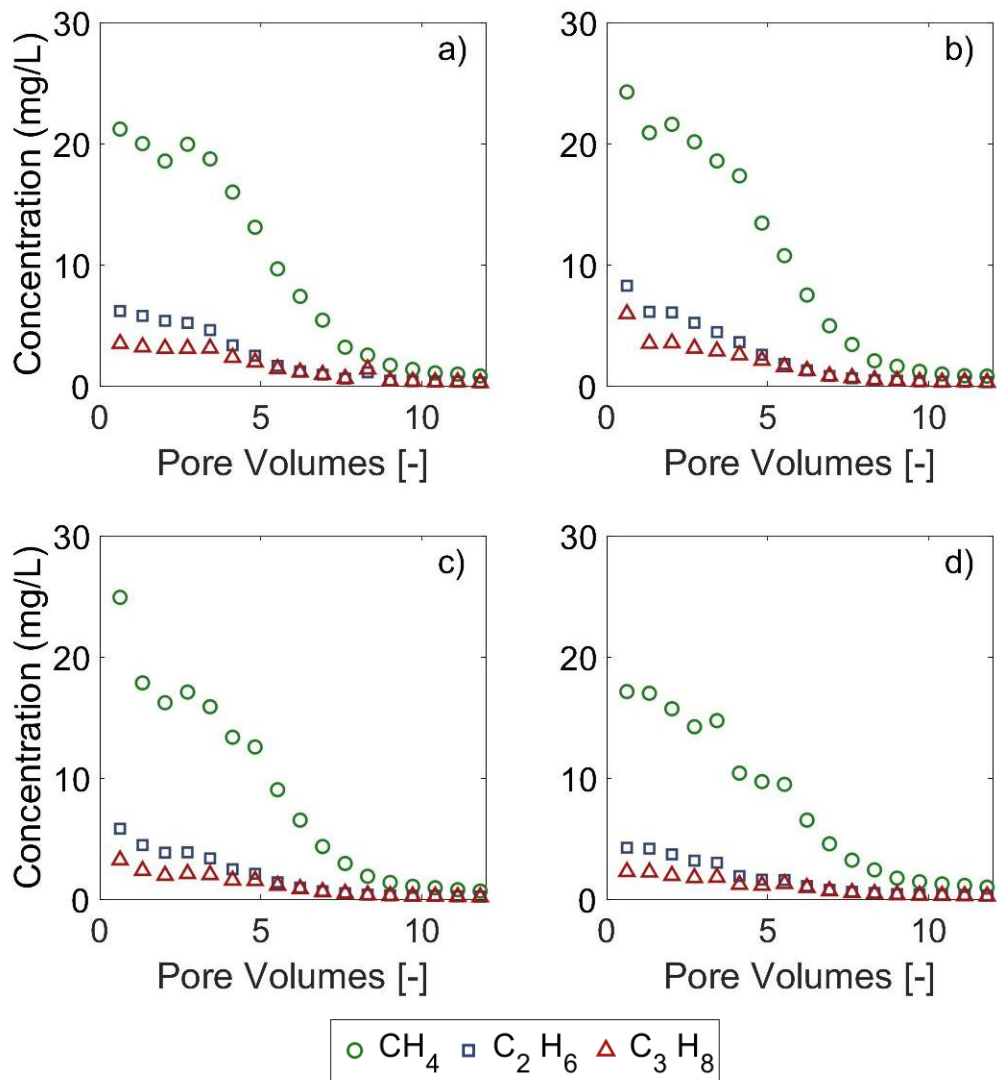


Figure A. 2. Measured aqueous effluent concentrations for the multicomponent experiments a) MC1 b) MC2 c) MC3 d) MC4.

Simulations were conducted to compare the sensitivity of gas persistence for varying background gas concentrations. Simulations were conducted at both atmospheric conditions and 30 m of hydrostatic pressure. It was determined that the total gas pressure in the system (approximated as the hydrostatic pressure) did not impact gas persistence when changing the relative background gas concentration.

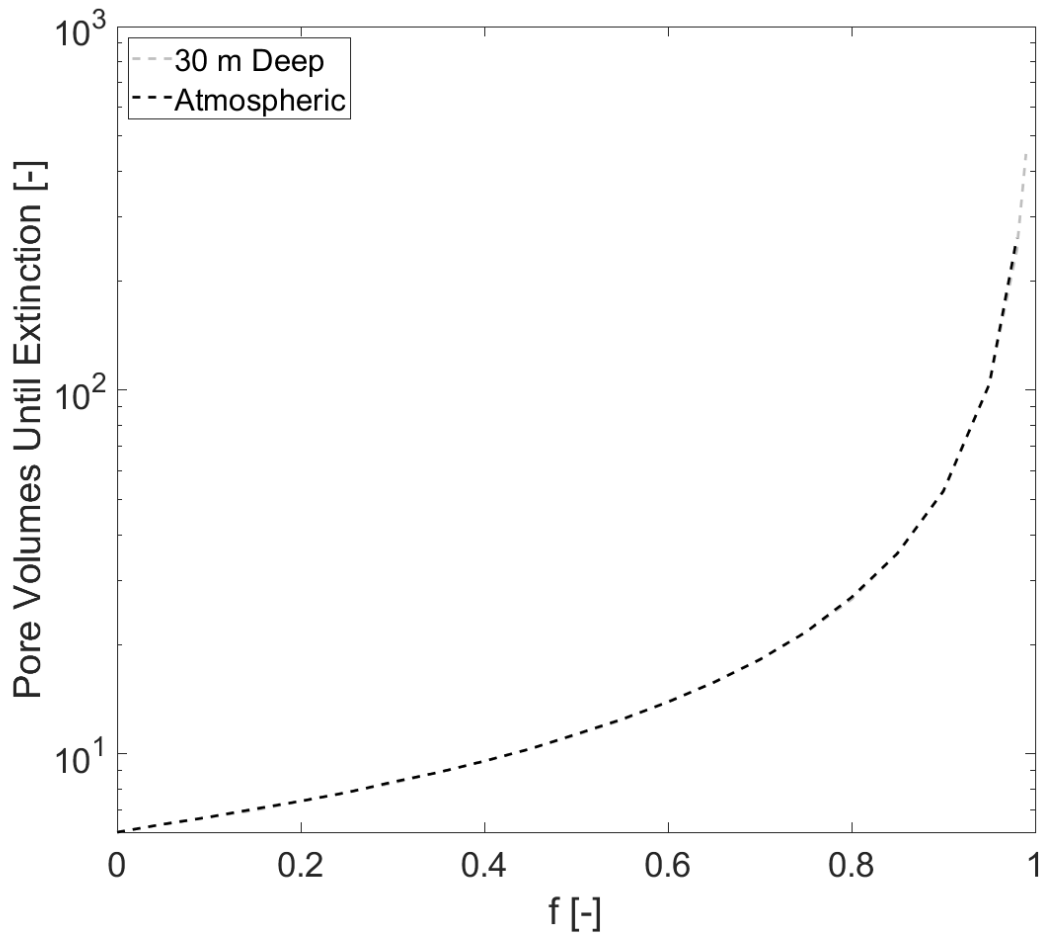


Figure A. 3. Time of extinction for a methane source with varying relative background gas concentration. The total gas pressure is simulated as atmospheric and as 30 m of hydrostatic pressure.

Laboratory experiments were conducted in which a multicomponent source (85% methane, 10% ethane, 5% propane) was dissolved using influent water sparged with CO₂ rather than air-equilibrated as in Chapter 2 (Figure A. 4.). Results showed that CO₂ concentrations quickly plateaued at 1100 mg/L. Methane, ethane and propane concentrations increased at 1 pore volume, and then decreased linearly before plateauing. Preliminary simulations with MIN3P were conducted, though further modification is required for the simulation to be valid as the simulation currently uses a surrogate CO₂ gas and does not consider the carbonate system or the loss of gas due to effervescence noted during the experiment. The use of influent background gases other than N₂ and O₂ may provide additional insights to the effects of multicomponent mass transfer on gas dissolution.

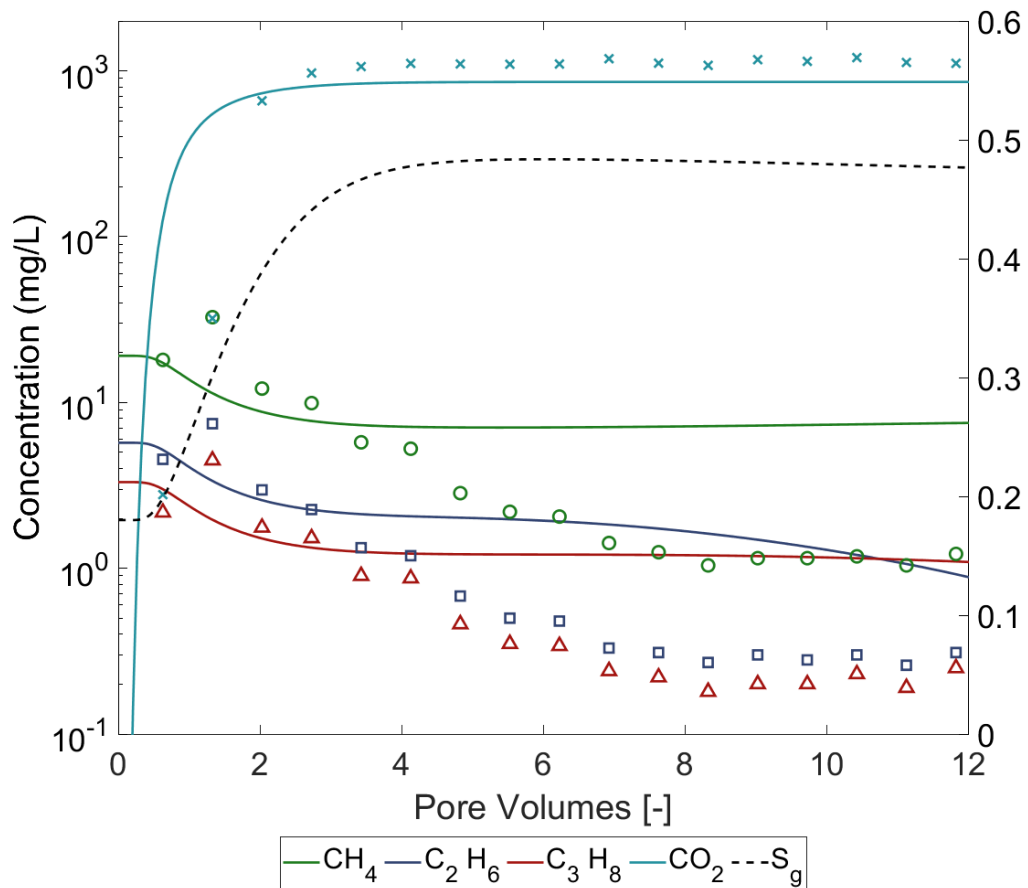


Figure A. 4. Measured (symbols) and simulated (lines) aqueous effluent concentrations for the multicomponent source experiment with CO₂ sparged influent. Experimental data points match the colours of the simulated data. Simulated average gas saturations throughout the column are shown as a dashed line Note: log scale on y axis.

Appendix B

Bromide Tracer Tests (Chapter 2)

A bromide tracer test was conducted in the experimental column to determine the dispersivity of the saturated sand pack. A 100 mg/L sodium bromide solution was pumped through the column at 2.5 mL/min, and 10 mL samples were collected at the outflow. These samples were then analyzed for bromide concentrations. Using MIN3P, the bromide breakthrough data was fitted with the advection-dispersion equation and it was determined that a dispersivity of 4.5 mm was the best fit. An offset of 0.37 pore volumes was used to fit the curve, which equates to 27 mL, to account for tubing between the influent reservoir and the column. Results are shown in Figure B. 1.

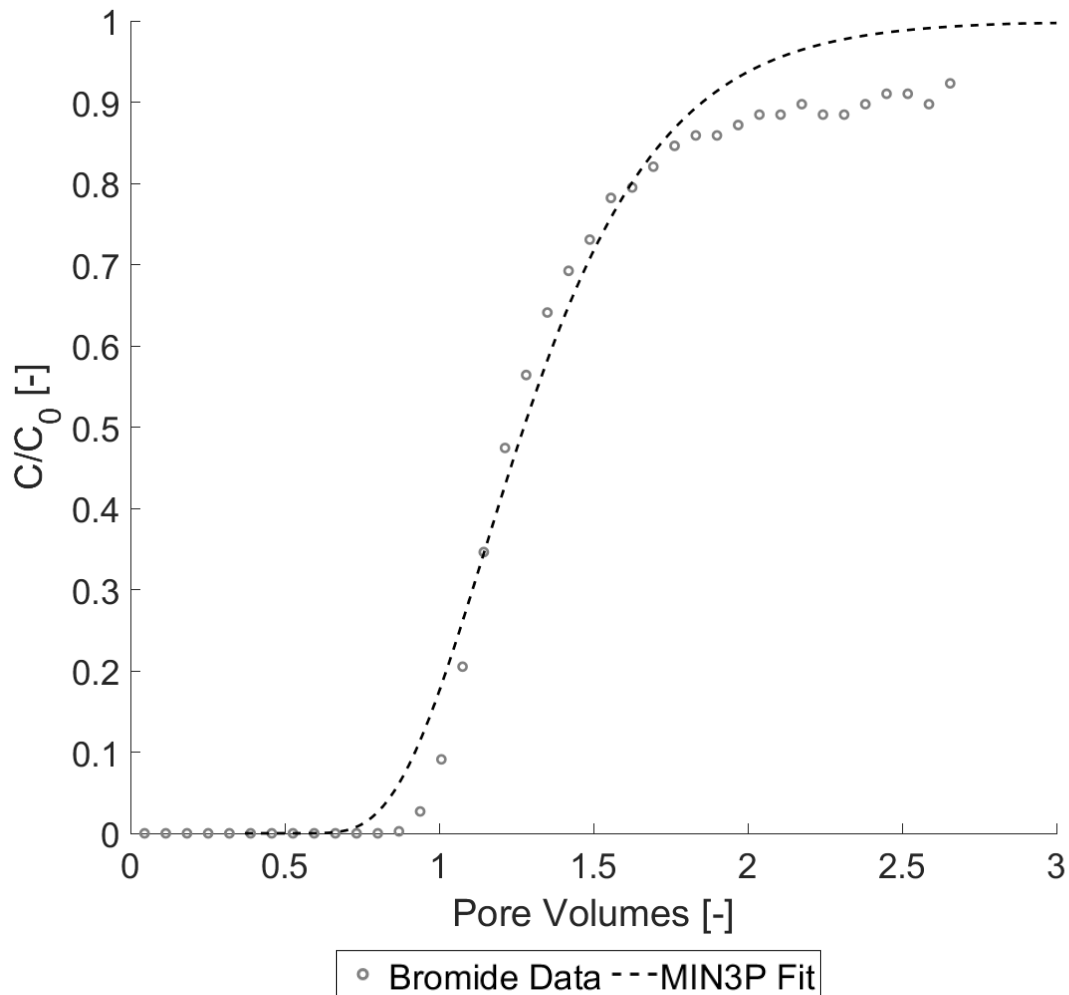


Figure B. 1. Bromide tracer test. Symbols show bromide sample data and dashed line is a line of best fit modeled in MIN3P.

Bromide tracer tests were conducted in the experimental column measuring conductivity to verify the dispersivity of the column for initially saturated and unsaturated conditions. A 100 mg/L sodium bromide solution was pumped through the column at 2.5 mL/min, and 10 mL samples were collected at the outflow. The conductivity of each sample was then measured with a conductivity probe, and it was determined that a dispersivity of 4.5 mm was a good fit for both conditions. An offset of 0.03 pore volumes was used to fit the curve, which equates to 2.2 mL, to account for tubing between the influent reservoir and the column (shortened tubing and earlier breakthrough compared to experiment in Figure B. 1.). Results are shown in Figure B. 2.

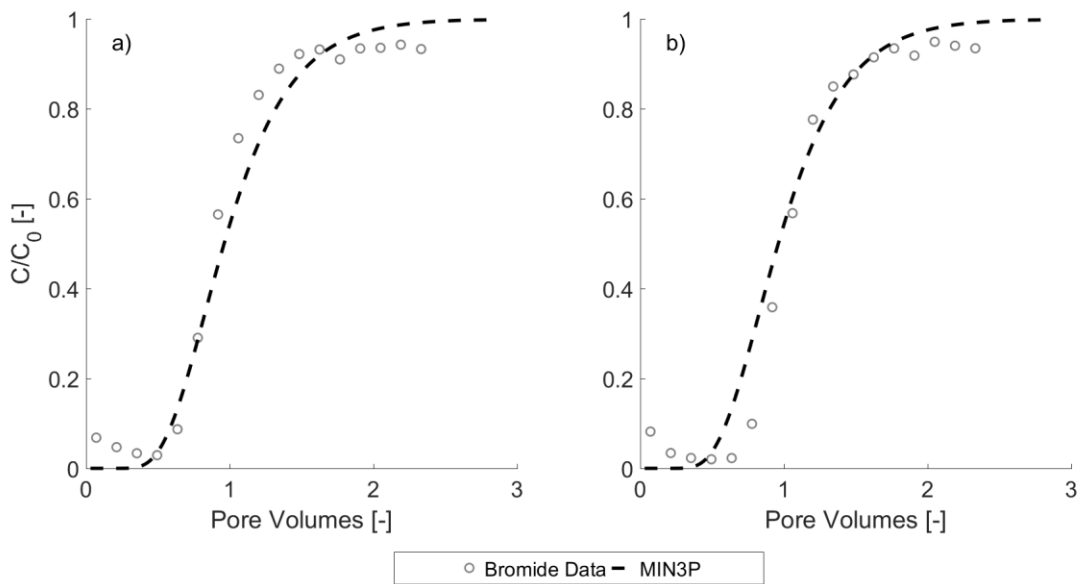


Figure B. 2. Bromide tracer test, measuring conductivity breakthrough for (a) saturated column and (b) unsaturated column. Symbols show conductivity sample data and dashed line is a line of best fit modeled in MIN3P.

Appendix C

Sand Characterization (Chapter 2)

To characterize the 20/30 sand used in experiments in Chapter 2, drainage curves were created by sampling the volume of water drained as capillary pressure was increased. First, a set of hanging column experiments were conducted and compared to Schroth et al. (1996) to verify that the hanging column method used was valid. Results are shown in Figure C. 1.

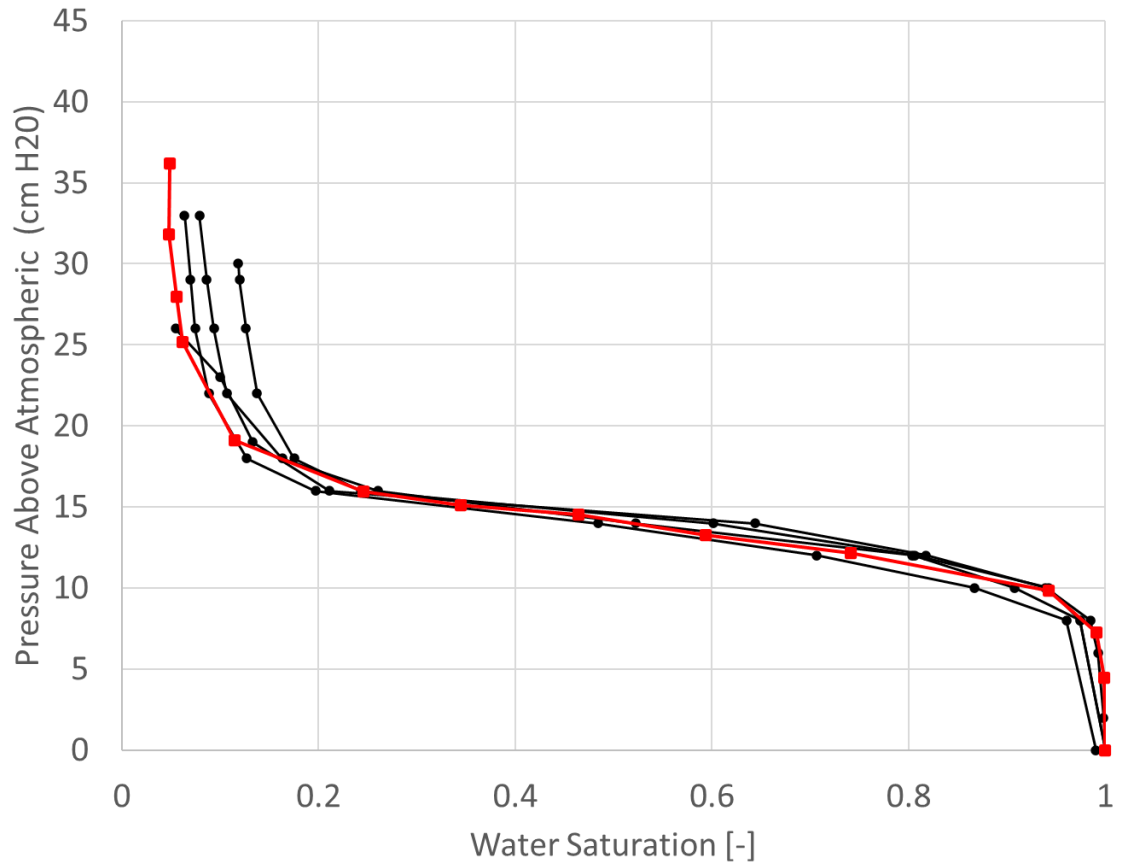


Figure C. 1. Hanging column drainage curves. The red line is drainage data for 20/30 sand from Schroth et al. (1996). Black lines are values collected for this thesis.

Following hanging column experiments, drainage was conducted by increasing the gas pressure at the top of the column using a mass flow controller as discussed in Section 2.2.1. Additionally, imbibition was conducted, and the final trapped gas saturation was determined. Drainage curves were collected for both single-component experiments (Figure C. 2) and multicomponent experiments (Figure C. 3).

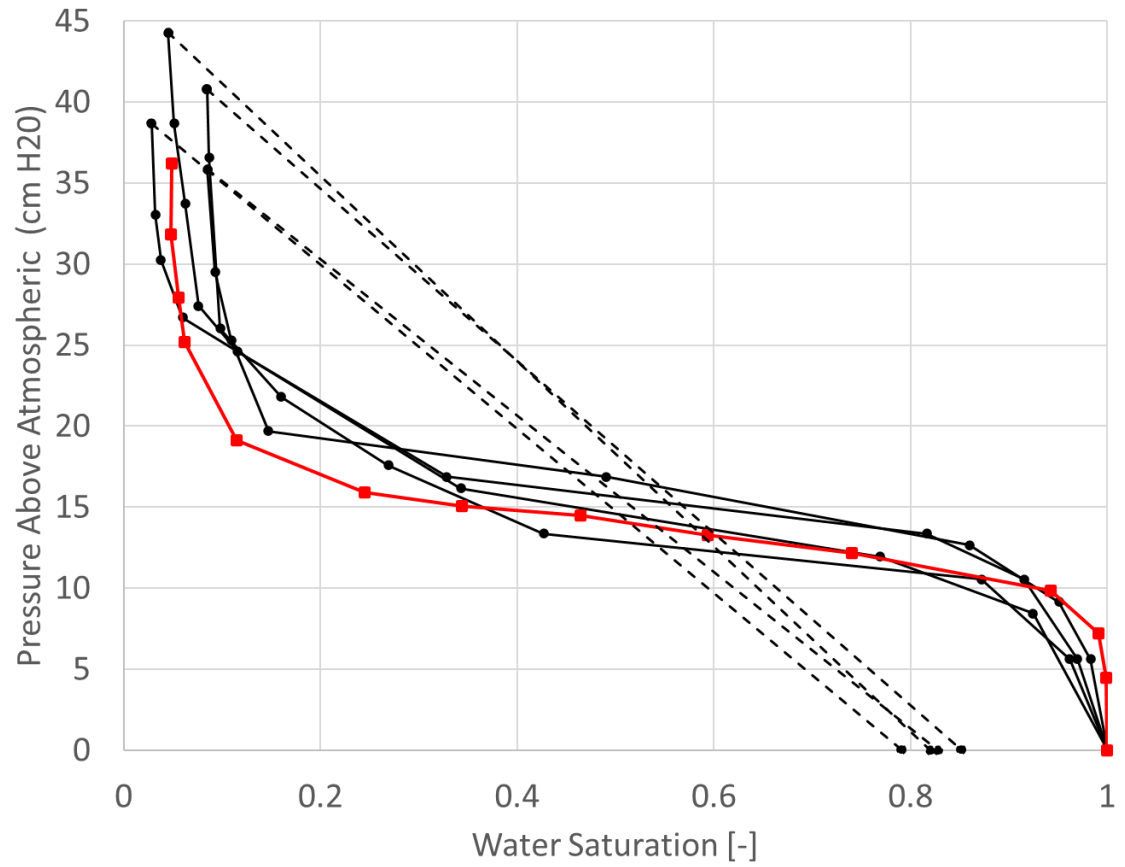


Figure C. 2. Drainage and imbibition data for single-component experiments (SC1-4). The red line is drainage data for 20/30 sand from Schroth et al. (1996). Drainage data for this thesis is shown in solid black lines, and imbibition start and end points are shown in dashed lines, and imbibition data was not collected at intermediate steps.

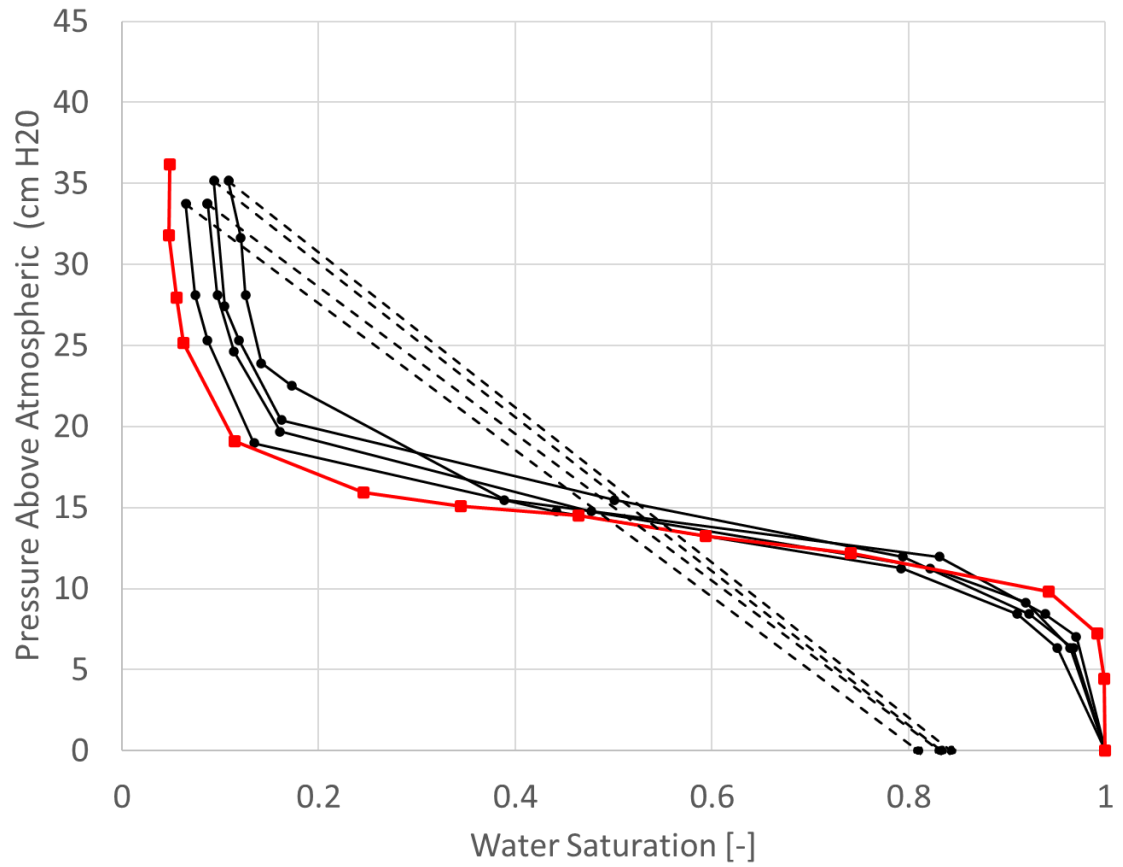


Figure C. 3. Drainage and imbibition data for single-component experiments (MC1-4). The red line is drainage data for 20/30 sand from Schroth et al. (1996). Drainage data for this thesis is shown in solid black lines, and imbibition start and end points are shown in dashed lines, and imbibition data was not collected at intermediate steps.

Appendix D

Experimental Apparatus (Chapter 2)

Photos were taken showing the experimental apparatus used in Chapter 2 as discussed in Section 2.2.1.

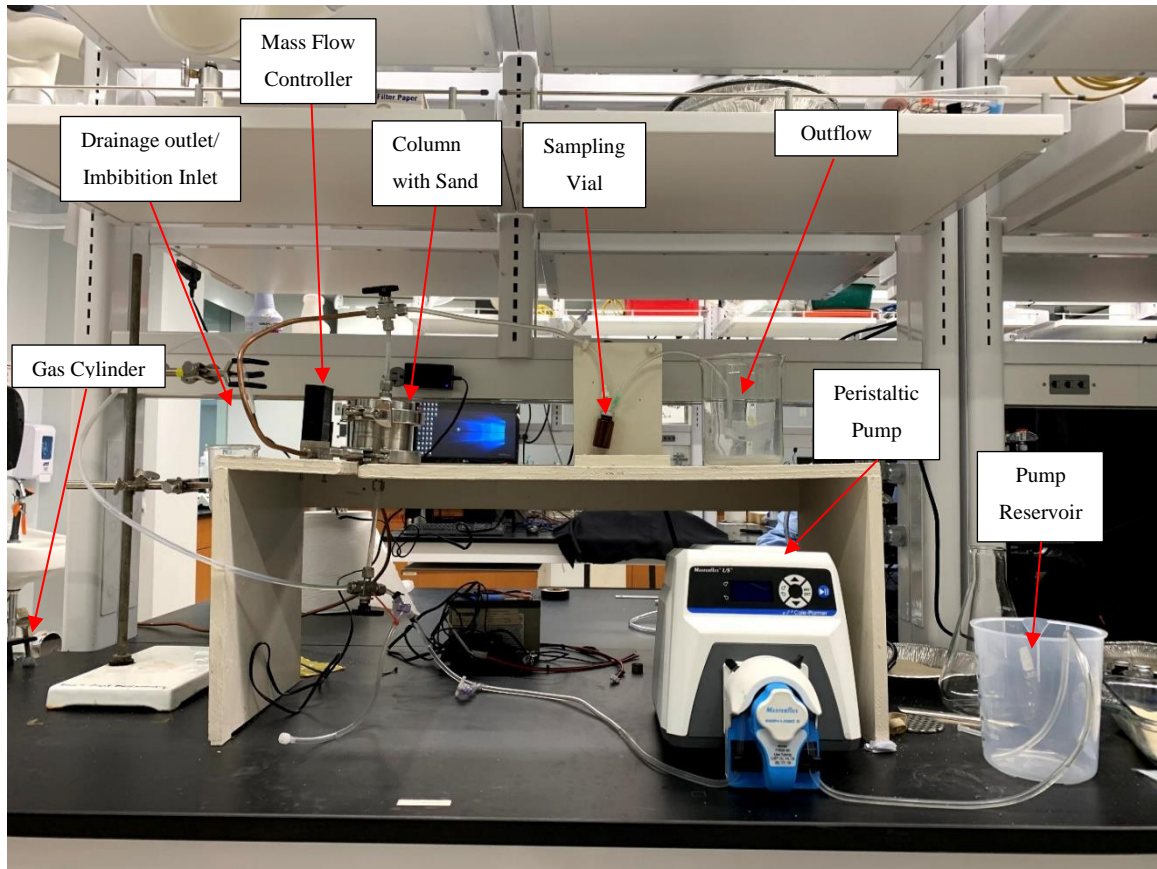


Figure D. 1. View of lab apparatus with labels corresponding to items shown in Figure 2.3.



Figure D. 2. Disassembled column showing from left to right: thin steel plate, collar, bottom cap with gasket, column, collar, top cap with gasket, and thick steel plate.



Figure D. 3. Bottom cap showing the filter placed between the thin steel plate and the gasket.



Figure D. 4. Assembled column – close up.

Appendix E

Methane Calibration Data (Chapter 2)

To measure the dissolved methane concentrations for SC-1 to SC-3, headspace gas chromatography was used to measure the gaseous concentration of methane in each sample vial. Calibration is required to relate sample area measured via GC to the methane concentration in the headspace. A unique calibration curve was measured for each experiment. Each calibration concentration was measured in triplicate, shown in red points.

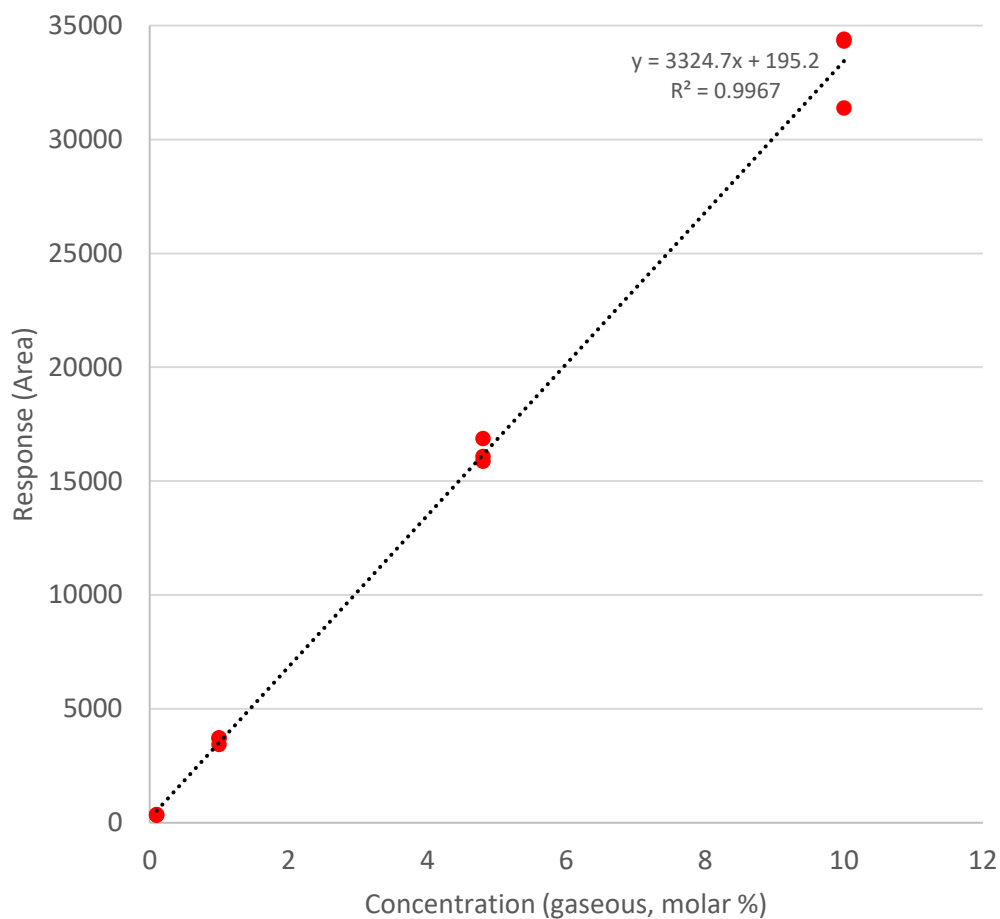


Figure E. 1. Calibration curve for SC1.

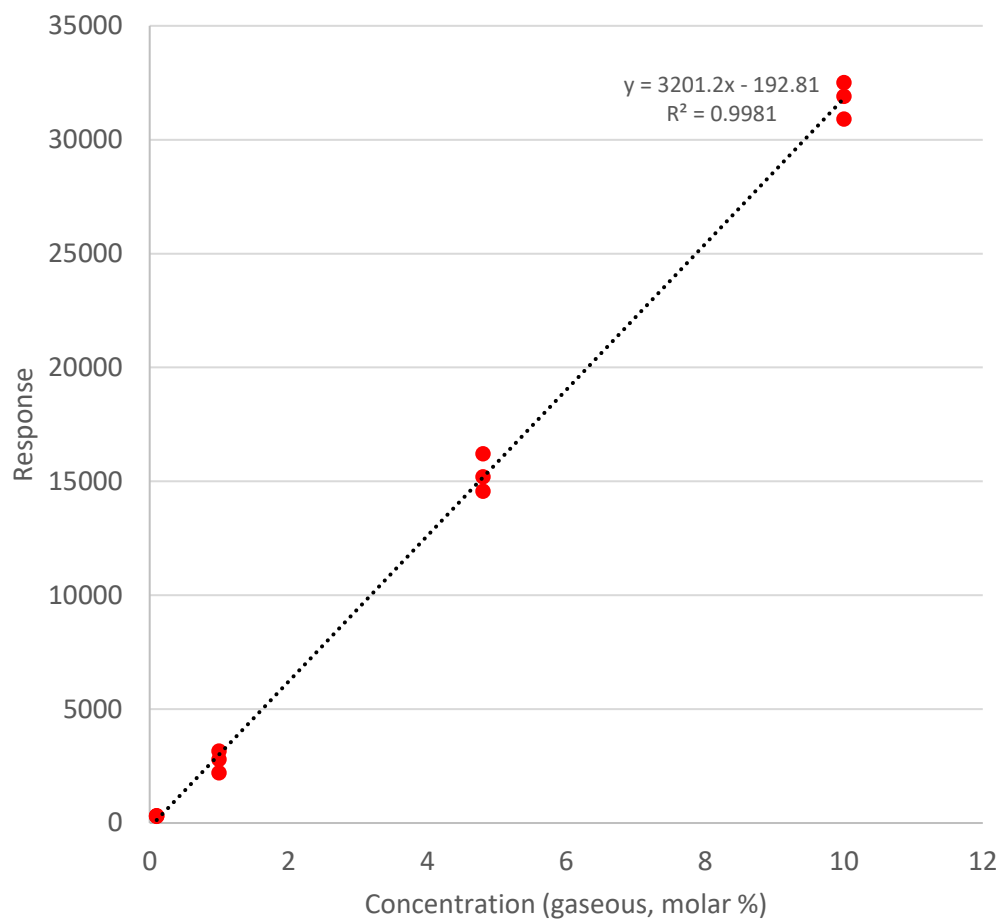


Figure E. 2. Calibration curve for SC2.

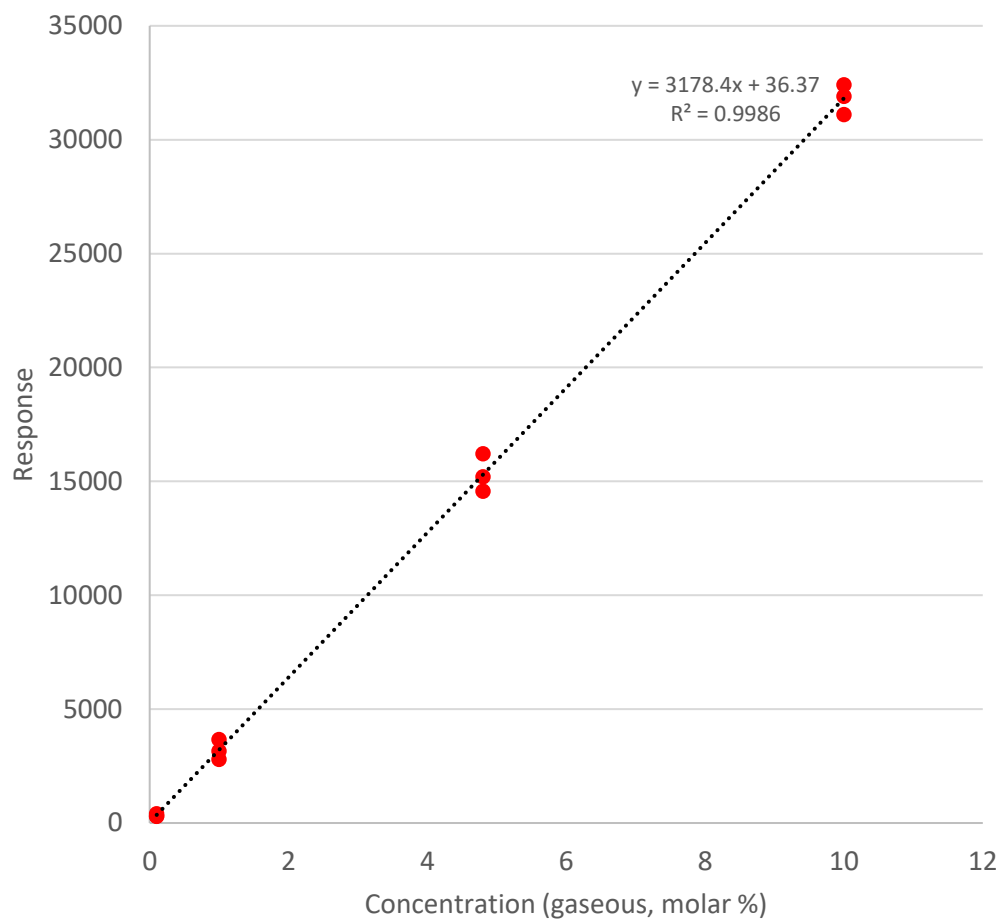


Figure E. 3. Calibration curve for SC3.